POLITECNICO DI MILANO

Facoltà di Ingegneria Industriale

Corso di Laurea in
Ingegneria Aeronautica

Nonlinear Continuous Turbulence

Design Loads Calculation Methods

Relatore: Prof. Sergio RICCI

Tutor: Ing. Manuel REYES GUITIAN

Tesi di Laurea di:

Marco BARBATI Matr. 736056

Anno Accademico 2010 - 2011

Ai miei genitori Giuseppe e Marisa

Index

List of Figures

List of Tables

Sommario

Questo lavoro presenta l'applicazione di tre metodi per il calcolo di carichi di disegno derivanti da turbolenza atmosferica continua per modelli dinamici di velivoli nonlineari. La tesi riporta una ricerca bibliografica sullo stato dell'arte dei metodi di calcolo per turbolenza continua lineare e non lineare, l'analisi e l'implementazione dei metodi piú interessanti da un punto di vista ingegneristico ed industriale e lo sviluppo di un nuovo metodo denominato *Statistical Method* (SM), ideato nel Dipartimento di Dinamica delle Strutture e Aeroelasticitá di Airbus Military, divisione del gruppo EADS-CASA, Getafe (Spagna). Viene presentata una prima valutazione dei metodi scelti su un semplice sistema test e quindi la loro applicazione ad un tipico modello industriale per il calcolo di carichi dinamici del velivolo *A400M*.

Parole chiave: Turbolenza Continua, carichi di progetto per sistemi non lineari, Matched Filter, Spectral Gust, Statistical Method, *A400M*.

Abstract

This paper presents a comparison between three methods for continuous turbulence (CT) design load calculation for nonlinear aircraft models. The paper provides a literature survey over linear and nonlinear CT methods, the comparison and the implementation of the most interesting ones and the development of a new method, referred to as *Statistical Method* (SM), developed by the Department of Structural Dynamics and Aeroelasticity of Airbus Military, EADS-CASA, Getafe (Spain). The methods have been applied at first to a simple dynamic test systems and then to an industrial dynamic model of the *A400M*.

Keywords: continuous turbulence, nonlinear design loads, Matched Filter, Spectral Gust, Statistical Method, *A400M*.

Chapter 1

Introduction to Continuous Turbulence design loads

The problem is the definition and the computation of design loads for nonlinear aircraft subjected to Continuous Turbulence. CT gust design methods are usually based on von Kármán Power Spectral Density (PSD) description of turbulence velocity and use frequency domain techniques to compute the loads. This definition of turbulence in the frequency plane represents the basic problems for nonlinear dynamic analysis, for which the principle of superposition no longer holds. On the contrary the time plane defined Discrete Tuned Gust (DTG) do not present problems related to the definition of the excitation and shows that aircraft nonlinearities, especially flight control nonlinearities (such as limiters and thresholds activity on control surfaces), cannot be neglected.
A practical method for nonlinear CT analysis should:

- give loads consistent to existing requirements (for a linear case),
- give time-correlated (or consistent, or balanced) loads,
- give nodal loads (see section 1.4),
- be straight-forward and time-saving (this point excludes local linearization).

So a number of methods have been developed in literature from the late 1980s, when the Federal Aviation Administration (FAA), the National Aeronautics and Space Administration (NASA) and parallel others European research centres such the National Aerospace Laboratory (NLR, Netherlands) started an initial evaluation of a candidate method for CT nonlinear analysis. These works result in several methods based mainly on time domain analysis with a stochastic or deterministic approach that will be shown in the next chapter.

1.1 Linear CT design loads

The definition of design loads of a linear aircraft subjected to continuous turbulence is given by EASA CS-25 regulations in AMC 25.341(b), Subpart C (ref. [2]). The regulations define two criterions to calculate CT design loads, the *Design Envelope Analysis*, based on PSD input-output relationship in critical points of the flight envelope, and the *Mission Analysis* criterion, based on the calculation of the probability (or frequency) of exceedance of a given load value during a typical flight profile. Hereafter when referring to CT design or time correlated loads we mean incremental load with respect to the *1g* flight load condition.

1.1.1 Design Envelope Analysis

For every load of interest named *y*, at all critical weights, weight distributions, speeds and altitudes the design value is defined as in equation 1.1, where $\overline{A_y}$ is the root mean square incremental load σ_y to root mean square gust velocity σ_g ratio (equation 1.2) and U_σ is the true gust velocity value given by regulations depending on aircraft speed and altitude. The power spectral density $\Phi_{yy}(\omega)$ can be calculated for a linear model as in equation 1.3, where $H_{yy}(i\omega)$ is the frequency response function between the gust input and the load *y*, while $\Phi_{ww}(\omega)$ is the von Kármán turbulence spectrum. For a more detailed treatment see reference [2].

$$y_{design} = U_\sigma \cdot \overline{A_y} \tag{1.1}$$

$$\overline{A_y} = \frac{\sigma_y}{\sigma_g} = \frac{\sqrt{\int_{-\infty}^{+\infty} \phi_{yy}(\omega) d\omega}}{\sigma_g} \tag{1.2}$$

$$\phi_{yy}(\omega) = \left| H_{yy}(i\omega) \right|^2 \phi_{ww}(\omega) \tag{1.3}$$

1.1.2 Mission Analysis

The mission analysis criterion is based on the concept of *frequency of exceedance N(y)*; for one or more flight profiles representing the expected aircraft utilization, divided into flight segments of width *t*, the average number of exceedances of the indicated values of the load in unit time (*N(y)*) should be calculated as a function of the load itself by means of equation 1.4. N_0 represents the average number of zero level crossing, P_1, P_2, b_1, b_2 are parameters given by

regulations as functions of altitude while $\overline{A_y}$ is the RMS ratio defined by dynamic analysis as in equation 1.2. All this quantities refer to the *i-th* time segment. The design (or limit) load is defined as the load which produce a frequency of exceedance of *2*1E-05* exceedances per hour. As before, for a more detailed explanation see reference [2].

$$N(y) = \sum tN_0 \left[P_1 \exp\left(-\frac{|y - y_{1g}|}{b_1 \overline{A_y}} \right) + P_2 \exp\left(-\frac{|y - y_{1g}|}{b_2 \overline{A_y}} \right) \right] \tag{1.4}$$

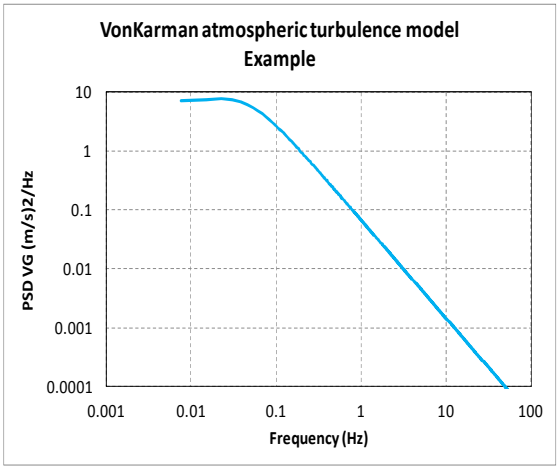

Figure 1.1. Von Kármán atmospheric model power spectral density.

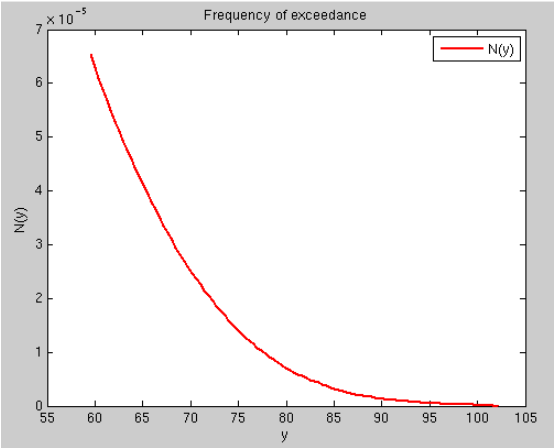

Figure 1.2. Typical frequency of exceedance curve.

1.2 Nonlinear CT design loads

Let us extract a paragraph over nonlinear continuous turbulence considerations from *CRD NPA309* [12]:

"It will normally be necessary to justify that the selected approach provides an equivalent level of safety as a conventional linear analysis and is appropriate to handle the types of non-linearity on the aircraft. This should include verification that the approach provides adequate statistical significance in the loads results. A methodology based upon stochastic simulation has been found to be acceptable for load alleviation and flight control system non-linearities. In this simulation, the input is a long, Gaussian, pseudo-random turbulence stream conforming to a Von Kármán spectrum with a root-mean-square (RMS) amplitude of 0.4 times U_σ (defined in Section 5.c (1) of this ACJ). The value of limit load is that load with the same probability of exceedance as U_σ of the same load quantity in a linear model [...]. When using an analysis of this type, exceedance curves should be constructed using incremental load values up to, or just beyond the limit load value. The non-linear simulation may also be performed in the frequency domain if the frequency domain method is shown to produce conservative results. Frequency domain methods include, but are not limited to, Matched Filter Theory and Equivalent Linearisation."

So for a nonlinear analysis the suggestion is to develop a time domain definition of the Design Envelope criterion which assures a level of safety equal to the same criterion applied to the linear model. As it can be seen in the next chapters this is the basic concept of the methods developed for CT nonlinear loads calculation.

1.3 Correlated loads

With time correlated loads it is intended the set of loads insisting in a section of the aircraft (or, more generally, any quantity in any position along the aircraft) at the instant of time at which the design load reaches its limit value. In time domain based methods this loads can be directly calculated, while in PSD based methods the calculation of the design loads in terms of RMS ratio looses the information about time correlation between two quantities. So we have to appeal to joint probability or cross-correlation definition for a stationary Gaussian random process involving a linear system (the definition for nonlinear systems will be carried out step by step in Chapter 2).
Following reference [10] the joint probability density function of two loads *y* and *z* with correlation coefficient ρ_{yz} is:

$$p_{yz}(y,z) = \frac{1}{2\pi\sigma_y\sigma_z\sqrt{1-\rho_{yz}^2}} \cdot \exp\left(-\frac{\left(\frac{y}{\sigma_y}\right)^2 - 2\frac{\rho_{yz}yz}{\sigma_y\sigma_z} + \left(\frac{z}{\sigma_z}\right)^2}{2(1-\rho_{yz}^2)} \right) \qquad (1.5)$$

$$\rho_{yz} = \frac{\int_0^{+\infty} \left[H_{yreal}(\omega)H_{zreal}(\omega) + H_{yimag}(\omega)H_{zimag}(\omega) \right] \phi_{ww}(\omega)d\omega}{\overline{A_y}\,\overline{A_z}} \qquad (1.6)$$

Hence the correlated load *z* to the design limit load *y* (or vice versa) can be calculated as follows:

$$z_{correl} = \rho_{yz} \cdot z_{design} = \rho_{yz} \cdot U_\sigma \overline{A_z} \qquad (1.7)$$

In the exponent of equation 1.5 it can be recognized an ellipse formula:

$$\left(\frac{y}{\sigma_y}\right)^2 - 2\frac{\rho_{yz}yz}{\sigma_y\sigma_z} + \left(\frac{z}{\sigma_z}\right)^2 = \left(\frac{U_\sigma}{\sigma_g}\right)^2 \left(1-\rho_{yz}^2\right) \qquad (1.8)$$

Any combination of loads *y* and *z* which belongs to the ellipse has the same probability density and represents a balanced load distribution.
Plotting the so called *equiprobability ellipse* (figure 1.4) we get the points of tangency, *T*, corresponding to the expressions for correlated load pairs given by equations 1.6, 1.7. The points of tangency to the ellipse given by lines AB, CD,

EF and GH represent an additional practical set of equiprobable load pairs that should be considered to establish critical design stresses, but will not be considered in the proceedings of this work. For more details see reference [12].

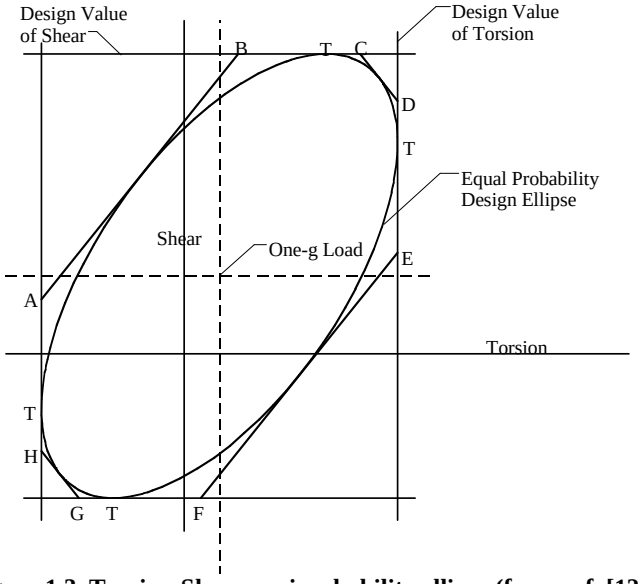

Figure 1.3. Torsion-Shear equiprobability ellipse (from ref. [12]).

1.4 Nodal loads

With the term nodal loads we intend the set of nodal forces that should be applied to the numerical Finite Element model to represent the considered load condition, in this case the continuous turbulence design load condition. It is clear that a PSD based method looses the information about nodal load distribution since it is based on an integral calculation. CT nodal loads can be recovered approximating the design point on the equiprobability ellipse with a DTG giving the same design and correlated loads. This is done varying the intensity and the shape of the discrete gust. Once the approximating DTG has been found nodal loads are obtained from the discrete displacements time history *{x(t)}* with summation of forces method (equation (1.9), where $\{F(t_0)\}$ is the nodal forces set, $\{\xi(t_0)\}$ is the modal displacements vector and t_0 is the instant of time in which the response reaches its maximum).

$$\{F(t_0)\} = [K]\{x(t_0)\} = -[M][\phi]\{\xi''(t_0)\} - [B][\phi]\{\xi'(t_0)\} + \{F_{ext}(t_0)\} \quad (1.9)$$

Chapter 2

Literature Survey over Nonlinear CT

Several methods have been available in the literature since the 80s. Two of them (Matched Filter theory and Spectral Gust) have been taken into account for their interesting characteristics, respectively reliability and time savings ability. Section 2.3 reports a brief description of methods which will not be considered in the proceedings of this work. A theoretical development of each method and a results comparison based on literature data is provided. The selected methods will be further implemented and compared with the Statistical Method developed by the Department of Structural Dynamics and Aeroelasticity of EADS-CASA, Airbus Military, Getafe (Spain), which is reported in section 2.5.

2.1 Matched Filter Based method (MF)

2.1.1 Linear MF Theory

The matched filter concept was originally developed for radar's signal post processing; it's an electronic filter designed to give a maximum response to a known input signal, which is called *matched waveform*. The idea is to apply this concept to the aircraft system, interpreting the series of a gust filter and the aircraft dynamics as the *filter* and looking for the *worst gust* waveform as a matched waveform. Thus the method is a *deterministic* representation of CT. A development of the matched filter theory and its application to gust loads calculation is here presented (for more details see ref. [1]).
Say $h_y(t)$ the unit impulse response of a linear dynamic system, the response of the system to an input $x(t)$ can be written as:

$$y(t) = \int_{-\infty}^{+\infty} h_y(t-t')x(t')dt' \tag{2.1}$$

The upper bound of $y(t)$ at a time $t=t_0$ is given by *Schwartz's* inequality:

$$|y(t_0)|^2 = \left|\int_{-\infty}^{+\infty} h_y(t_0 - t')x(t')dt'\right|^2 \leq \left|\int_{-\infty}^{+\infty} h_y^2(t_0 - t')dt'\right|\left|\int_{-\infty}^{+\infty} x^2(t')dt'\right| \quad (2.2)$$

Substituting *x(t)* with a specific waveform given by $x(t) = \frac{1}{|K|}h_y(t_0 - t)$, and applying *Parseval's* theorem we obtain:

$$|y(t)|_{\max} = |y(t_0)| = \frac{1}{|K|}\left|\int_{-\infty}^{+\infty} h_y^2(t_0 - t')dt'\right| = \frac{1}{|K|}\frac{1}{2\pi}\left|\int_{-\infty}^{+\infty} H_y^*(\omega)H_y(\omega)d\omega\right| = \frac{\sigma_{h_y}^2}{|K|} \quad (2.3)$$

Where σ_{h_y} is the Root Mean Square (RMS) value of the impulse response and *K* is an arbitrary constant. It's guaranteed that y_{max} is reached at t_0 since the integrand is always positive. The waveform *x(t)* is referred to as matched to *y(t)* because it maximizes the response. The definition of the constant *K* can be related to the level of probability of encountering a waveform of a given energy level. In fact a measure of the waveform energy can be:

$$U_{x,t_0} = \int_{\tau}^{\tau+t_0} x^2(t)dt = \frac{1}{K^2}\int_{\tau}^{\tau+t_0} h_y^2(t_0 - t)dt = \frac{\sigma_{h_y}^2}{K^2} \quad (2.4)$$

So we get:

$$K = \frac{\sqrt{U_{x,t_0}}}{\sigma_{h_y}} \quad (2.5)$$

As mentioned before $U_{x,T}$ is a measure of the energy of the waveform and is related to the probability density of *x(t)* by:

$$p(x(t),T) = \frac{1}{Z}\exp\left(-\frac{U_{x,T}}{2\sigma_x^2}\right) \quad (2.6)$$

$$Z = \int_x \exp\left(-\frac{U_{x,T}}{2\sigma_x^2}\right) \quad (2.7)$$

In conclusion, for all the excitation waveform of a given energy $U_{x,T}$ the *maximum response* of a linear system (equation (2.8)) is the result of a *matched excitation* waveform (equation (2.9)) possessing an energy $U_{x,T}$ and a probability density *p(x(t),T).*

$$|y|_{\max} = \sqrt{U_{x,t_0}}\,\sigma_{h_y} \tag{2.8}$$

$$x(t) = \frac{\sqrt{U_{x,t_0}}}{\sigma_{h_y}} h_y(t_0 - t) \tag{2.9}$$

Thus the maximum response of the system and the corresponding excitation waveform can be known simply by the impulse response of the system and its RMS value. The operation sequence can be seen in figure 2.1.

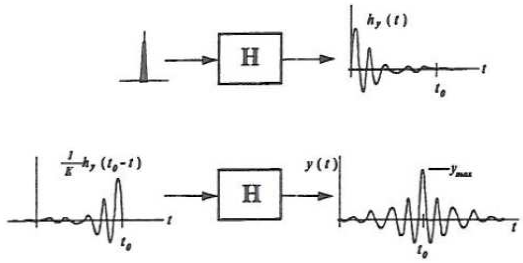

Figure 2.1. Linear Matched Filter sequence.

To apply this method to continuous turbulence load calculation we have to:

- relate the impulse input to continuous turbulence,
- relate the waveform energy measure $U_{x,T}$ to the regulations.

First, continuous turbulence is defined in frequency domain as a power spectrum, the *von Kármán* one. A power spectrum can be obtained as in equation (2.10), where $G(i\omega)$ is the transfer function of a gust filter which approximates the von Kármán spectrum and *WN* is a white noise. $G(i\omega)$ is referred to as a "filter" since equation (2.10) can be represented in the time domain as the response of a filter to a unit impulse input. So the system dynamics *H* represented in figure 2.1 is given by the series of the gust filter dynamics and the aircraft dynamics.

$$\phi_{vK}(i\omega) = |G(i\omega)|^2 \cdot WN \tag{2.10}$$

Second, from the *EASA CS-25, AMC 25.341 (b)* requirements (ref. [2]) we have:

$$y_{design} = U_\sigma \overline{A} = U_\sigma \frac{\sigma_y}{\sigma_g} \tag{2.11}$$

Where U_σ is the design gust velocity, given by regulations, and σ_g is the RMS value of the turbulence. Thus, comparing equation (2.11) with equation (2.8), we have:

$$\sqrt{U_{x,t_0}} = \frac{U_\sigma}{\sigma_g} \tag{2.12}$$

$$|y|_{\max} = \sqrt{U_{x,t_0}}\,\sigma_{h_y} = \frac{U_\sigma}{\sigma_g}\,\sigma_{h_y} = y_{design,PSD} \tag{2.13}$$

So the maximum response of the MF procedure y_{max} represents the Design Envelope criterion design loads $y_{design,PSD}$ if the matched excitation waveform $x(t)$ energy level $U_{x,T}$ comply with equation (2.12).
The application of the method to a linear aircraft system is depicted in figure 2.2, where $G(i\omega)$ indicates the gust filter transfer function while $H(i\omega)$ represents aircraft dynamics.

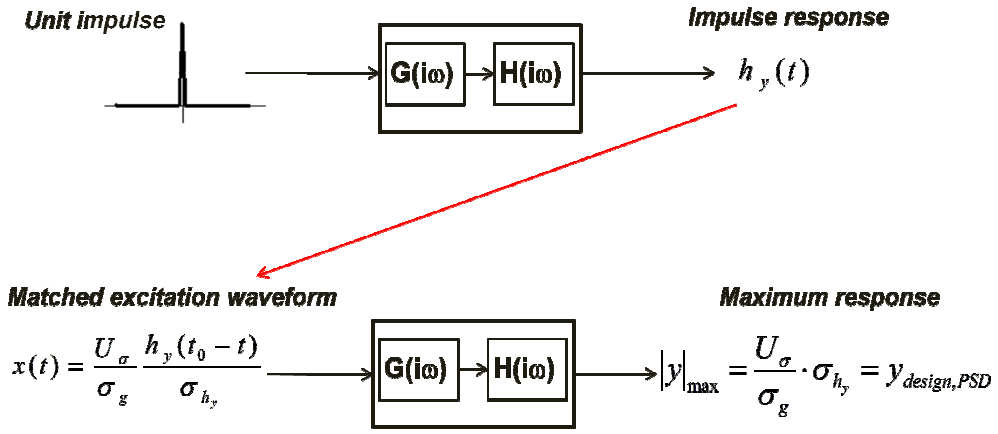

Figure 2.2. Matched Filter theory for aircraft continuous turbulence analysis.

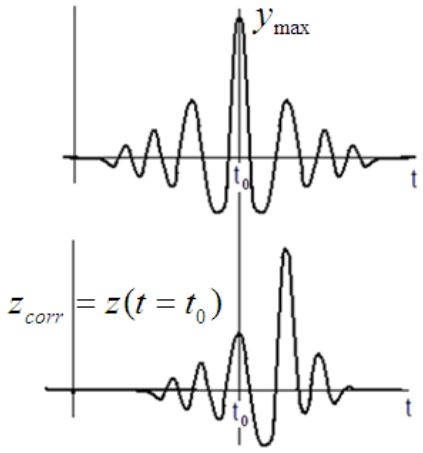

Figure 2.3. Matched Filter theory for aircraft continuous turbulence analysis, correlated loads.

Comments:

- The worst gust profile (matched to the maximum load y_{max}) can be obtained as an intermediate result between the gust filter and aircraft dynamics in the second row of the operational flow.
- The method allows the calculation of *time-correlated loads* (values of the others output of the system at the time t_0, when y reaches its maximum, figure 2.3).
- The method provides *nodal loads*, since operates on actual time histories known in every node of the aircraft model.
- The procedure has to be repeated for every design load that has to be maximized, because every load is maximized by its own matched excitation (i.e. by its own impulse response function).

Obviously there's no convenience to run the MF method for a linear aircraft, since it reproduce the results of the linear PSD analysis with a bigger calculation effort (PSD method needs only one analysis to calculate all design and time-correlated loads). Matched filter interest is greater for a *nonlinear* analysis, since it's a fully time domain method, while frequency domain based method as PSD method cannot be applied.

2.1.2 Nonlinear MF application

When nonlinearities cannot be neglected the superposition principle no longer holds, so the magnitude of the output is not necessarily proportional to the magnitude of the input. The authors (ref. [3]) propose a *search procedure* based on numerical optimization for the matched excitation waveform *x(t)* that maximizes y_{max}. Two search procedure are available: a *one dimensional* (1D) search procedure, which varies the value of the initial impulse strength keeping fixed the shape of the excitation waveform, and a *multi dimensional* (MD) search procedure, which starting from the results of the 1D procedure uses a numerical optimization of the excitation shape under the constraint of unit RMS. It's demonstrated in the literature that the MD search procedure has a huge computational effort and it added a slight 1% more on design loads than the 1D procedure. Thus only the 1D search procedure will be carried out in this paper, because the MD procedure is felt to be unpractical for engineering use.
The 1D-MF method for nonlinear systems follows faithfully the linear procedure, but with an iterative procedure to search the maximum load y_{max}. The only value which is varied is the initial impulse strength *k* (figure 2.4). We can notice that the design load is the maximum of the $y_{max}(k)$ values, functions of *k*, obtained at the end of each iterative step. With system dynamics it is intended the series between aircraft dynamics and gust filter. The computational effort is the same as the linear MF analysis multiplied by the number of steps needed to reach the maximum[1].

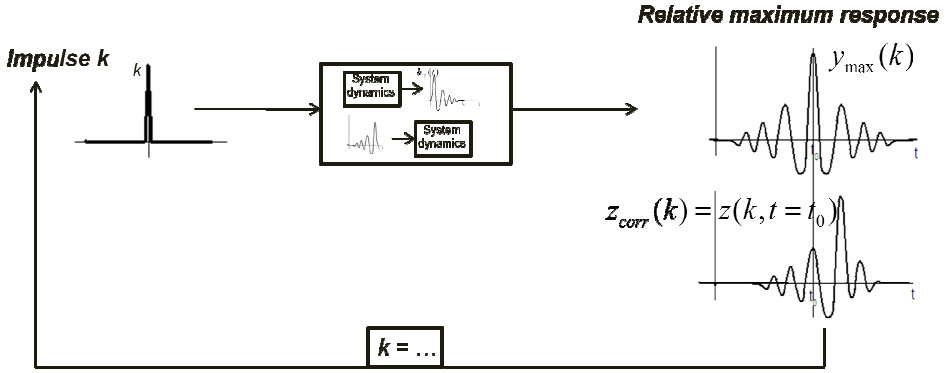

Figure 2.4. Matched Filter with one dimensional search procedure for nonlinear systems.

[1] Note that there isn't a mathematical justification in the maximum reached, it can both be a relative or an absolute one.

2.2 Spectral Gust (SG)

The SG method is a direct translation in time domain of the *JAR* random gust load calculation criterion, which is based on frequency defined PSD concept. The SG seems to be very interesting because it needs only one step to derive all the design values of interest. Moreover it's consistent with Design Envelope Analysis and provides time-correlated loads. The mathematical bases of the SG method are now described, for an extended treatment see ref. [4].
The RMS definition of design load per unit gust intensity, given by *EASA CS-25, AMC 25.341 (b)* is:

$$y_{design} = U_\sigma \overline{A} \tag{2.14}$$

$$\overline{A} = \frac{RMS_y}{RMS_g} = RMS_y = \left(\int_0^{+\infty} \phi_y(\omega) d\omega \right)^{1/2} = \left(\int_0^{+\infty} \left| H(\omega) \right|^2 \phi_{VK} d\omega \right)^{1/2} =$$

$$= \left(\int_0^{+\infty} \left| H_y(\omega) G(\omega) \right|^2 d\omega \right)^{1/2} = \left\| H_y G \right\|_\omega \tag{2.15}$$

Where $\Phi_{VK}(\omega)$ is the *von Kármán* spectrum, $H_y(\omega)$ is the aircraft dynamics frequency transfer function, $G(\omega)$ the gust filter transfer function (see equation (2.10)). The symbol $\|.\|_\omega$ denotes an energy norm defined in frequency domain. Through the *Parseval's* theorem we get:

$$\left\| H_y G \right\|_\omega = \left(\int_0^{+\infty} \overline{H_y G} H_y G d\omega \right)^{1/2} = \left(\pi \int_{-\infty}^{+\infty} \left| h_y * g \right|^2 dt \right)^{1/2} = \sqrt{\pi} \left\| h_y * g \right\|_t \tag{2.16}$$

Where $\|.\|_t$ denotes the energy norm in time domain, $\overline{(.)}$ is the conjugation operation and $(a * b)$ indicates the convolution between *a* and *b*. Thus the design gust load can be defined as:

$$y_{design} = U_\sigma \sqrt{\pi} \left\| h_y * g \right\|_t = \left\| h_y * (U_\sigma \sqrt{\pi} g) \right\|_t \tag{2.17}$$

The second term of the convolution is referred to as *Spectral gust* (equation (2.18)), while *g(t)* is the time domain representation of the gust filter function through the Laplace inverse transform operation L^{-1}. Since $\bar{A}$ has been defined for unit gust intensity, the RMS value of *g(t)* is unit.

$$u(t) = U_\sigma \sqrt{\pi} \cdot g(t) \tag{2.18}$$

$$g(t) = L^{-1}\left(G(s)\right) \tag{2.19}$$

So the design load calculation criterion becomes:

$$y_{design} = \left\| h_y * u(t) \right\|_t = \left\| y(t) \right\|_t \tag{2.20}$$

In conclusion the design load is the energy norm of the response *y(t)* (however it's calculated, with a linear or nonlinear model) to an input $u(t) = U_\sigma \sqrt{\pi}\, g(t)$. Time-correlated loads can be calculated through the following time definition of the crosscorrelation coefficient:

$$z_{corr} = y_{design} \rho_{zy} = y_{design} \frac{\int_0^{+\infty} y(t) z(t) dt}{\left\| y \right\|_t \left\| z \right\|_t} \tag{2.21}$$

Equation (2.20) and (2.21) represent the greatest advantage of the SG method over MF and similar methods: just one analysis is needed to calculate all design and time-correlated loads in every section of the aircraft. The drawbacks are the lack of nodal loads, since the calculation of design and time-correlated loads is based on an integral operation, and the non-unique definition of the spectral gust *u(t)*, because of the number of different von Kármán spectrum time domain representation that exist. For this work, the time domain representation of the gust filter *g(t)* will be generated as the Fourier inverse transform of the frequency response function of the filter *G(s)* to an impulsive input.

2.3 Other methods

This section reports a brief literature survey over other methods that will not be investigated in the proceedings of this work.

2.3.1 Indirect Deterministic PSD (IDPSD)

The IDPSD is a translation of the continuous PSD frequency domain criterion into a deterministic time domain procedure. The resulting method is very similar to MF theory but presents two main differences:

- the input is not an impulse but a specific waveform,
- the first system is *linearized*.

Because it's very similar to MF and according to literature (refs. [5], [6] and [7]) it produces results very similar to MF method with almost the same calculation effort, it has not been considered in this work. For a deeper development of the method see the above mentioned references.

2.3.2 Stochastic Simulation (SS)

The SS method is implemented in the same way both for linear and non linear analysis. It requires the following steps:

- Calculate load time histories $y(t)$ in response to a number of approximation of a Gaussian white noise (which is, because of the gust filter, the response of the airplane model to a Gaussian turbulence with a von Kármán PSD and a given σ_g);
- Identify load peaks near a prescribed value or within a specified range (given by another load prediction method). The highest peaks within a time span of $2t_0$ are extracted, centered on t_0 and lined up in time;
- Average the time history at each point in time, producing the final time history, on which statistical quantities will be calculated.

The same procedure has to be done on gust profiles and correlated loads, at the instants of time corresponding to the maximized load extraction, and has to be repeated for every design load. The method has proved to be reliable but it requires long simulation times (time responses of 1000 seconds order), to ensure that the input signal approximates a true random process and so that the final waveforms are as smooth as possible: moreover the counting procedures to find design levels and correlated loads usually takes a very long time. So, comparing the calculation effort required with others methods such as MF and SG, it is felt

to be unpractical for this work. For an extended treatment see references [1], [6] and [7].

2.3.3 Statistical Discrete Gust (SDG)

The SDG method is an attempt to bridge the gap between *Discrete Gust* models and *Continuous Turbulence* models representing atmospheric turbulence as a series of discrete gusts. These gusts have a deterministic shape (simple ramp, *(1-cos)* ramp, wavelets, wavelets with entropy correction factor, and many others) determined by a series of parameters like the distance between a ramp and the next one, the gust length and so on. The gusts are fed into the system dynamics and responses are calculated. An optimization procedure varies the gust parameters to reach a relative maximum in the considered response: this is the design load. It's immediately clear that the first drawback of the SDG method is that it requires an optimization procedure for every design load, with a number of parameters that grow up with the number of gusts considered. Second, the method lacks of a strong mathematical justification. Third, the different implementations, based on different gust shape definitions, could affect the results. In conclusion also the SDG method has been rejected for the use needed for this work. For a more complete explanation see reference [6].

2.4 Results comparison from literature data

To make a first evaluation of the methods before the practical implementation a wide literature survey has been carried out. The outcome of this work is a results comparison based on references [6] and [7]. No calculation has been carried out in this section: data in this paragraph refers only to simulations made by the National Aerospace Laboratory NLR (Netherlands) on three nonlinear aircraft models:

- *Noback* model: 2 degrees of freedom (DOF) large transport aircraft with load alleviation through ailerons.
- *F100* model: medium-sized transport with "Fokker-100-like" characteristics with load alleviation through ailerons.
- *A310* model: an Airbus A310 model with load alleviation through ailerons and spoilers.

For a wider description of these models see the above mentioned references. Nonlinearities are introduced by limits on the control surface deflections (non symmetrical for the *A310* model). The reported results regard either the linear or non-linear versions of these models.

2.4.1 Figures and tables

Figures from 2.5 to 2.8 show the results of the calculations for the three aircraft models and five calculation methods. Table 2.1 reports CPU times comparison based on the A310 model results. The notation is the same as used in this paper, except for as follows:

- *y,des* = design load value of load *y*;
- *nonlin* = closed loop system, nonlinear (aileron limited deflection) load alleviation;
- *nolim* = closed loop system, linear (aileron unlimited deflection) load alleviation;
- *nocon* = open loop system (linear);
- *Stoch. Simul.* = Stochastic Simulation result;
- *PSD* = standard PSD result;
- *POS* = "positive" design load case (A310 model only);
- *NEG* = "negative" design load case (A310 model only).

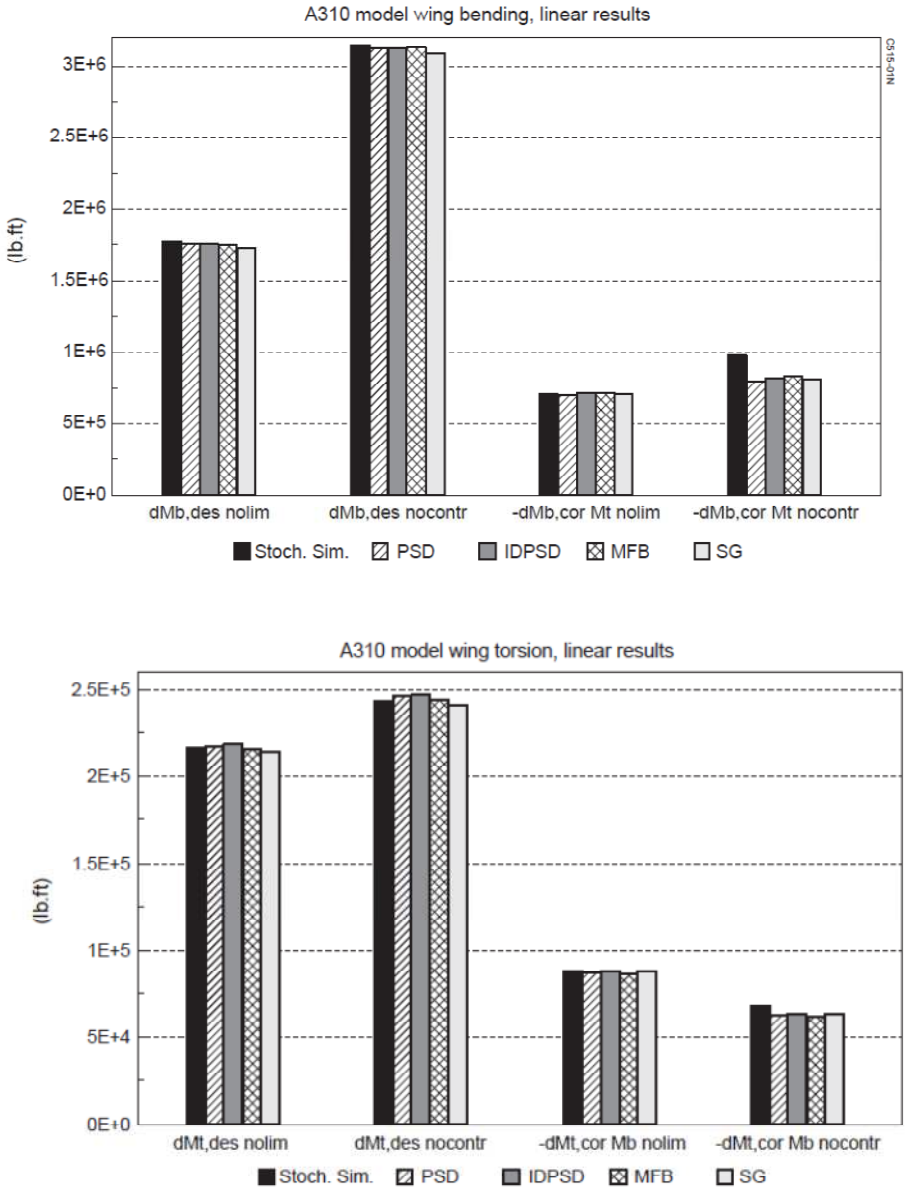

Figure 2.5. A310 linear model: Stochastic Simulation, deterministic methods and standard PSD wing bending moment and torsion comparison.

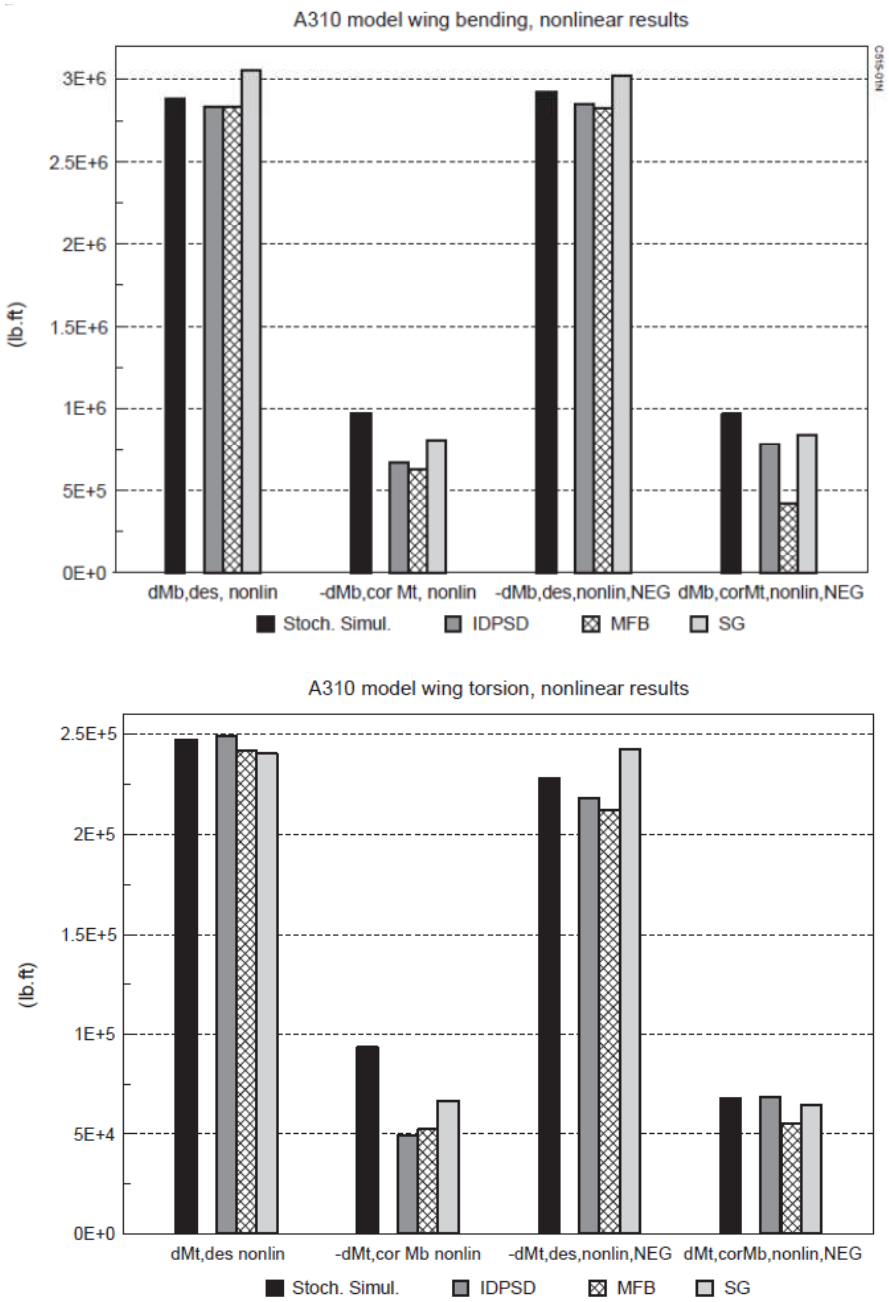

Figure 2.6. A310 nonlinear model: Stochastic Simulation and deterministic methods wing bending moment and torsion comparison.

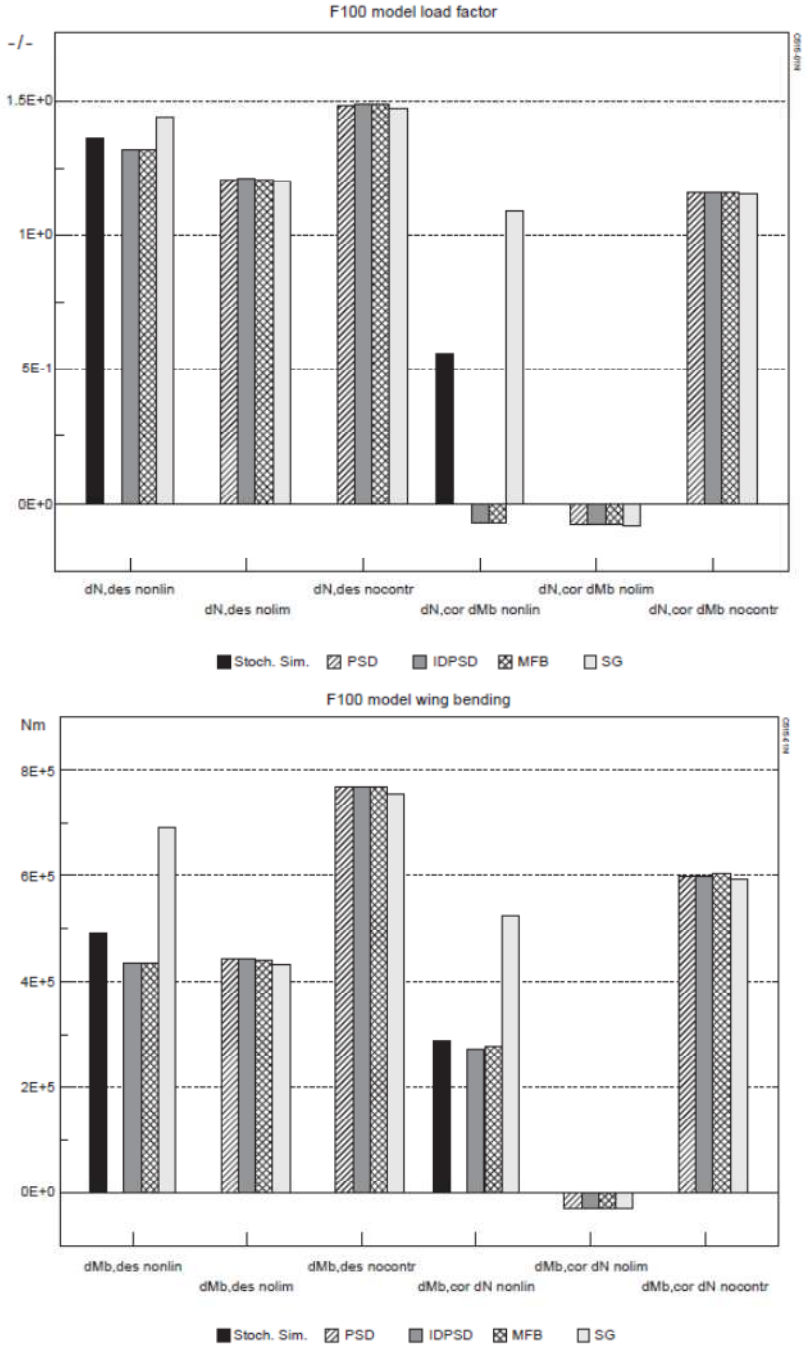

Figure 2.7. Fokker F100 linear and nonlinear models: Stochastic Simulation, deterministic methods and standard PSD load factor and wing bending moment results.

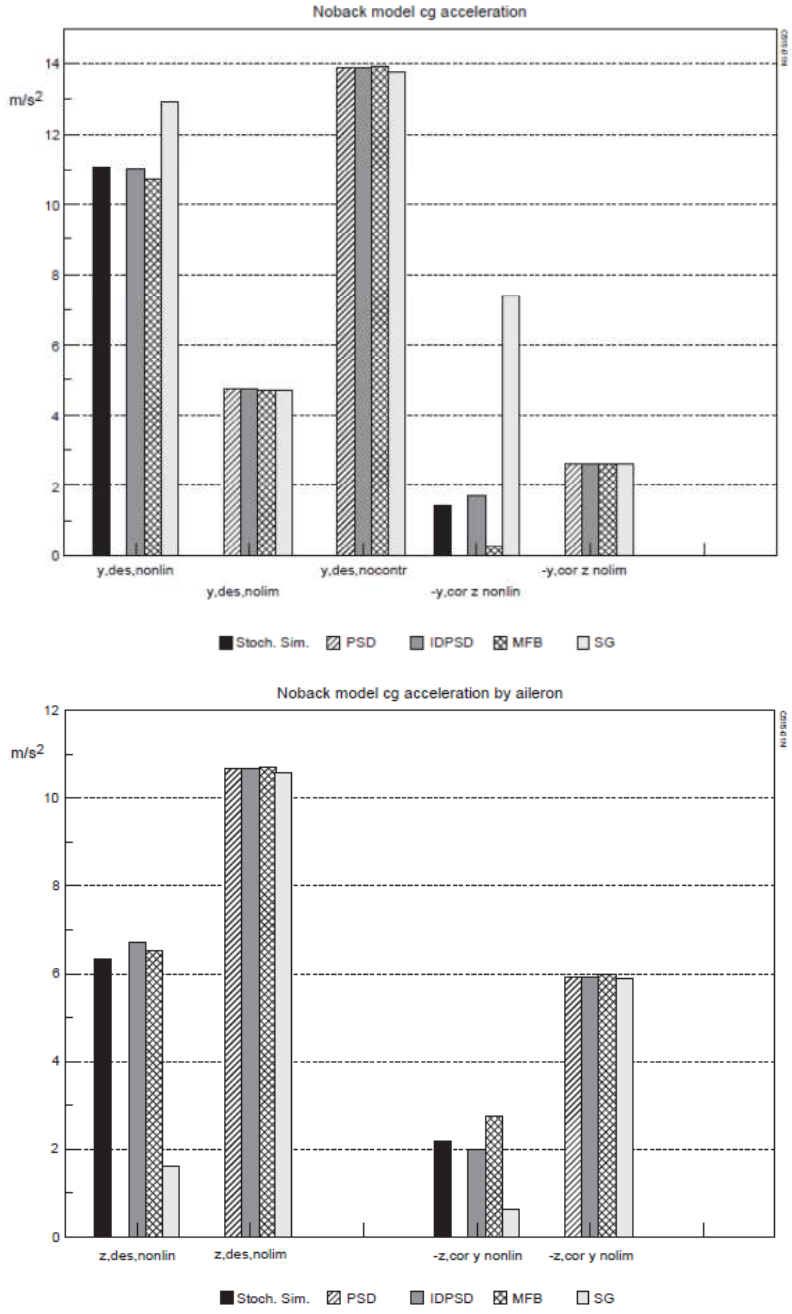

Figure 2.8. Noback linear and nonlinear models: Stochastic Simulation, deterministic methods and standard PSD load factor and wing bending moment results.

Method	Total length of responses [s]	CPU time [s]
SS	1250	1067
MF	450	76
SG	135	17
IDPSD	540	86

Table 2.1. Stochastic Simulation and deterministic method CPU times comparison.

2.4.2 Comments

The bar charts show that for the linear cases (*nolim*, *nocon*) the SS and the deterministic methods (MF, SG, IDPSD) comply with the standard PSD results both for design and time-correlated loads.

When nonlinearities are activated the results of deterministic methods begin to spread around the SS results (which are brought as reference in [6]). As mentioned above MF and IDPSD give very similar results that reasonably approach the SS: only in one case of time-correlated load calculation (load factor increment for the *F100* model) the results are really different, with an error even in the sign of the load. However there isn't a result that can be taken as an absolute reference, because of the stochastic and nonlinear nature of the problem. The SG procedure differs appreciably from the others method, both for design and time-correlated loads. Its great interest remains the time calculation savings that it permits, clearly shown in table 2.1. For this reason, nevertheless it doesn't demonstrate to be sufficiently reliable (at least in this brief literature survey), it will be taken into account in the proceedings of this work.

2.5 Statistical Method (SM)

A method for the calculation of continuous turbulence design load for nonlinear aircraft models based on *CRD NPA309* has been applied in *EADS-CASA, Airbus Military Structural Dynamic and Aeroelasticity Department, Getafe (Spain)*. For this reason it is reported in this chapter but it was not considered in the results comparison based on literature data shown above. The SM method is very interesting for the following two reasons:

- It doesn't present any kind of approximation or simplification on aircraft dynamics, nonlinearities, turbulence representation or other.
- It requires a fixed number *N* of analysis to calculate all design and time-correlated loads along the aircraft.

The idea is to represent in the time domain the frequency defined PSD criterion transforming the von Kármán PSD into a discrete gust time history, on which calculate the aircraft response. The problem is in the fact that from a PSD function only the magnitude of the original time domain signal can be calculated, not the phase angle. So, to avoid this uncertainty, a number *N* of random phase vectors are considered obtaining *N* gust time histories (equation (2.22)):

$$w_g(t) = \sum_k \sqrt{\phi_{VK}(\omega_k)\Delta\omega} \cdot \cos(\omega_k t + \psi_k) \tag{2.22}$$

Where ψ is a random phase vector.
Feeding these gusts into the aircraft dynamics we obtain *N* response time histories (for design and time-correlated loads) of which we can calculate the *Probability of Exceedance P(y)* curve, simply counting the number of times that the *i-th* time history $y_i(t)$ (the system response to the *i-th* gust w_{gi} *(t)*) is above the given level *y**. Hence the design load is calculated as the load which has the probability of exceedance level prescribed or, graphically, as the intersection between the averaged *P(y)* curve (averaged along the *N* response time histories) and the given level $P(y)_{design}$ (see section 2.5.2).

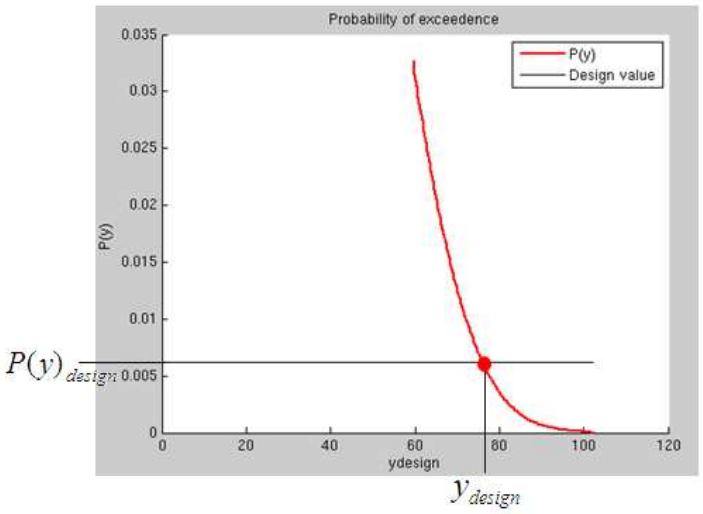

Figure 2.9. Frequency of exceedence curve and design load definition example.

Now to calculate the time-correlated loads let plot the design value of *y(t)* on the generic time history $y_i(t)$, figure 2.10. The intersections between $y_i(t)$ and the design value define the instants of time at which the response reach the design value. So for the definition of time-correlated loads we just have to take the value of the correlated $z_i(t)$ of interest at these time instants and averaged them homogeneously (equation (2.24)).

$$y_{design} = y(\overline{P(y)}) \tag{2.23}$$

$$z_{correlated} = \frac{1}{N}\sum_i \left(\frac{1}{N_{point}} \sum_j P(t_j, z_{ij}) \right) \tag{2.24}$$

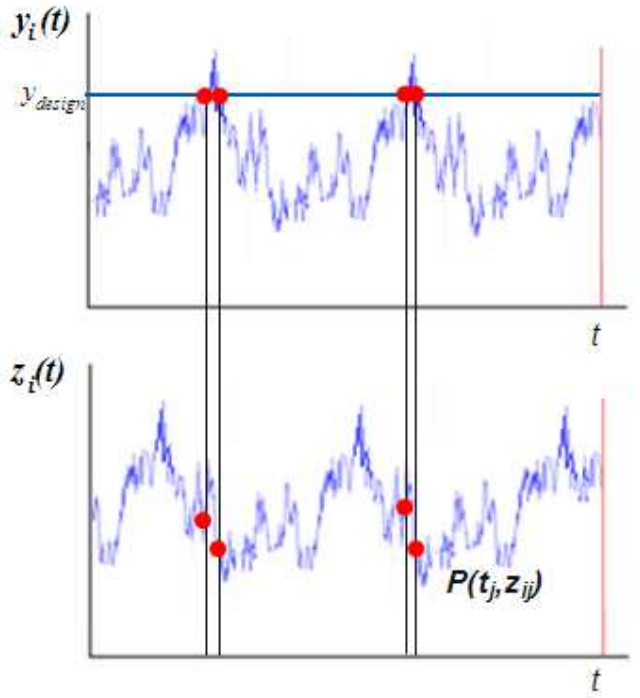

Figure 2.10. Definition of time-correlated loads.

The method starts from pure statistical considerations and doesn't require any kind of iterative procedure to find the maximum of the response. Inasmuch, the shape of the gusts required for the calculation of design and time-correlated loads does not depend on the specific output considered, with a great savings of time respect to MF and similar methods when the number of design (and time-correlated) loads that has to be calculated overcomes the number of time responses *N*. A minor drawback of the SM is that it doesn't provide *nodal loads*.

2.5.1 Gust time histories generation

The development of the gust time histories generation procedure is carried out by an in-house code of AI-Military widely describe in reference [11], hence only the most important conclusions of this work are here reported.
Gust time histories can be generated through equation (2.22) or directly from von Kármán PSD using numerical IFFT:

$$w_g(t) = IFFT(W_g(i\omega)) \tag{2.25}$$

$$W_g(i\omega) = \left|W_g(i\omega)\right| \cdot \exp\left(i\psi(\omega)\right) \tag{2.26}$$

Where ψ is still a random phase vector.
The resulting time history and the quality of the von Kármán spectrum approximation of the re-transformed time history depend on IFFT parameters, such as period T_{max} (which determines the frequency resolution *df*), sampling frequency f_{max} (which determines the time resolution *dt*) and consequently the number of samples in the signal. It was found out that the RMS error of the re-transformed time history with respect to the original von Kármán spectrum RMS is slightly dependent on the maximum frequency f_{max}, while it has a great dependence with T_{max}. So great attention must be put in the frequency resolution *df* to ensure that the IFFT generated time history has a representative RMS value (figure 2.11)

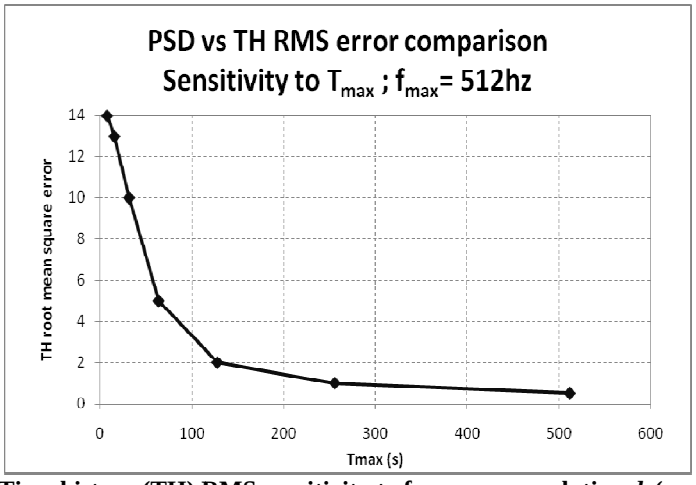

Figure 2.11. Time history (TH) RMS sensitivity to frequency resolution d_f (or period T_{max}).

After the RMS quality check a time history post processing is needed to ensure that the aircraft excitation starts in zero and with a smooth gradient, mainly to avoid numerical problems to the solver. The IFFT generated $w_g(t)$ has a random nature, so in general it is not assured that it starts with a zero amplitude. Two solutions are available: an *(1-cos)* smoothing of the initial and final step (figure 2.12), which produces a significant modification of the time history spectrum and RMS (figure 2.13), and a time shift procedure to use as starting point the first crossing by zero of the time history (figure 2.14). This procedure respects the von Kármán spectrum approximation, also if an additional smoothing is

applied (figure 2.15). For the proceedings of this work both procedures will be applied.

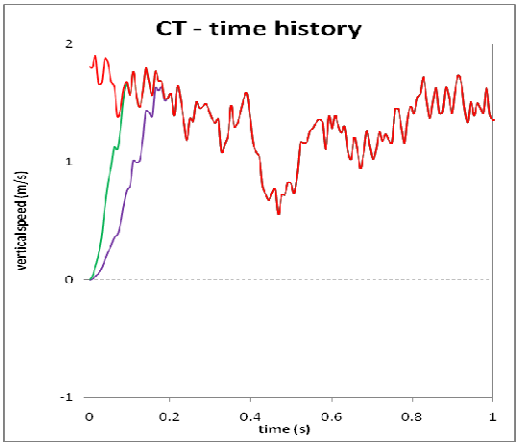

Figure 2.12. Time history smoothing to avoid step starts of the excitation (period of the smoothing function: 0.1s (green) and 0.2s (violet)).

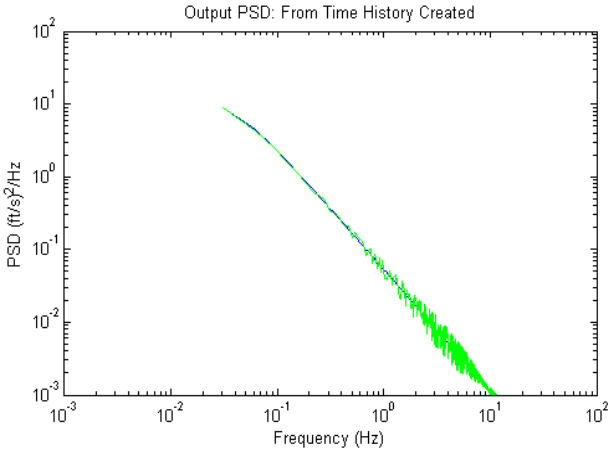

Figure 2.13. Smoothed TH (0.1s) PSD modification.

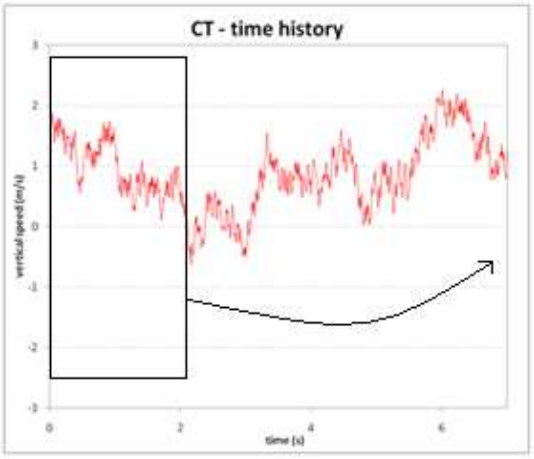

Figure 2.14. Zero shift procedure (the cut segment is then pasted at the end of the signal).

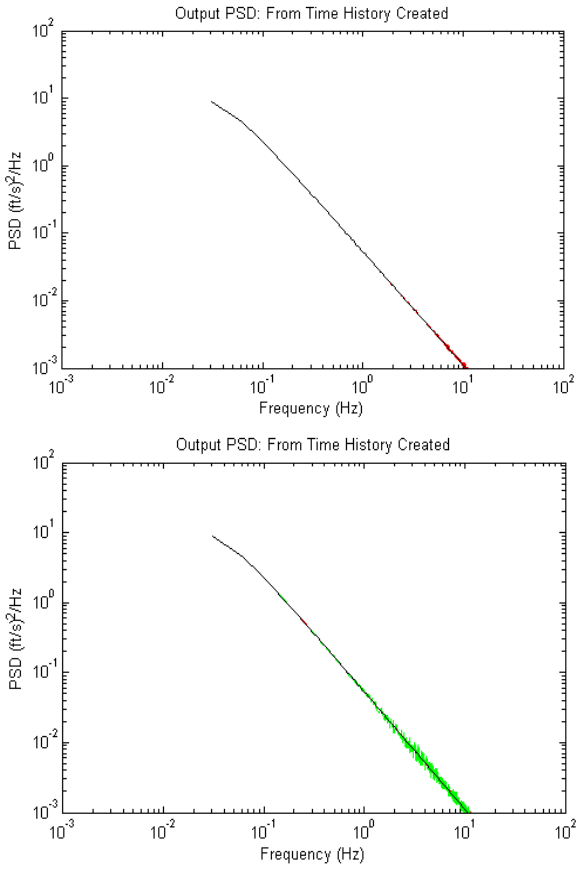

Figure 2.15. Zero shift and zero shift + smoothing (0.1s) TH PSD modification.

2.5.2 Counting procedure

For each response time history a *Probability of Exceedance P(y)* curve must be built. To build the curve a sweep of exceedance levels *y* is defined and, for each level, the number of points of the time history *y(t)* which overcome the level *y* is accounted for (figure 2.16); hence dividing for the total length of the response *y(t)* we obtain *P(y)*, that is the number of exceedances in unit time. Repeating this procedure for all the *N* time responses and averaging the curves we obtain the *averaged probability of exceedance* curve related to a pseudo-random Gaussian gust input (figure 2.17).
The design load value is found checking the intersection of the probability of exceedance curve obtained from the simulations with the design probability level defined as $\overline{P(y)} = 0.0062$ (figure 2.9). The design level $\overline{P(y)}$ derives from the regulations suggestion to perform the simulation with a turbulence intensity equal to 0.4 times the design turbulence intensity U_σ (section 1.2), from which it can be deduct that the design load is the one with a Gaussian probability of occur equal to $1/0.4\sigma = 2.5\sigma$.

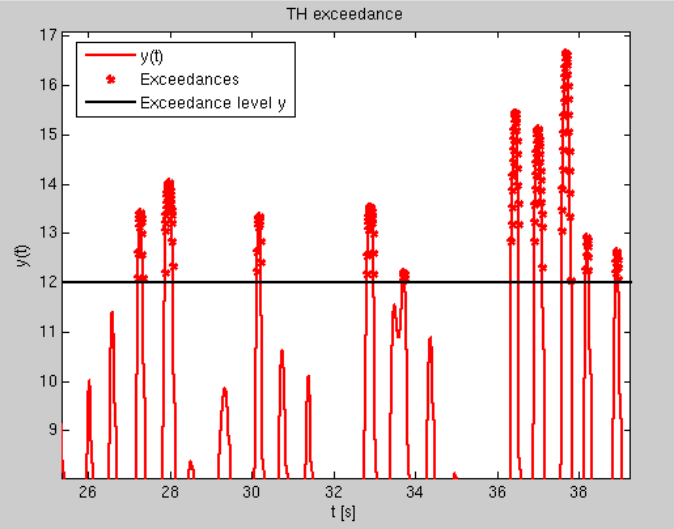

Figure 2.16. Counting procedure example.

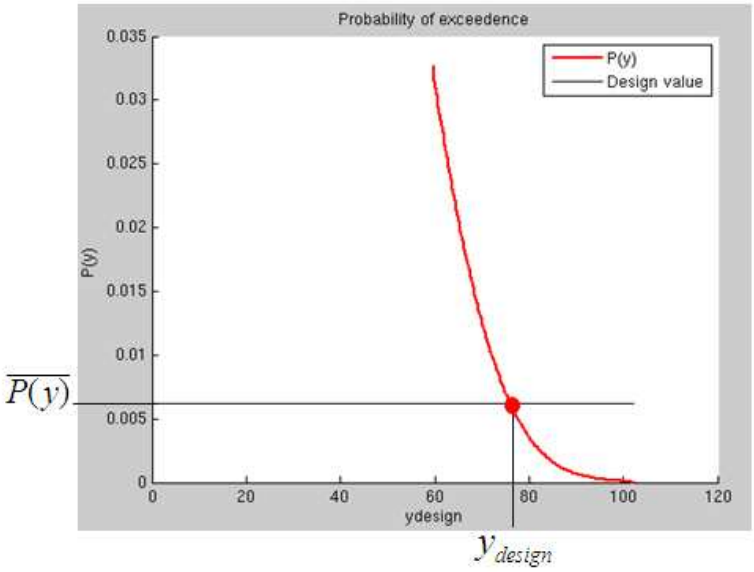

Figure 2.17. Averaged probability of exceedance curve.

Chapter 3

Application to a test system

The three selected methods (MF, SG, SM) have been implemented on a simple 2 degrees of freedom dynamic model for a first evaluation of effectiveness, reliability and performances.

3.1 Description of the test system

The system is made by two masses (m_1, m_2) and two couples of linear spring-damper elements (c_1,k_1,c_2,k_2), connected as showed in figure 3.1. The two degrees of freedom are represented by the absolut displacements of the masses, while the external forces can be applied directly to the first and/or to the second mass. The values of mass, stiffness and damping were varied during the evaluation of the characteristics of the methods. A tipical frequency response function of the system is depicted in figure 3.2.

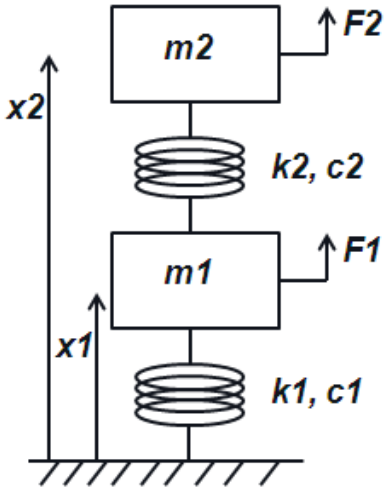

Figure 3.1. Two DOF test system description.

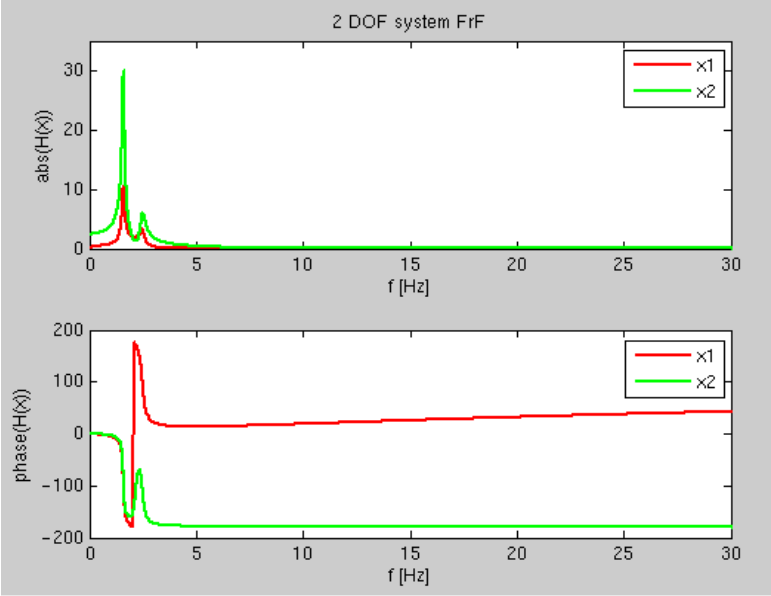

Figure 3.2. Test sytem frequency response functions.

3.1.1 Nonlinearity

For reasons of simplicity and limited calculation effort required the nonlinearity is introduced in the system "a posteriori", with a "load alleviation-like" block placed after the system dynamics, see figure 3.3. The alleviation block can act over one of the two degrees of freedom (x_1 or x_2), called "control load", when this one overcomes a user defined level refer to as cut-off value; the nonlinear block multiplies the part of the original signal which overcomes the cut-off by an alleviation factor *AF* selected by the user. The other DOF is affected by the nonlinearity in an indirect way, proportionally to the time by time ratio between the original control load and alleviated control load (figure 3.4 and equations (3.1), (3.2), (3.3)). This is only one of the possible implementations of nonlinearity blocks, but it is clear that a design load calculation method, to be referred to as solid and reliable, must work efficiently with almost any kind of nonlinearity.

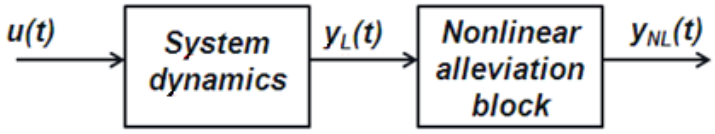

Figure 3.3. "A posteriori" nonlinearity application.

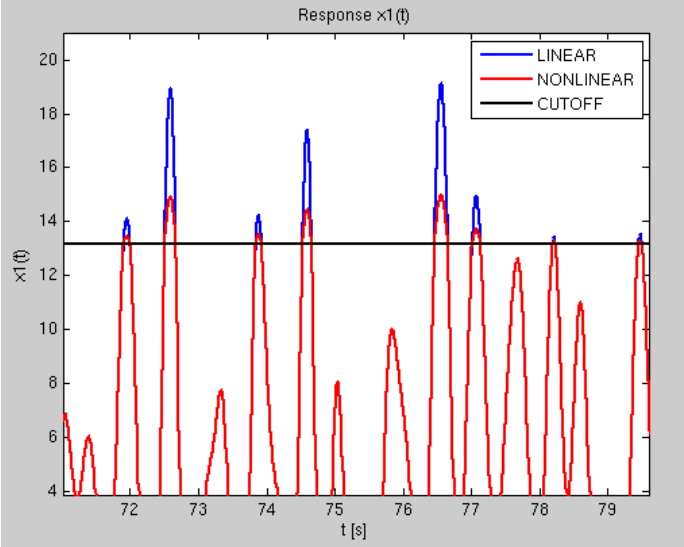

Figure 3.4. Alleviation block action over control load.

$$y_{control,all}(t_i) = y_{cutoff} + \left(y_{control}(t_i) - y_{cutoff}\right) \cdot AF \tag{3.1}$$

$$K_{cutoff}(i) = \frac{y_{control,all}(t_i)}{y_{control}(t_i)} \tag{3.2}$$

$$y_j(t_i) = y_j(t_i) \cdot K_{cutoff}(i),\ j \neq control \tag{3.3}$$

3.2 Input filter and Von Kármán spectrum approximations

To represent a valid test-bench for the application of the methods to the *A400M* model, the input forces F_1, F_2 have been modelled as gaussian noises with a von Kármán power density spectrum. Depending on the method considered, a von Kármán gust filter has been used to obtain the correct PSD starting from a gaussian white noise; the results in terms of design loads has proven to be quite dependent on the von Kármán spectrum approximation.
Von Kármán spectrum is defined by equation (3.4) its denominator has a rational exponent; hence it is not possible to obtain exactly the von Kármán spectrum through a rational filter defined as in equation (3.5). Two approximations available in literature have been considered in the preliminar phase of this work: the standard NASA filter and the Hoblit filter (refs. [7], [8], [9]).
The filters differ in numerator and denominator order, as shown in table 3.1. Figure 3.5 shows the power spectra comparison: it can be notice that the PSD of the impulse response of the Hoblit filter has a better approach to the von

Kármán spectrum, while the NASA filter represent a good approximation only for frequencies up to 2-3 Hz (or for reduce frequencies $L\omega/V$ up to 20, where L is the characteristic gust length, ω the angular frequency and V the aircraft speed, see ref. [8]).

$$\phi_{vK}(\omega) = \sigma_g^2 \frac{L}{\pi V} \frac{1+\frac{8}{3}(1.339(L/V)\omega)^2}{\left[1+(1.339(L/V)\omega)^2\right]^{11/6}} \tag{3.4}$$

$$G(s) = \sigma_g \sqrt{\frac{L}{\pi V}} \frac{[1+a(L/V)s][1+b(L/V)s][1+c(L/V)s]}{[1+A(L/V)s][1+B(L/V)s][1+C(L/V)s][1+D(L/V)s]} \tag{3.5}$$

Filter	a	b	c	A	B	C	D
NASA	2.618	0.1298	0	2.083	0.823	0.0898	0
Hoblit	2.187	0.1833	0.021	1.339	1.118	0.1277	0.0146

Table 3.1. Gust filters parameters.

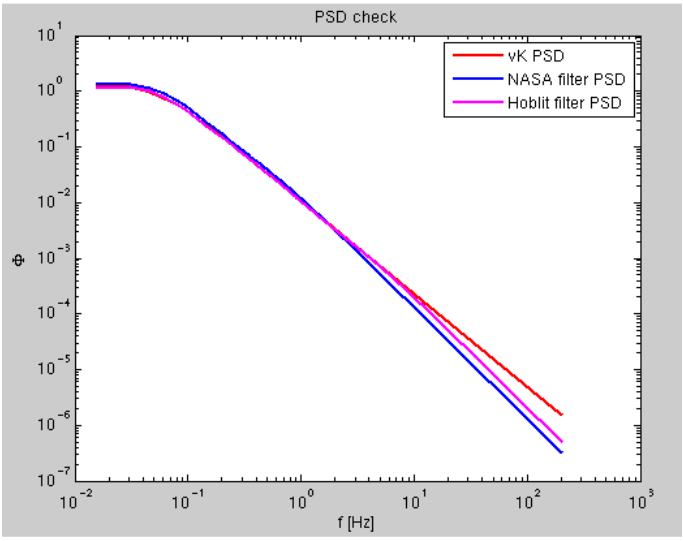

Figure 3.5. Von Kármán vs. gust filter PSD comparison (unit gust intensity).

A results comparison based on the linear model (whose design loads can be calculated without spectra approximations through linear PSD theory as reference) is provided in section 3.4.3. As a result of this comparison the Hoblit filter has been chosen for the methods that require a gust filter to generate the critical gust waveform, such as MF and SG.

3.3 Intermediate results overview and discussion

This section reports figures and comments about the intermediate steps of MF, SG and SM, useful to validate and comprehend the functioning of the three methods taken into account.

3.3.1 Matched Filter

The operation flow of the MF method is as follows in figures from 3.6 to 3.12. The method consists in generating the impulse response functions of the system through an impulsive excitation (iteratively scaled by a factor *k* for the nonlinear model). The impulse responses are then reversed in time, shifted, scaled by their own root mean square value and fed again into the system dynamics to obtain the matched response (every load has its independent matched excitation) and time-correlated loads. It is important to notice that with "system dynamics" we mean the series of the dynamics of the 2 DOF system (named *H*) with the gust filter (named *G*).

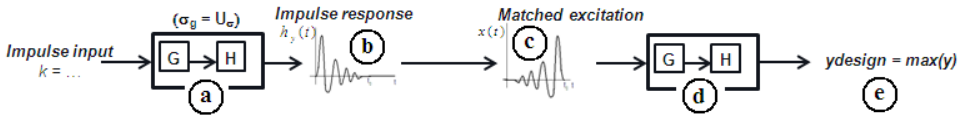

Figure 3.6. Matched Filter operation flowchart.

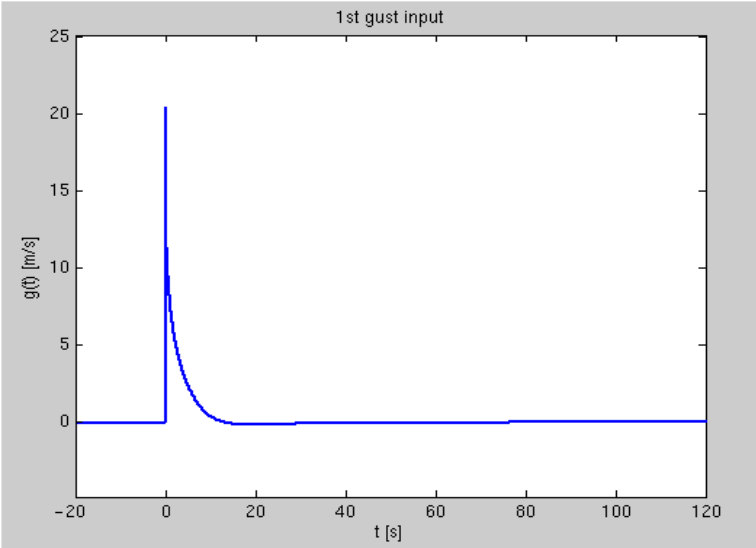

Figure 3.7. MF a) First gust input to aircraft dynamics.

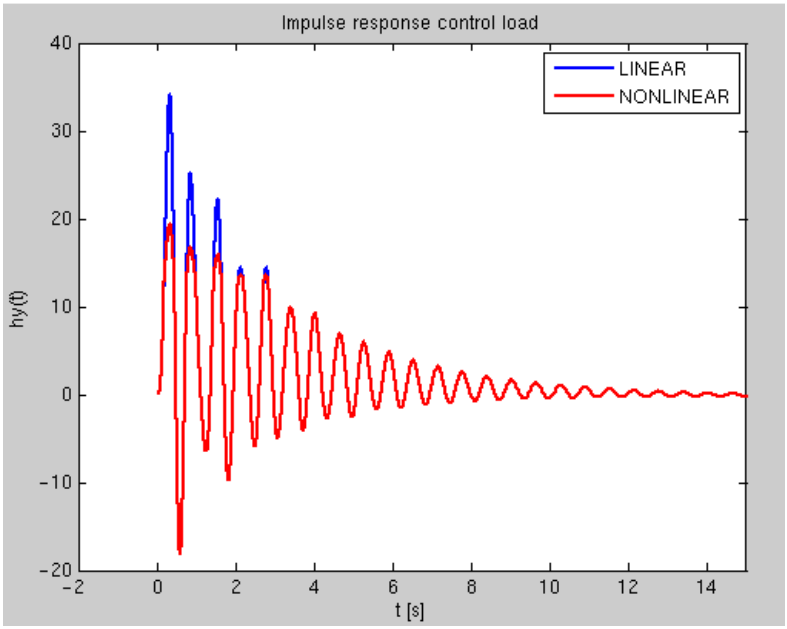

Figure 3.8. MF b) Control load impulse response, linear (alleviation nonlinearity off) and nonlinear model (*k*=2).

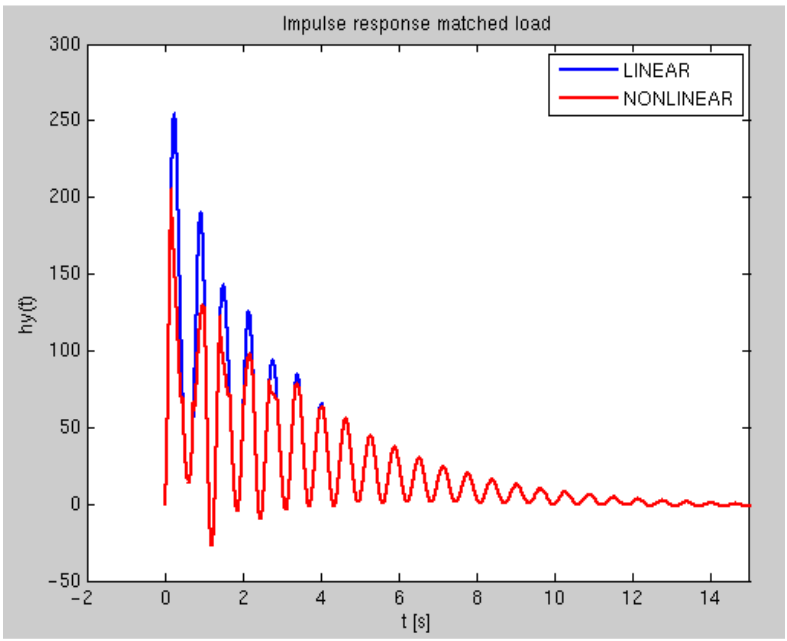

Figure 3.9. MF b) Matched load impulse response, linear (alleviation nonlinearity off) and nonlinear model (*k*=2). In this example the control load is different from the matched load.

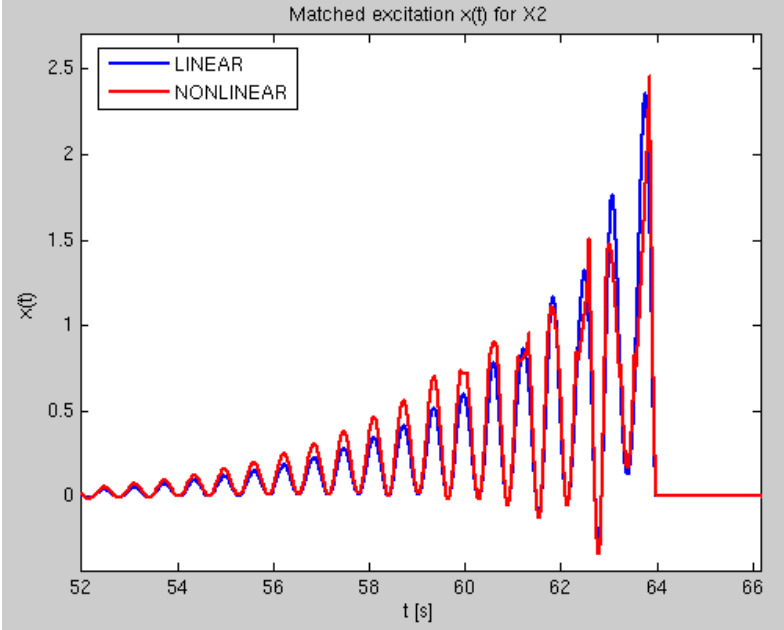

Figure 3.10. MF c) Matched excitation, linear (alleviation nonlinearity off) and nonlinear model (*k*=2).

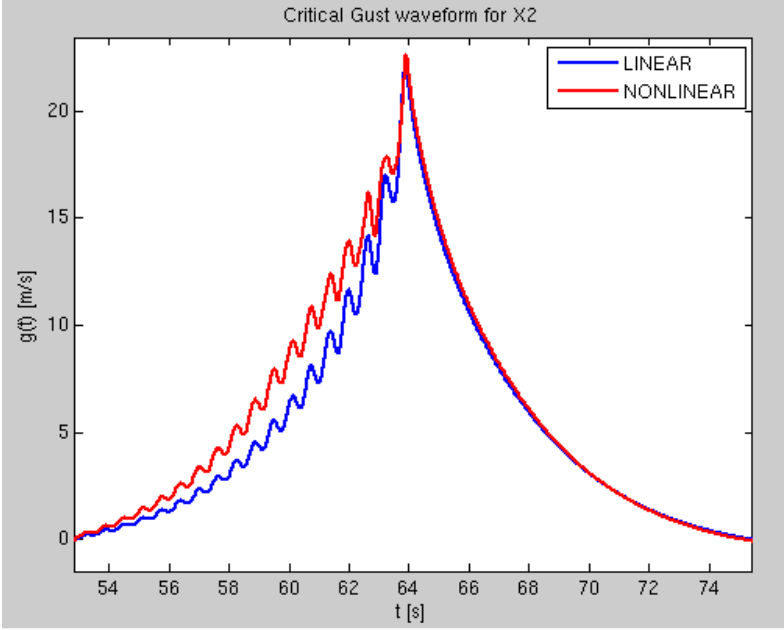

Figure 3.11. MF d) Critical gust waveform (originated from the matched excitation fed through the gust filter), linear (alleviation nonlinearity off) and nonlinear model (*k*=2).

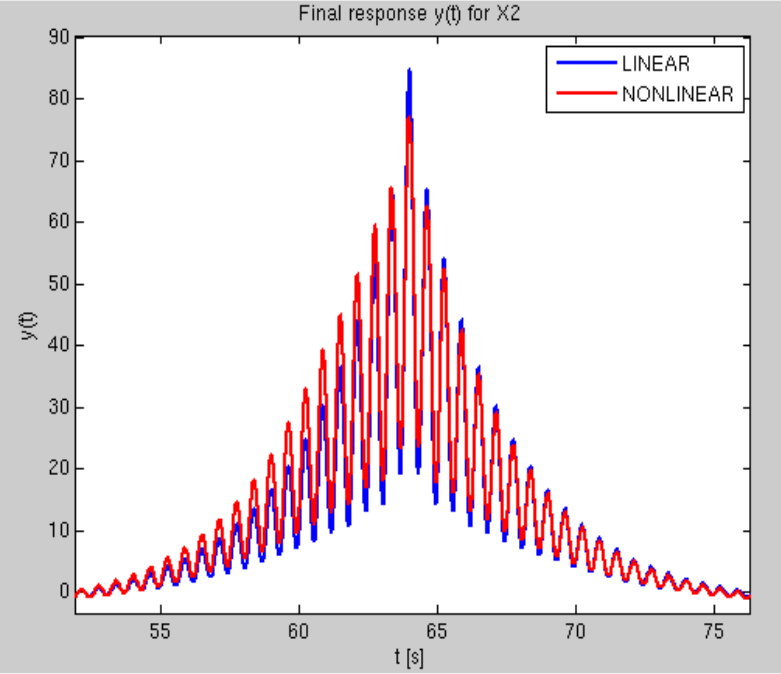

Figure 3.12. MF e) Final matched response (the maximum reached represents the design load), linear (alleviation nonlinearity off) and nonlinear model (*k*=2).

3.3.2 Spectral Gust

The SG method consists in exciting the system with the so called spectral excitation that is a waveform generated from the time domain transformation of the gust filter: so in this case the system dynamics refers only to the aircraft dynamics, as specified in figure 3.13, the filter is only used to generate the spectral gust. Design and time-correlated loads are then calculated as a norm of the final response and by means of a time defined correlation coefficient.

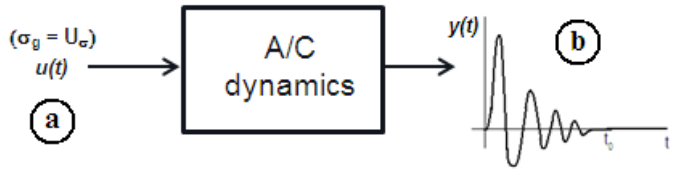

Figure 3.13. Spectral Gust operation flowchart.

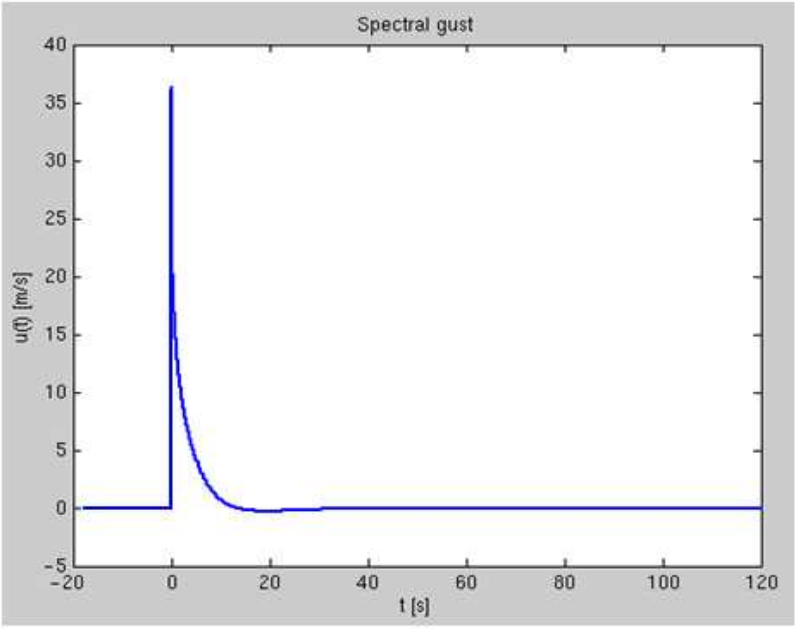

Figure 3.14. SG a) Spectral Gust u(t), input to aircraft dynamics.

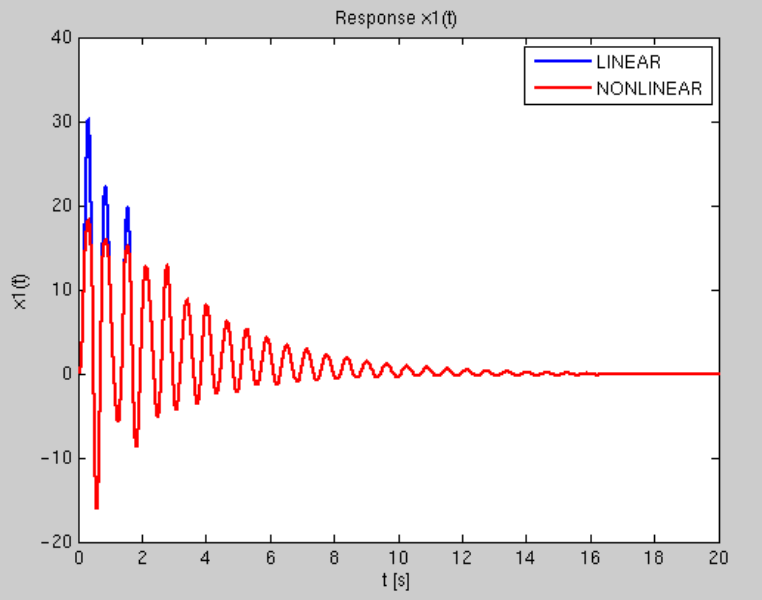

Figure 3.15. SG b) Control load final response, linear (alleviation nonlinearity off) and nonlinear model.

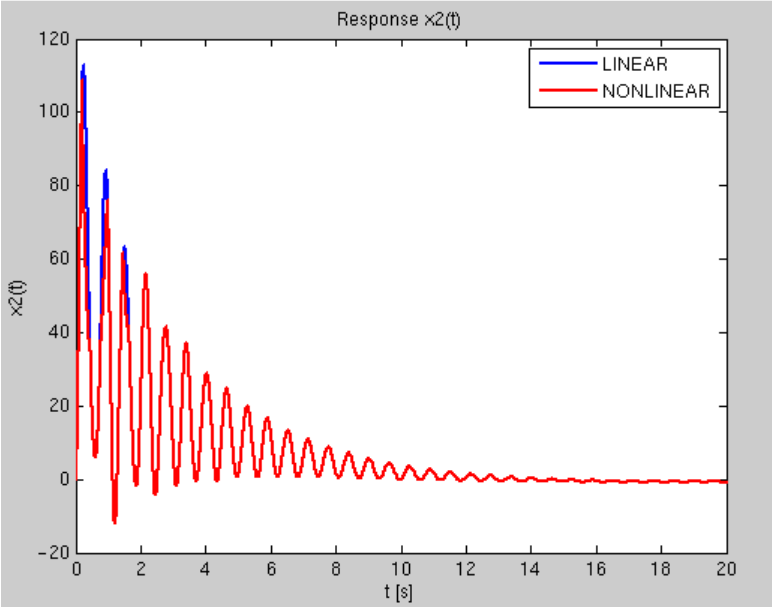

Figure 3.16. SG b) Final response of the 2nd load (in this example affected indirectly from the nonlinearity), linear (alleviation nonlinearity off) and nonlinear model.

3.3.3 Statistical Method

The SM, as the SG, only consists in time responses calculation and post processing of them. The input signal is generated as described in section 2.5.1 and again the system dynamics refer only to the aircraft dynamics. Figures from 3.17 to 3.20 reports the waveforms obtained.

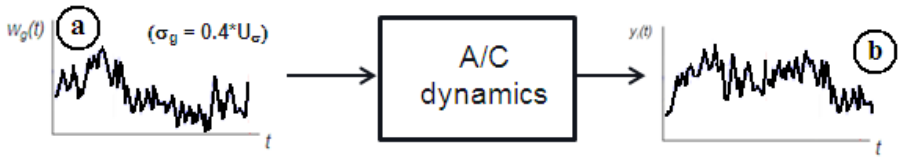

Figure 3.17. Statistical Method operation flowchart.

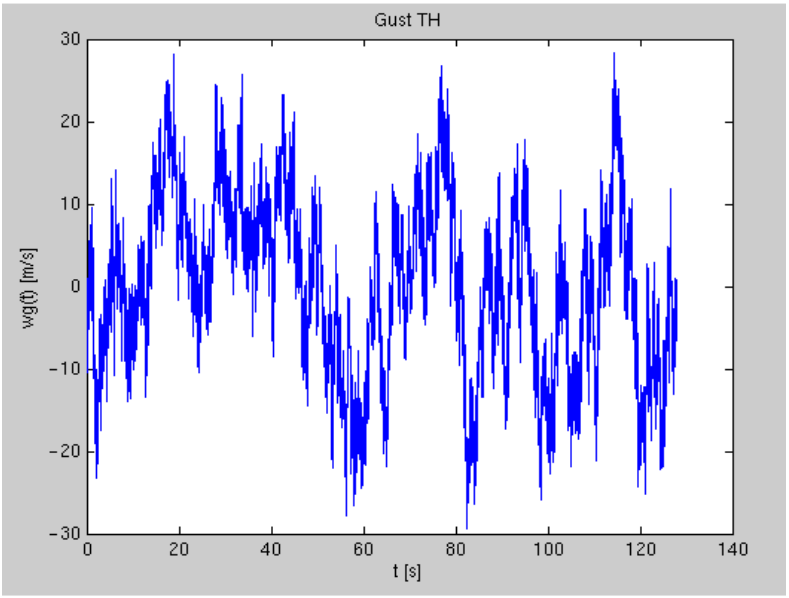

Figure 3.18. SM a) Patch of random Gaussian turbulence, generated from von Kármán power density spectrum.

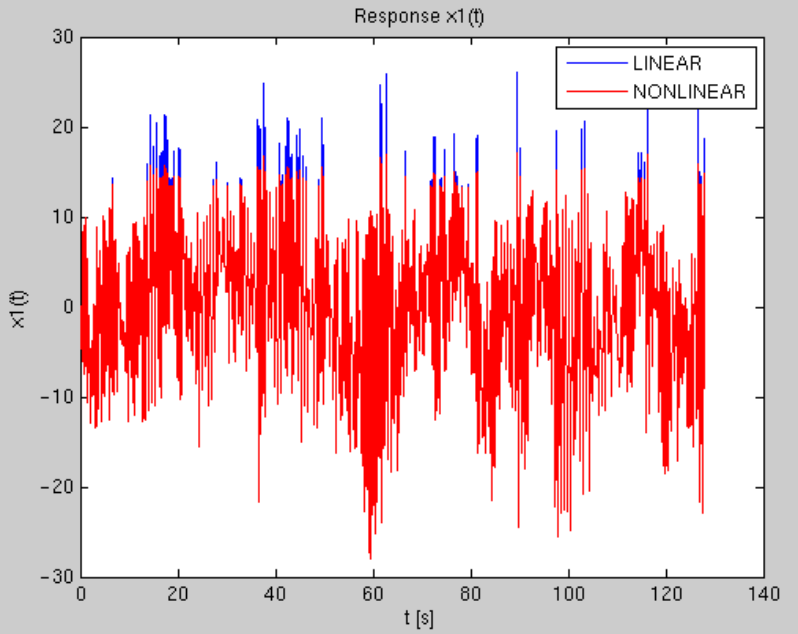

Figure 3.19. SM b) Control load final response, linear (alleviation nonlinearity off) and nonlinear model.

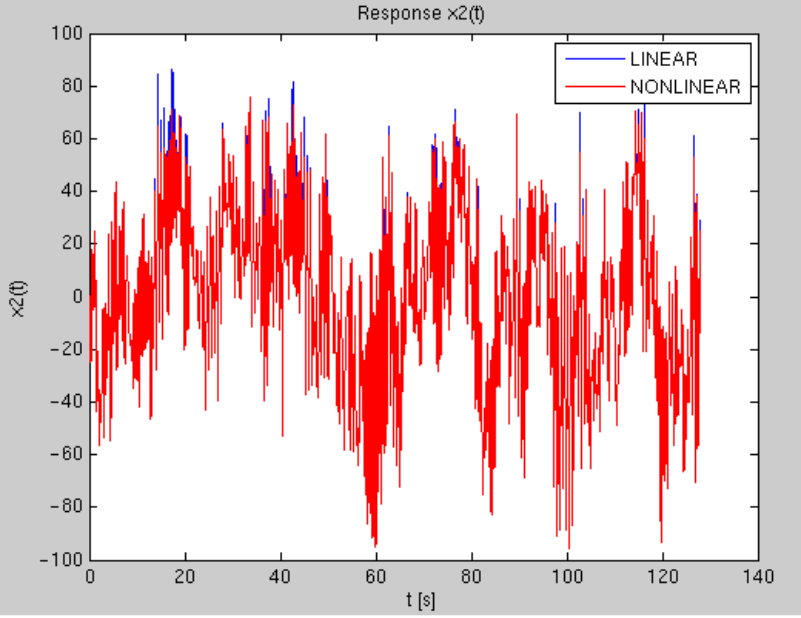

Figure 3.20. SM b) Final response of the 2nd load (in this example affected indirectly from the nonlinearity), linear (alleviation nonlinearity off) and nonlinear model.

3.4 Results comparison

3.4.1 Linear model

With the term "linear model" we refer to the 2 DOF model above mentioned without the nonlinear alleviation block. The design load calculation has been performed with the three methods selected using as reference the standard linear PSD formulae (see section 1.1). The results are reported in tables from 3.2 to 3.5 and graphically in figures 3.21, 3.22.

DOF	PSD	MF	SG	SM
X_1	21.98	21.77	21.78	21.61
X_2	85.05	84.78	84.80	83.37

Table 3.2. Linear results comparison, design loads.

DOF	PSD	MF	SG	SM
X_1 correlated	19.40	18.88	18.89	18.75
X_2 correlated	75.06	73.50	73.53	72.65

Table 3.3. Linear results comparison, correlated loads.

DOF	PSD	MF	SG	SM
X_1 % error	-	-0.95	-0.89	-1.67
X_2 % error	-	-0.33	-0.30	-1.99

Table 3.4. Linear results comparison, design loads percentual error with respect to linear PSD.

DOF	PSD	MF	SG	SM
X_1 correlated % error	-	-2.68	-2.63	-3.35
X_2 correlated % error	-	-2.08	-2.04	-3.21

Table 3.5. Linear results comparison, correlated loads percentual error with respect to linear PSD.

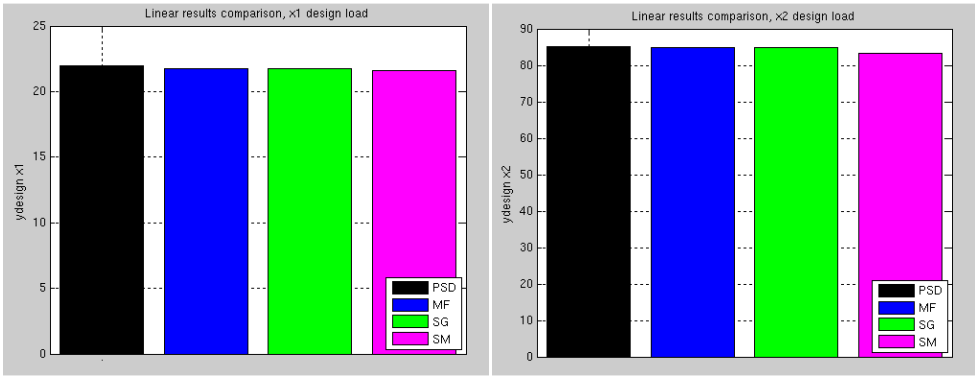

Figure 3.21. Linear results comparison, x_1 (left) and x_2 (right) design loads.

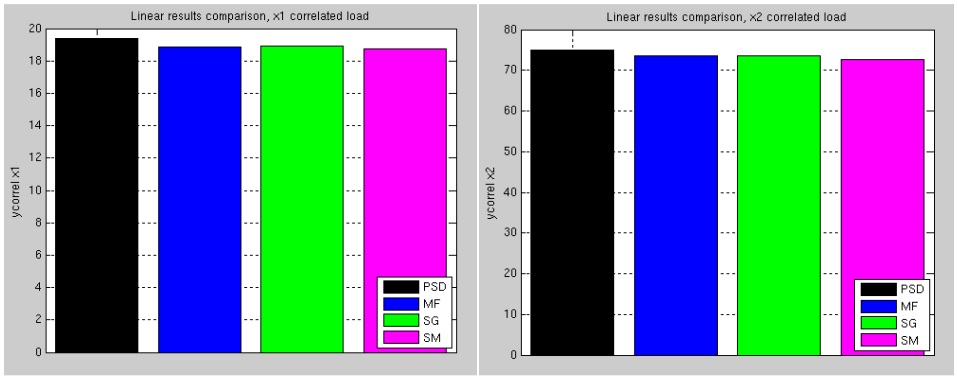

Figure 3.22. Linear results comparison, x_1 correlated to x_2 (left) and x_2 correlated to x_1 (right).

The three methods approach very well the linear PSD design and time correlated loads. The maximum error is encountered for the SM about the 3% around the reference value: this suggests a possible improvement of the counting procedure which will be carried out in the next *A400M* model implementation.

3.4.2 Nonlinear model

The results obtained for the nonlinear model are reported in tables 3.6, 3.7 and in the subsequent figures in terms of design loads versus cut-off value. For a cut-off greater than the control load linear design value (*% cutoff >100*) the results shall be equal to those obtained for the linear model.

MF procedure and SM show a reasonable behavior: they "feel" the load alleviation nonlinearity and give the correct design load when the nonlinearity is shut down, that is when the cutoff value lays over the linear PSD design load Figure 3.27 shows a typical variation of the results for the MF method in terms of design load versus the initial impulse strength sweep. The SG method shows a completely different trend that doesn't seem to be reasonable, because design and time correlated loads continue to grow up still in the linear field (figures from 3.23 to 3.26, *cutoff>1*).

% cutoff (X_1)	X_1 MF	X_1 SG	X_1 SM	X_2 MF correl.	X_2 SG correl.	X_2 SM correl.
60	15.76	18.60	15.71	53.22	62.86	52.78
100	21.77	21.26	21.68	73.50	72.02	72.89
140	21.77	21.78	21.61	73.50	73.53	72.65

Table 3.6. Nonlinear results comparison for different cut-off levels (cut-off on x_1), design load DOF x_1, correlated load DOF x_2.

% cutoff (X_1)	X_2 MF	X_2 SG	X_2 SM	X_1 MF correl.	X_1 SG correl.	X_1 SM correl.
60	70.13	75.17	70.39	13.90	15.56	12.69
100	84.78	83.45	82.37	18.88	18.34	18.00
140	84.78	84.80	82.37	18.88	18.89	18.60

Table 3.7. Nonlinear results comparison for different cut-off levels (cut-off on x_1), design load DOF x_2, correlated load DOF x_1.

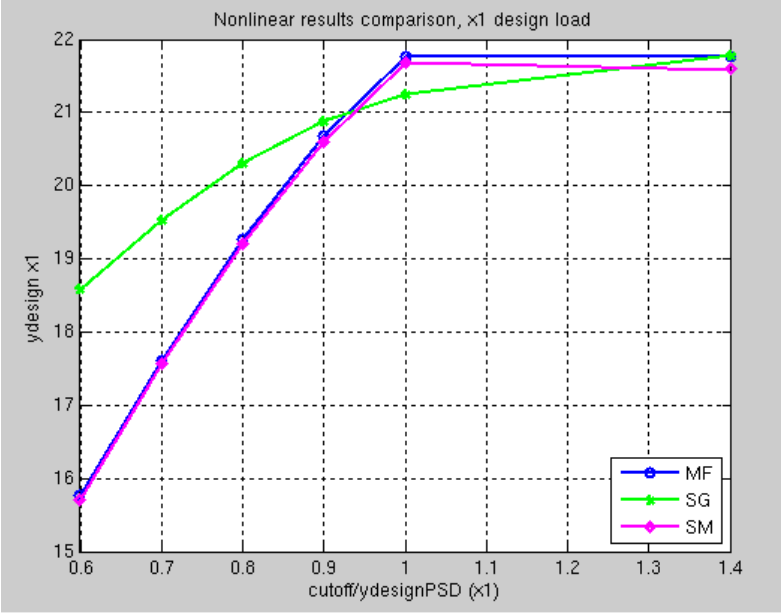

Figure 3.23. Nonlinear results comparison for different cut-off levels (cut-off on x_1), design load DOF x_1.

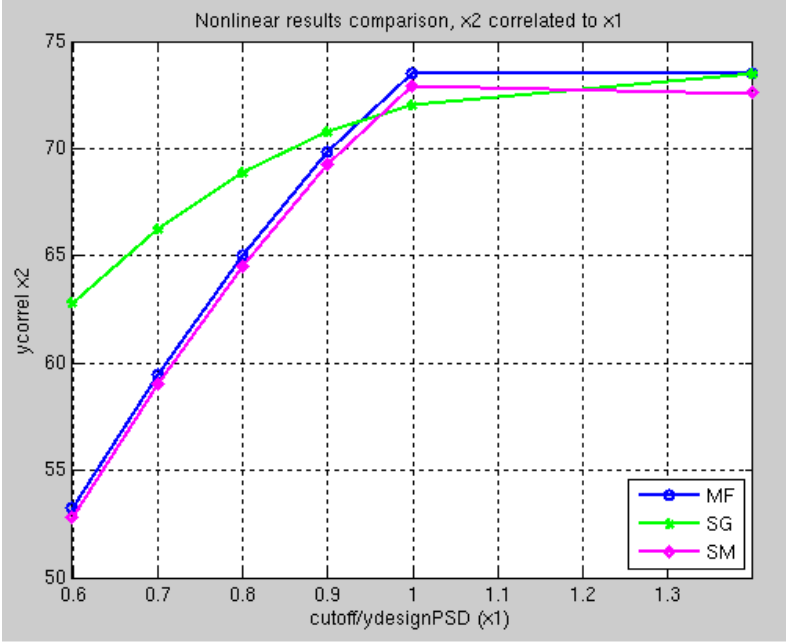

Figure 3.24. Nonlinear results comparison for different cut-off levels (cut-off on x_1), DOF x_2 correlated to x_1.

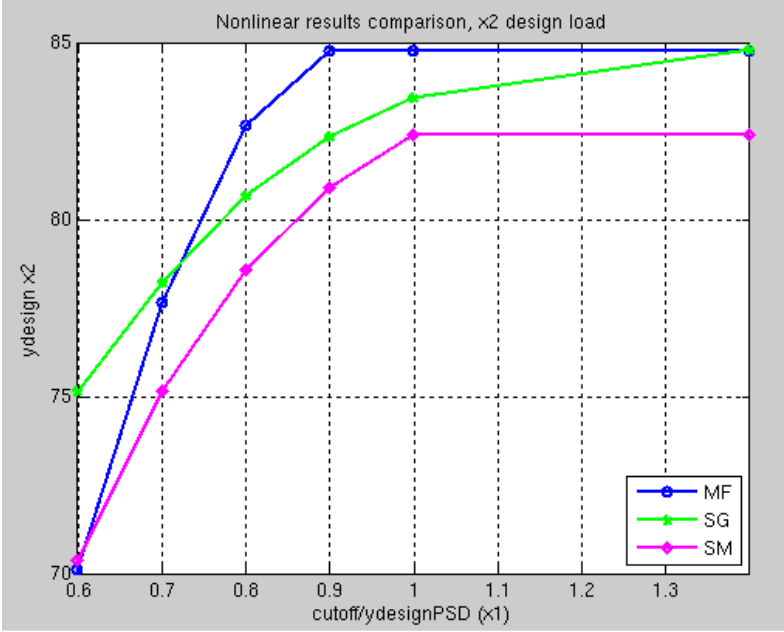

Figure 3.25. Nonlinear results comparison for different cut-off levels (cut-off on x_1), design load DOF x_2.

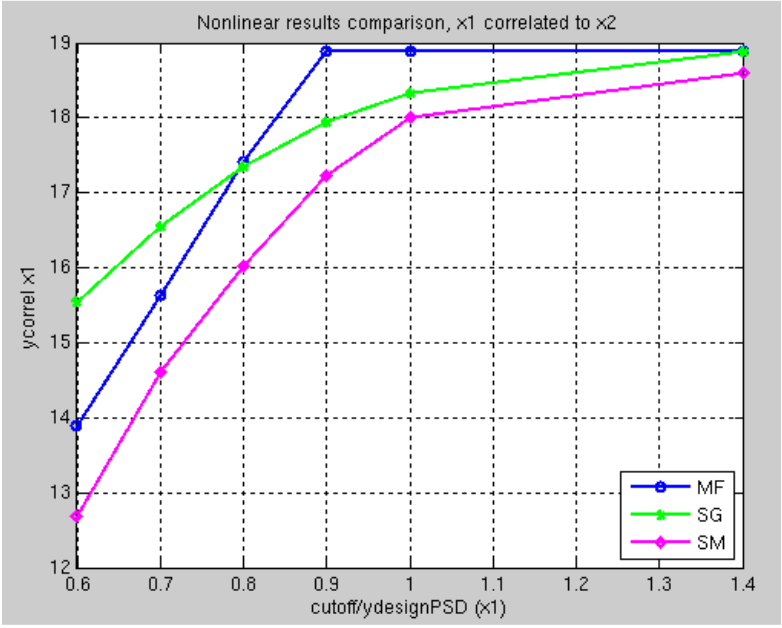

Figure 3.26. Nonlinear results comparison for different cut-off levels (cut-off on x_1), DOF x_1 correlated to x_2.

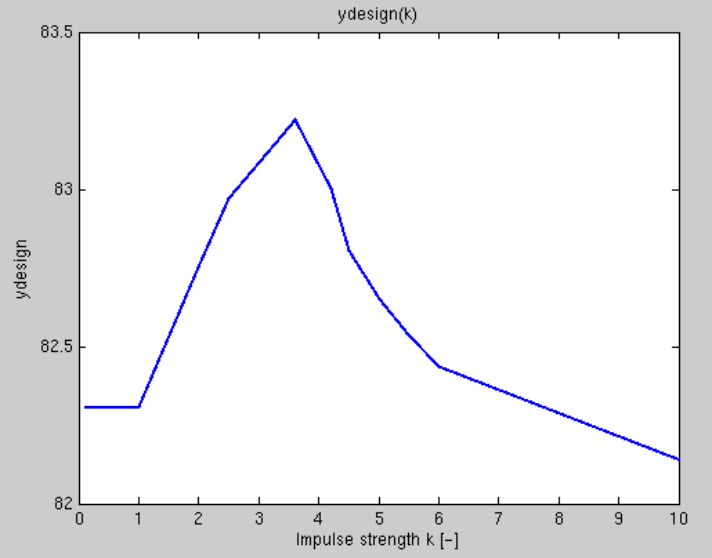

Figure 3.27. Nonlinear model, typical design load variation with initial impulse strength sweep (MF).

3.4.3 Nonlinear model calculation times

CPU times for the nonlinear analysis performed are reported in table 3.8. It can be seen that the SG is by far the cheapest method, because it requires only one response analysis to calculate all the design and time correlated loads of interest. SM time is quite bigger than the other methods because it requires a fixed number (*N=60*) of response analysis independently on the number of design stations: in this case only two combinations of design – time correlated loads have to be calculated. This is a disadvantage but for bigger models with several design station this fact could permit a big time saving, with only a little increment for loads recovery and post processing times (while for example MF method requires a number of complete analysis proportional to the number of design stations). Finally MF number of responses *NR* and CPU time is depicted with a star symbol *(*)* because it depends by case duration of the one dimensional search procedure: the reported results are for a typical number *k=15* of iterations.

Method	Length of responses [s]	Number of responses	CPU time [s]
MF	90	*NR**	24.6 *(*)*
SG	40	1	1.6
SM	128	60	41.6

Table 3.8. Nonlinear model design and time correlated loads calculation, CPU times.

3.4.4 Filter influence over results

As said before (see section 3.2) two von Kármán spectrum approximations have been tested. A results comparison based on the linear 2 DOF model is here presented, with linear PSD loads used as reference. The results are displayed only for MF and SG methods because the SM doesn't require a gust filter to generate the gust waveforms. As a result of this data comparison the Hoblit gust filter has been chosen.

Filter	DOF	PSD	MF	SG
NASA	X_1 % error	-	-2.65	-6.91
	X_2 % error	-	-6.95	-2.63
Hoblit	X_1 % error	-	-0.95	-0.89
	X_2 % error	-	-0.33	-0.30

Table 3.9. Gust filter influence over results, linear model design loads.

Filter	DOF	PSD	MF	SG
NASA	X_1 correlated % error	-	-7.23	-7.19
	X_2 correlated % error	-	-2.94	-2.92
Hoblit	X_1 correlated % error	-	-2.68	-2.63
	X_2 correlated % error	-	-2.08	-2.04

Table 3.10. Gust filter influence over results, linear model correlated loads.

Chapter 4

Application to *A400M* dynamic model

4.1 Model description

4.1.1 Aircraft general description

The *A400M* is a versatile, state-of-the-art military transport aircraft offered as a response to the European Staff Requirement (ESR), set out by eight European NATO nations, Belgium, France, Germany, Italy (withdrawn), Portugal (withdrawn), Spain, Turkey and the United Kingdom, and was designed according to the joint air force requirements of those countries. The *A400M* has excellent tactical performance, enabling all forms of aerial delivery, low level and steep descent manoeuvres. It is capable of operating in areas with poor infrastructure and from short or unpaved runways with full ground operations autonomy. The *A400M* is designed with built-in air-to-air refuelling capability and can be configured as a tanker in less than two hours. Its speed envelope is such that it can refuel a wide range of helicopters, fighters and large transport aircraft. The aircraft can be refuelled in flight.
Figure 4.1 shows the *A400M* general arrangement in a three-view plot. Specific features are listed and illustrated here below for wing (table 4.2), Horizontal Tail Plane (table 4.3) and Vertical Tail Plane (table 4.4). For reasons of industrial confidentiality only a brief description of the aircraft modelling will be presented.

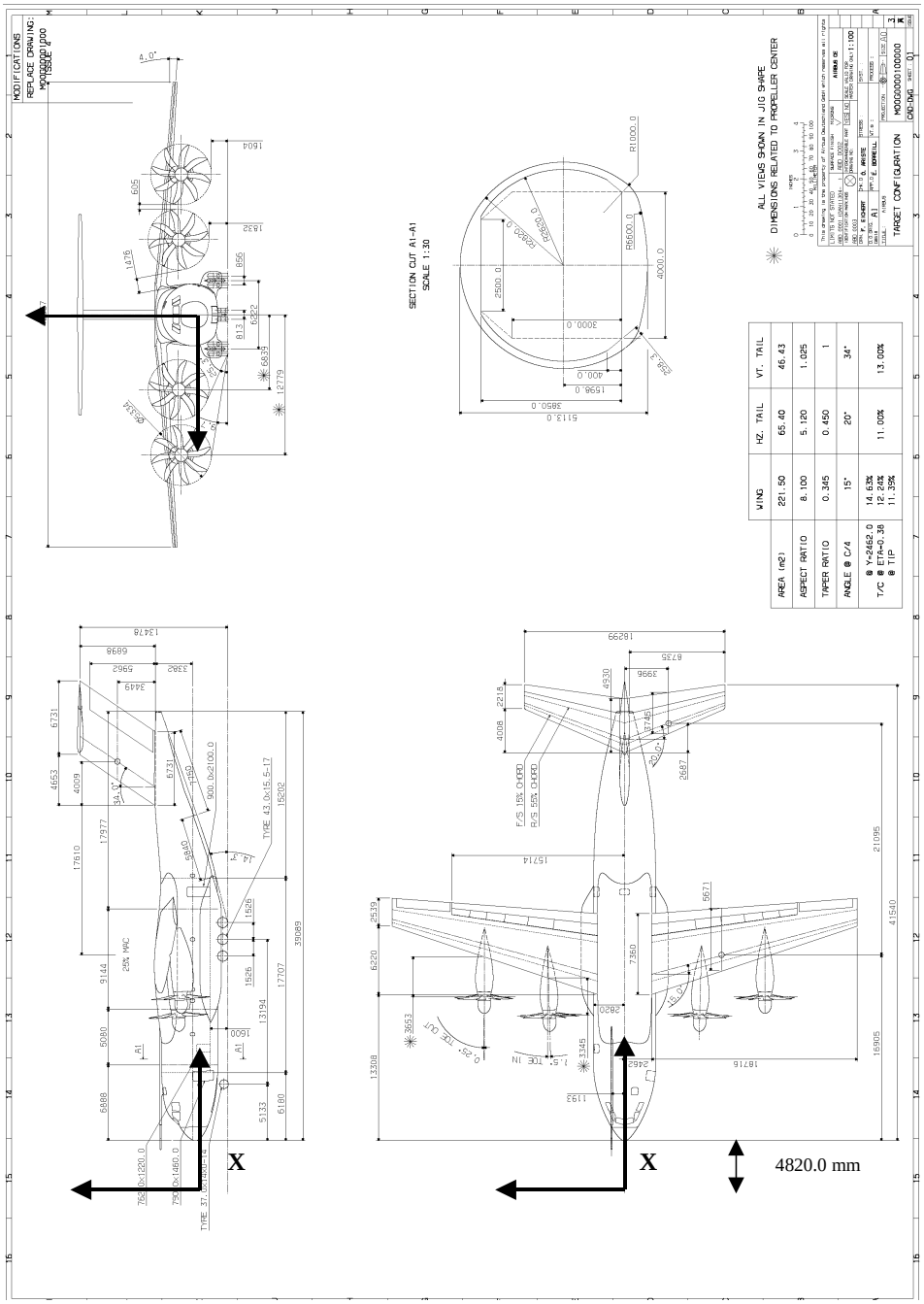

Figure 4.1. *A400M* general arrangement.

Parameter	
Overall length [m]	41.5
Wingspan [m]	42.4
Overall height [m]	14.7
Max. speed [Mach]	0.72
Max. WTO [t]	136.5
Max. WOE [t]	76.5
Max. Payload [t]	37
Max. Range [km]	8797
Number of troops/paratroops	116

Table 4.1. *A400M* general characteristics.

Parameter	Definition
Wing Reference area	S_{ref} = 221.50 m^2
Wing Mean aerodynamic chord	c = 5.671 m
Wing Span	b = 42.357 m
Wing Sweep (1/4 c)	Λ = 15 deg
Wing Anhedral	Γ = 4 deg
Aileron reference area	S_{ail} = 3.94 m^2

Table 4.2. *A400M* wing arrangement.

Parameter	Definition
HTP Reference area	S_{ref} = 67 m^2
HTP Mean aerodynamic chord	c = 3.824 m
HTP Span	b = 18.844 m
HTP Sweep (1/4 c)	Λ = 32.5 deg
HTP Anhedral	Γ = 0 deg
Elevator reference area	S_{elev} = 17.495 m^2

Table 4.3. *A400M* HTP arrangement.

Parameter	Definition
VTP Reference area	S_{ref} = 46.43 m^2
VTP Mean aerodynamic chord	c = 6.7309 m
VTP Span	b = 6.8983 m
VTP Sweep (1/4 c)	Λ = 0 deg
VTP Anhedral	Γ = 34 deg
Rudder reference area	S_{rud} = 11.59 m^2

Table 4.4. *A400M* VTP arrangement.

4.1.2 Dynamic model assembly

The FE model of the *A400M* and the main coordinate reference system are illustrated in figure 4.2. The structural components are condensed to a single collector super-element representing the stiffness of the aircraft. Stiffness matrix of this super-element are saved in a MSC.NASTRAN database file and then read as an External Super-element in the MSC.NASTRAN runs of the dynamic model.
Assembly and condensation are made in three steps:

- Phase 1: Assembly of fuselage and VTP and condensation into a super-element (figure 4.3).
- Phase 1-2: Extraction of fuselage-VTP super-element stiffness matrix from the MSC.NASTRAN database and division by 2 to use it in the half (symmetric) A/C model.
- Phase 2: Assembly of fuselage-VTP super-element (full or half) with wings and HTP FEM models (both sides or R/H side) and condensation into a super-element.

The mass model consists of concentrated masses (MSC.NASTRAN CONM2 entries) associated to reference grid points that are connected to the structure with RBE3 entries.

4.1.3 Unsteady aerodynamic model

The aerodynamic model is a MSC.NASTRAN Doublet-Lattice Method (DLM) unsteady model accounting for:

- Lifting surfaces: wing, horizontal stabilizer and vertical stabilizer.
- Control surfaces: ailerons, elevator and rudder.
- Fuselage.
- Nacelles.

The structural-aerodynamic model interconnection is obtained by interpolating the displacement of the structural grid points by means of surface splines. Additional structural points have been created for the interpolation of nacelles and fuselage areas; these new points are rigidly connected respectively to pylon mass and fuselage frame reference points.
The DLM unsteady aerodynamic model has been corrected in terms of pressure coefficients in order to match up the aerodynamic derivatives available from flight mechanics data. Corrections applied depend on Mach number, inflow angle, flaps configuration and airbrakes setting *AB-in* and *AB-out*. An example

of the areas affected by the corrections for a 30 degrees flap configuration is shown in figure 4.6.

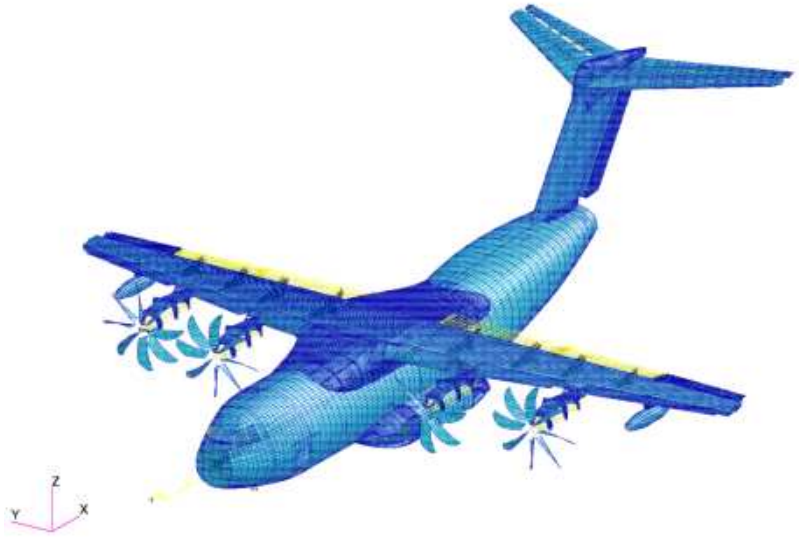

Figure 4.2. *A400M* FE model.

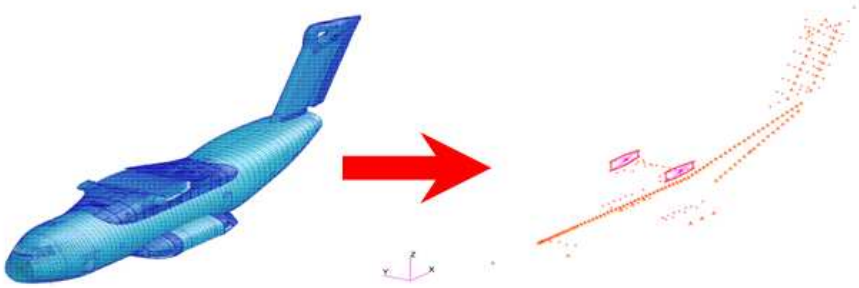

Figure 4.3. Phase 1: fuselage-VTP superelement condensation.

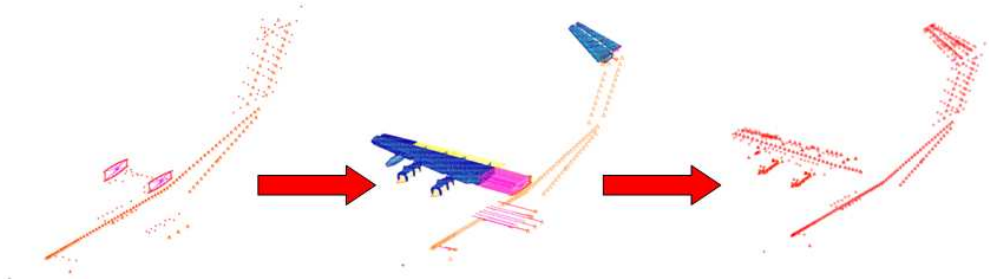

Figure 4.4. Phase 2: fuselage-VTP superelement + R/H wing + R/H HTP and condensation.

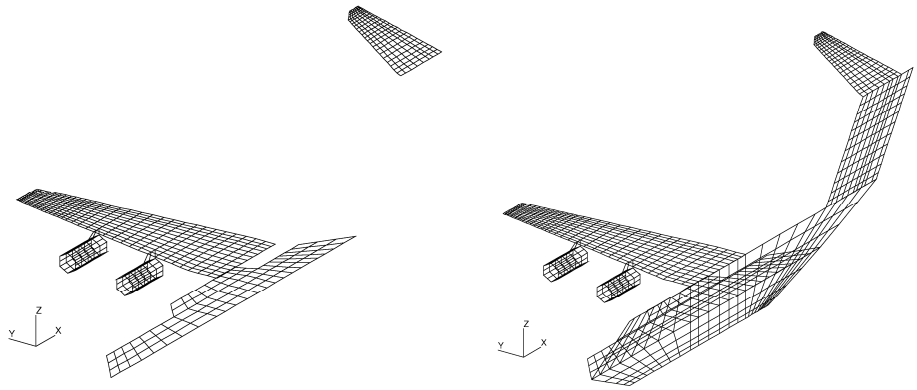

Figure 4.5. A400M symmetric and antisymmetric DLM unsteady aerodynamic models.

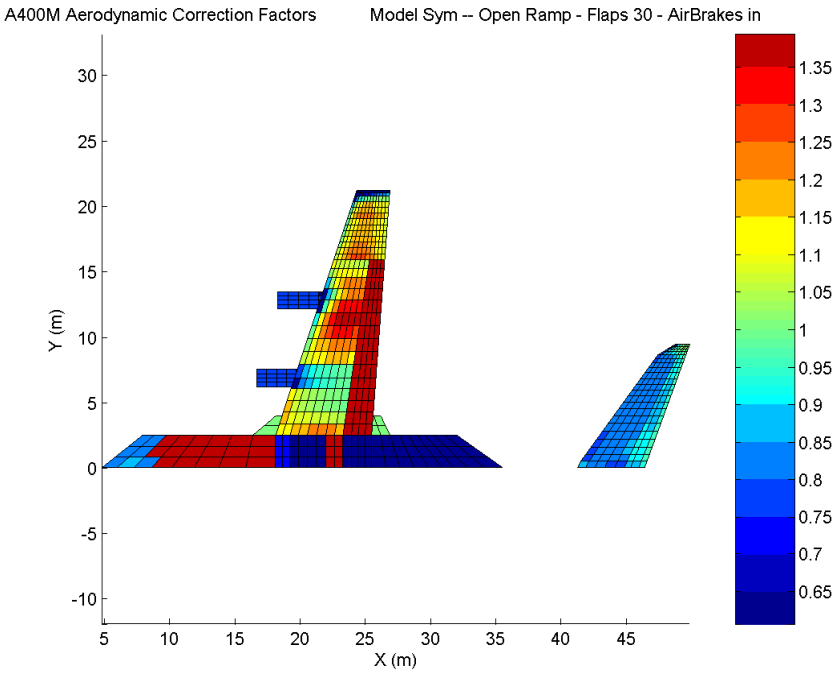

Figure 4.6. A400M symmetric DLM unsteady aerodynamic model pressure corrections for flaps 30 degrees configuration, *AB-in*.

4.1.4 Nonlinear FCS

Figure 4.7 reports a general scheme of the linear/nonlinear Flight Control System (FCS) implemented in the *A400M* DTG loads calculation model. It is based on a two level control logic which input parameters are pitch angle *TETA*, pitch angular velocity *Q1*, altitude *Z*, vertical speed *VZ* and normal load factor *NZ1* (measured in a node corresponding to avionic bay position, next to pilots cabin). Others parameters are aircraft speed, Mach number, center of gravity position and mass. The first block (LIN - pilotage) is fully linear and comprehends the pilot control logic. The second block (MLA - Maneuvering and gust Load Alleviation) comprehends the nonlinear gust load alleviation logic which can be selected in a range of three different laws:

- NLX: normal load alleviation law, reads as input *NZ1* (figure 4.7), achieves to maintain the horizontal trim.
- LLF or ALT: fixed altitude law, reads as input *NZ1*, *Z* and *VZ*, achieves to maintain the horizontal trim and the specified flight altitude.
- VSX: vertical speed limitation law, reads as input *NZ1*, *Z* and *VZ*, achieves to maintain the horizontal trim and holds the vertical speed measured at avionic bay position.

Besides the specific task all the laws alleviate wing root bending moment and act through elevators and ailerons.

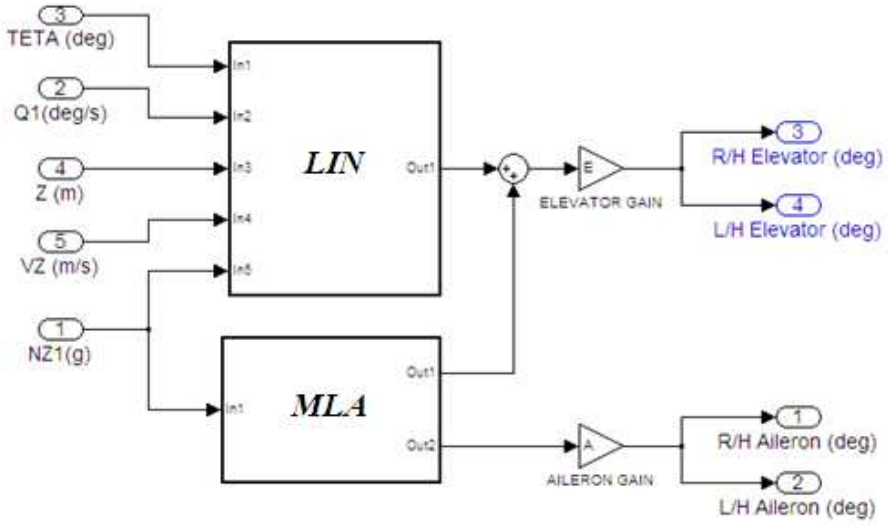

Figure 4.7. *A400M* linear/nonlinear Flight Control System (FCS).

For the tasks needed in this work (reliability and simplicity in results interpretation) only NLX law has been taken into account. This law implements a classical load alleviation logic taking as input vertical load factor *NZ1*: when *NZ1* reaches *0.3g* (where *g* is the gravity acceleration) the MLA starts to work ordering a proportional negative (upwards) symmetric deflection of the ailerons $\delta_{aileron}$. The consequence of this deflection is a decrease in wing tip lift distribution which has a positive influence over wing root bending moment, while others components can increase or decrease depending on aircraft dynamics (it is typical a wing root torsion moment increment). Nonlinearities reside in the nonlinear proportional law $NZ1/\delta_{aileron}$ (which is intrinsically nonlinear and has a further unidirectional control logic which avoids undesired aileron vibrations acting only for positive load factor increments) and in a saturation limit over aileron deflection. The nonlinear MLA block resets 5 seconds after the last time instant in which $NZ1(t_i)>0.3g$. The elevator is controlled consequently to achieve the horizontal trim of the aircraft.

4.2 Loads calculation procedure

4.2.1 General scheme

Loads responses calculation is carried out in a three step procedure as illustrated in figure 4.8. The three steps respectively consist in:

- Generation of generalized mass, stiffness, damping and AIC matrices with MSC.NASTRAN.
- Gust response calculation with DYNRESP in terms of modal and control surfaces displacements, in time or frequency domain.
- Loads recovery with DYNLOAD (an in-house code for loads recovery and modal response post processing), with displacements method (DM) or summation of forces (SOF) procedures.

DYNRESP is a software package developed by the Karpel Dynamic Consulting Ltd. (algorithm, formulation and user interface), EADS-CASA Airbus Military (requirements, beta site and first user) and ISCFDC (code development and maintenance) during the *A400M* design process [13]. The code covers a wide variety of dynamic capabilities including modal and control-surface response to discrete gust, maneuver command and direct forces, control system of most general architecture, fully nonlinear elements, 1P and gyroscopic effects, resulting loads separation into time histories of excitation, aerodynamic response and inertial forces for summation of forces or mode displacements loads calculations.

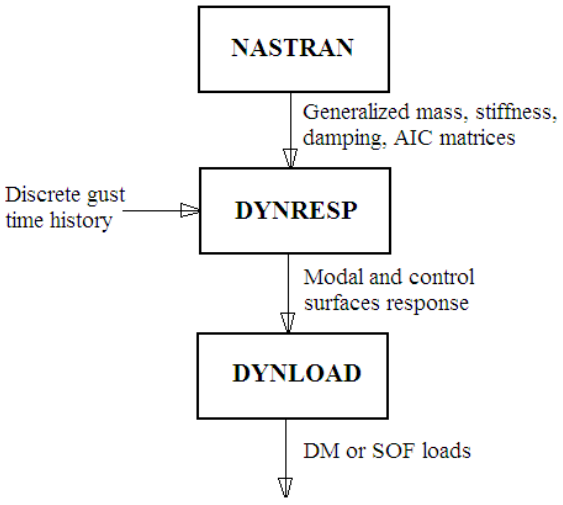

Figure 4.8. Load calculation flowchart.

4.2.2 Dynamic gust response with DYNRESP

Discrete gust responses used in this work have been calculated using DYNRESP.
The formulation is based on second order frequency domain equations of motion in generalized coordinates (equation (4.1)):

$$\begin{aligned}&\left(-\omega^2[M_{hh}]+i\omega[B_{hh}]+[K_{hh}]+q[Q_{hh}(i\omega)]\right)\{\xi(i\omega)\}=\\&=\left(-\omega^2[M_{hc}]-q[Q_{hc}(i\omega)]\right)\{\delta(i\omega)\}-q\{Q_{hg}(i\omega)\}\frac{w_g(i\omega)}{V}\end{aligned} \tag{4.1}$$

The left-side matrix coefficient matrices are the generalized mass, damping, stiffness and aerodynamic influence coefficient (AIC) matrices associated with modal displacement $\{\xi(i\omega)\}$, while the right-side terms expresses the generalized aerodynamic forces due to a single sinusoidal gust velocity of amplitude $w_g(i\omega)$ and excitation term due to control-surface commanded deflections $\{\delta(i\omega)\}$.
The AIC matrices of equation (4.1) are interpolated from several $[Q_{hh}(k)]$, $[Q_{hc}(k)]$ and $\{Q_{hg}(k)\}$, where k is a tabulated value of the reduced-frequency $k=\omega L/V$ and $L=REFC/2$ is the reference length. The tabulated matrices can be imported by either NASTRAN or ZAERO at several k values (typically 15).
The current version of DYNRESP deals with mass configurations for which the normal modes are calculated by MSC.NASTRAN. The generalized diagonal mass and stiffness matrices, and of equation (4.1) are obtained from NASTRAN. The diagonal terms in the damping matrix are usually calculated by equation (4.2), where ω_i and ξ_i are the modal frequency and damping ratio associated with the *i-th* mode.

$$B_{ii}=2\xi_i M_{ii}\omega_i \tag{4.2}$$

Additional transfer functions can be defined to include sensors and actuators dynamics in the system. The control system can be included by means of SISO transfer functions, MIMO elements defined in state space form and zero-order junctions. The final formulation of the closed-loop aeroservoelastic system is symbolic given in equation (4.3). Figure 4.9 shows a general flow chart about the construction of the system and the possible solutions.

$$\left[\overline{A_v}(i\omega)\right]\{X_v(i\omega)\}=\{B_{vw}(i\omega)\} \tag{4.3}$$

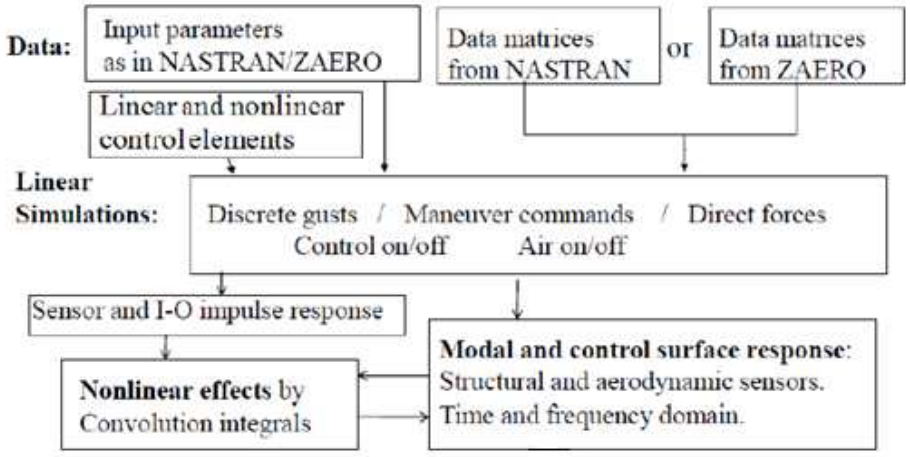

Figure 4.9. General DYNRESP flowchart.

For more details on the formulation of system (4.3) see ref. [13]. Further details will be now given about the formulation and the resolution of the nonlinear problem, where nonlinearities derive from nonlinear elements of the control system.

4.2.3 Nonlinear aeroservoelastic response

The calculation of aeroservoelastic response to deterministic excitations with nonlinear control elements with DYNRESP is based on a three-stage process that combines frequency-domain linear aeroservoelastic response, impulse response to control inputs and time-domain simulations of the nonlinear elements. A typical interconnection scheme of an aeroelastic plant with a control system that includes nonlinear elements is shown in figure 4.10. The NLi boxes represent nonlinear elements. The ITFi boxes represent isolated linear element that interacts with the nonlinear elements. The outputs y_i and the inputs u_i of the main linear block are inputs and outputs to the combined block, called NLIL, of nonlinear and isolated elements.

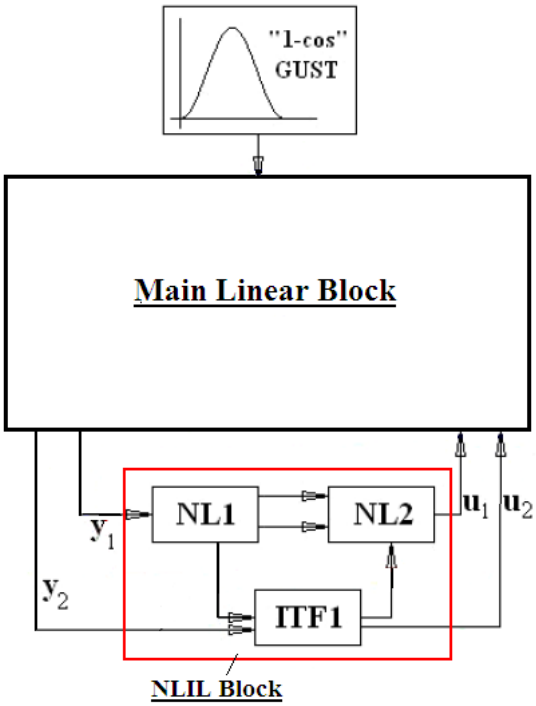

Figure 4.10. Aeroservoelastic system with discrete gust excitation and nonlinear elements.

As said before the calculation of the nonlinear aeroservoelastic response is based on a three-step process:

- Stage 1: calculation of the frequency domain responses of the main linear block to the external excitations $\{Y_L(i\omega)\}$ and to units u_i inputs $[Y_{LU}(i\omega)]$ with the NLIL block disconnected.
- Stage 2: time domain transformations of the Stage 1 frequency response vectors using IFFT techniques ($\{y_L(t)\}, [y_{LU}(t)]$).
- Stage 3: the impulse response functions of the main block inputs $[y_{LU}(t)]$ are used to add the nonlinear effects to the linear gust response by using convolution integrals (equation (4.4)).

$$\{y(t)\} = \{y_L(t)\} + \int_0^t [y_{LU}(t-\tau)]\{u(\tau)\}d\tau \qquad (4.4)$$

Vector $\{u(\tau)\}$ represents the control input to the main linear block and it's generated as the response of the NLIL block to the output $y_i(t)$ of the main linear block. The NLIL response is calculated solving directly the algebraic (static)

NLi elements and through the 4-th order Runge-Kutta integration method for the isolated linear elements ITFi.
The process results in modal and control-surface response functions, in the frequency domain or in the time domain, for subsequent summation of force or mode displacement loads computations.

4.2.4 Gyroscopic and *1P* loads

Rotating engines installed on vibrating structure introduce "one per revolution" (1P) and gyroscopic forces and moments at the engine grid points that represent the engine hubs. These additional loads are not negligible for aircraft with big propellers like the *A400M*.
With 1P loads we intend loads generated by the propeller disc in incidence. These loads are reduced to two shear forces and two moments applied to propeller hub which magnitudes are calculated by "whirl flutter derivatives" provided by the propeller fabricant. 1P loads depend on rotational speed of the propeller (i.e. engine speed) only by means of these derivatives: furthermore they depend on blades surface, propeller diameter, altitude, speed, hub displacements and rotations. Hence they can be introduced in equation (4.1) through an incremental non symmetric stiffness matrix $[\Delta K_{hh}]_P$ and an incremental non symmetric damping matrix $[\Delta B_{hh}]_P$ due to generalized aerodynamic forces and moments applied to the engine hubs (equation (4.5), (4.6)) which depend on the local incidence angles α and β of the hub.

$$[\Delta K_{hh}]_P = [\phi_{Hh}]^T [K_{1P}][\phi_{\alpha h}] \tag{4.5}$$

$$[\Delta B_{hh}]_P = [\phi_{Hh}]^T [B_{1P}][\phi_{\alpha h}] \tag{4.6}$$

Matrix $[\phi_{Hh}]$ represents the modal displacements at the hub (subscript *H*), $[\phi_{\alpha h}]$ is the matrix of modal incidence angles while $[K_{1P}]$, $[B_{1P}]$ contains combinations of whirl flutter derivatives. The local incidence angles can be measured by adding small vanes at the engine hub points, free to rotate about *y* and *z* directions (where *y* and *z* are perpendicular to engine hub direction *x*, see figure 4.11) hence able to follow the local stream orientation; combinations of the vane rotations and the hub rotations provide the local incidence angles.

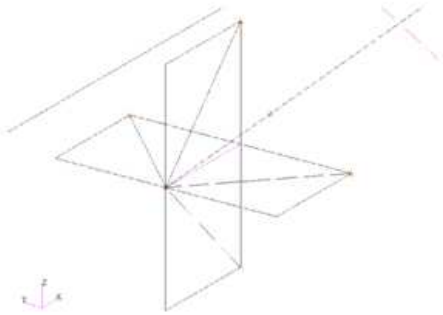

Figure 4.11. Incidence sensor (vane) at propellers hub.

The effects of gyroscopic forces are introduced in a similar way to 1P effects by adding an incremental non symmetric damping matrix $[\Delta B_{hh}]_g$ in equation 4.1 that reflects the gyroscopic moments in certain rotational directions at the hubs due to angular velocities in other directions.
Figure 4.12 depicts the contribution of gyroscopic and 1P effects in an example of *(1-cos)* discrete tuned gust response performed with the actual *A400M* model. The response is referred to horizontal tail plane root section bending moment calculated with summation-of-forces method. It can be seen that gyroscopic effect is almost negligible with respect to 1P effect, also in a section of the aircraft not directly connected with the engines and propellers installation. It is important to say that 1P effects are not negligible along any section of the aircraft and it is not necessarily a negative (heaviest) contribution, so it has to be taken into account for a reliable design load calculation.

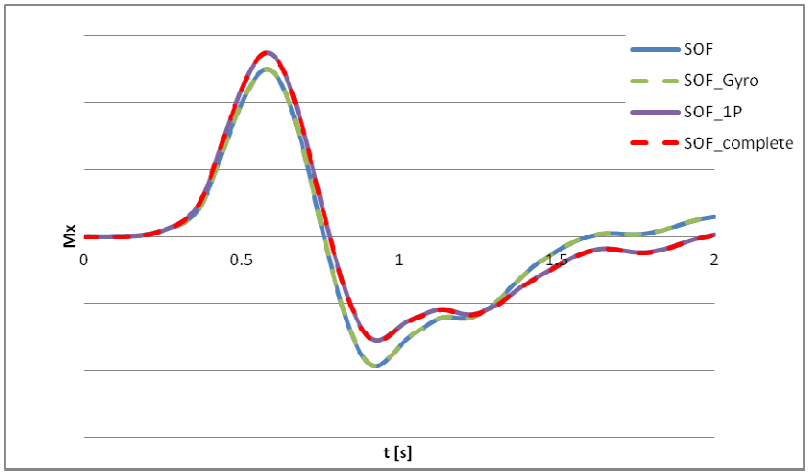

Figure 4.12. Gyroscopic and 1P effects on discrete tuned gust response (horizontal tail plane root section bending moment M_x).

4.3 Intermediate results overview and discussion

Like it has been done in chapter 3 for the 2 DOF test system here will be reported all the intermediate results in terms of excitations and responses for the three methods selected. Hereafter the term “linear model” refers to the FCS OFF model while with “nonlinear model” it will be intended the FCS ON model with the NLX loads alleviation logic. The responses have been calculated for the following design station (the correspondence load component-design station is shown in table 4.5 and figure 4.13):

- WRS_W06: wing root section (hereafter WRS);
- HRS_M02: horizontal tail plane root section (hereafter HTP).

Paragraph 4.3.1 reports the results of a linear/nonlinear discrete tuned gust analysis useful to introduce and explain the aircraft behaviour during gust response (aircraft loads, control surfaces displacements) and to give an order of magnitude for the nonlinear CT design loads.
In sections 4.3.2 to 4.3.4 only results regarding WRS section will be shown, while section 4.4 reports quantitative results for all the design section considered.

Design station	Load component	Denomination
WRS	Fz	WRS3
WRS	Mx	WRS4
WRS	My	WRS5
HTP	Fz	HTP3
HTP	Mx	HTP4
HTP	My	HTP5

Table 4.5. Design section-load component correspondences.

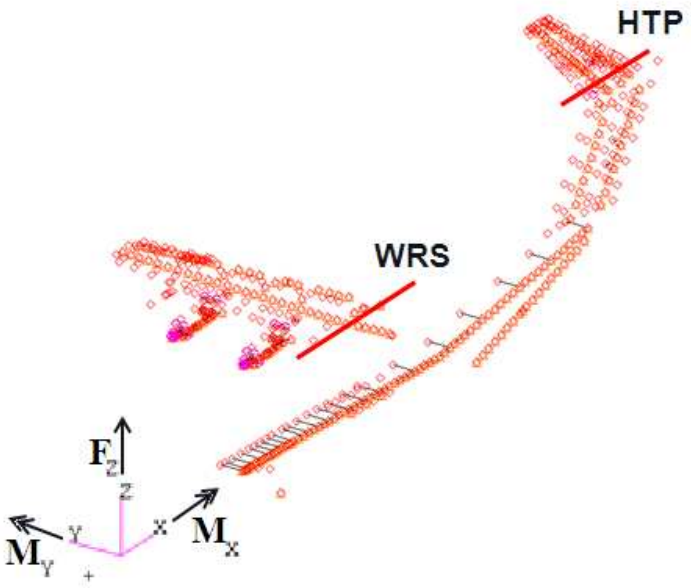

Figure 4.13. Design section location and load components denomination.

4.3.1 Discrete Tuned Gust analysis

This section reports results for the DTG analysis performed as indicated by certification requirements (refs. [2] and [12]). The role of this paragraph is to introduce and explain the behaviour of the aircraft during a gust response with the nonlinear FCS activated. This is done because the linear or nonlinear DTG is a simple deterministic response and the resolution is "exact", so a lot of qualitative conclusions can be caught from this analysis about FCS behaviour, control surfaces displacements, entity of loads alleviation (or magnification!).
Figure 4.14 reports the input *(1-cos)* discrete gusts for 9 gust gradients *H* included in a range from 30 to 350 ft.

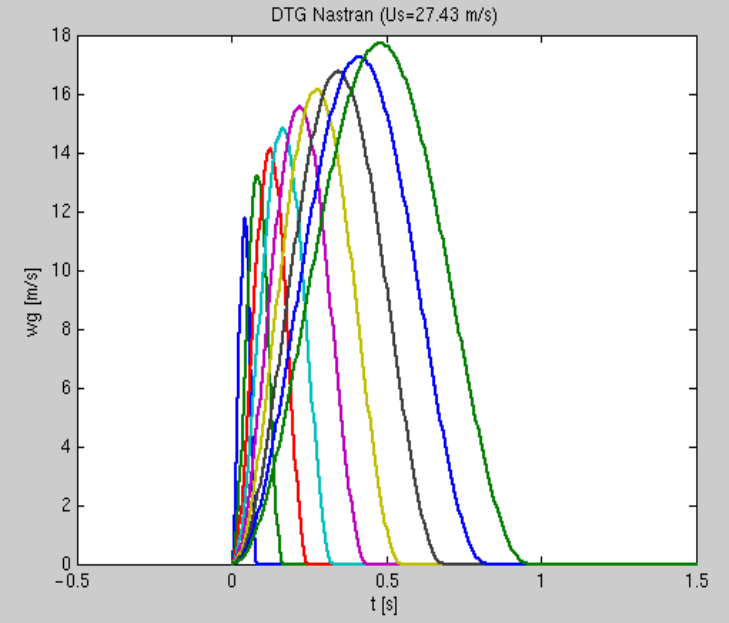

Figure 4.14. Discrete tuned gusts (H = 30-350 ft).

Responses are calculated as in section 4.2.3 and modal vectors for structural and control surfaces displacements and inertia and aerodynamic forces vectors for summation of forces recovery are available. With these informations we can rebuild the event dynamic which is shown in figures from 4.15 to 4.17. Finally figure 4.18 resumes elevator, aileron and load factor time histories.

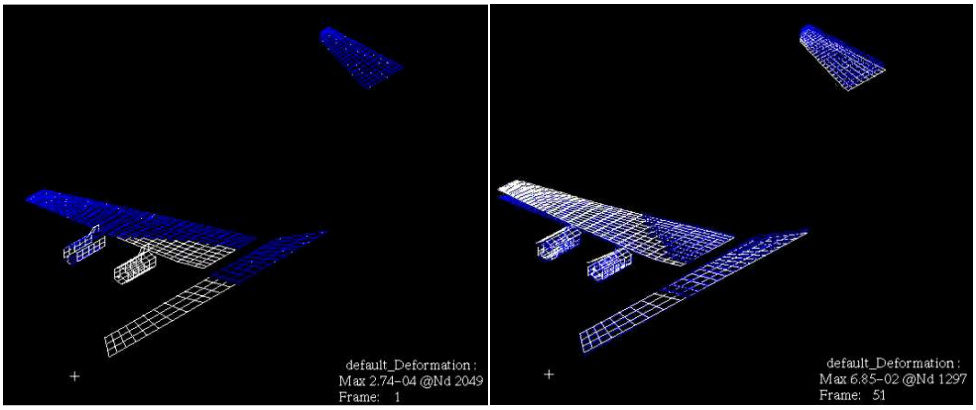

Figure 4.15. DTG response, initial undeformed condition (left) and first structural displacements (right).

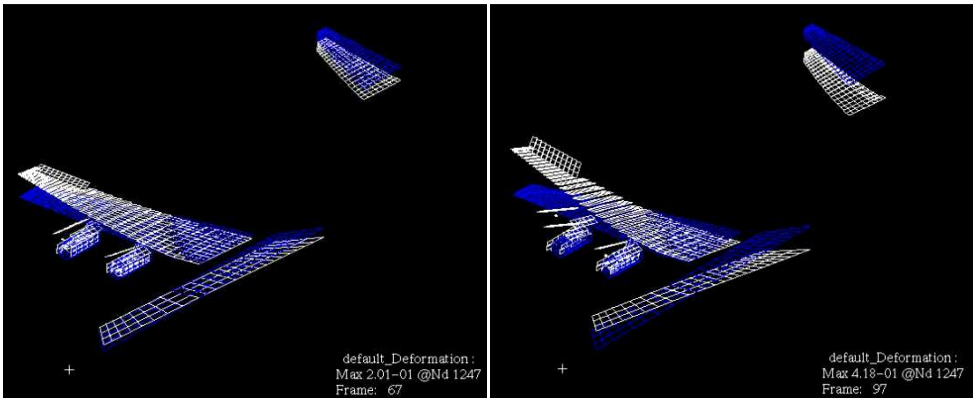

Figure 4.16. DTG response, aileron first (left) and maximum deflection (right) with wing maximum upward deflection. Note the elevator begins to deflect too.

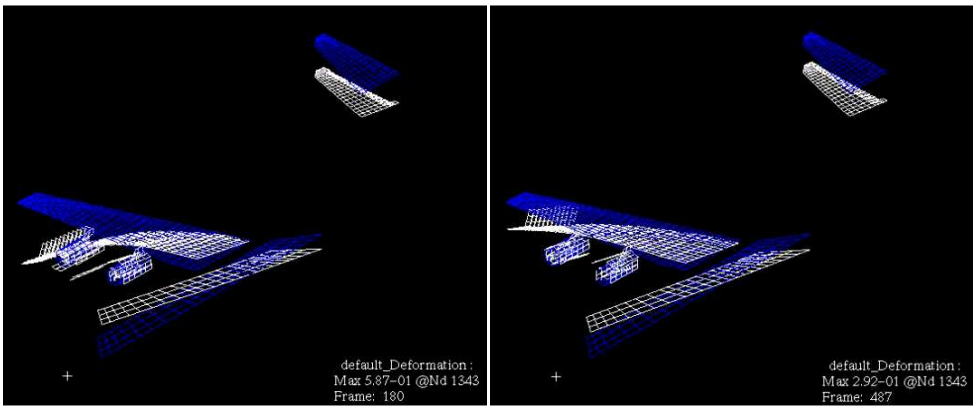

Figure 4.17. DTG response, maximum wing downward deflection (left) and asymptotic conditions (right).

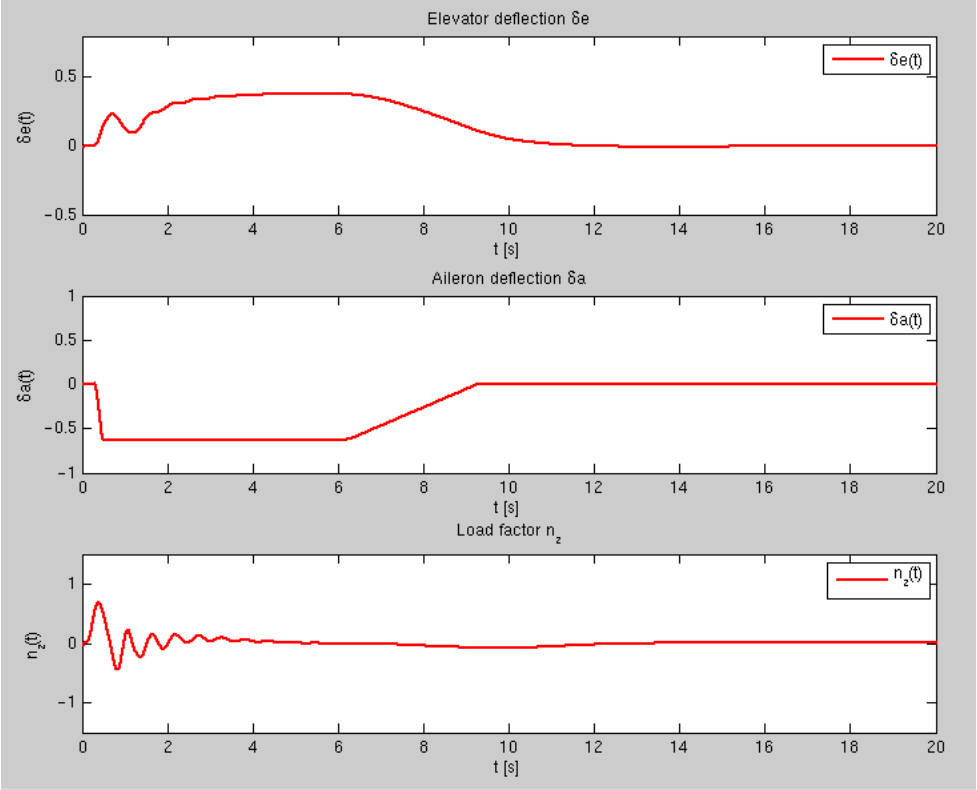

Figure 4.18. DTG response, control surfaces and CG load factor.

Comments:

Looking to the above images we can understand and explain the dynamic of the aircraft encountering a gust field and see the intervention of the nonlinear FCS. Figure 4.15 shows the initial undeformed conditions and the linear response of the aircraft responding to the gust excitation: at this point the nonlinear FCS isn't still working. When the load factor reaches the *0.3g* level the FCS commands a certain aileron deflection, while the aircraft continues to respond to the gust field (figure 4.16). The elevator begins to deflect to maintain the horizontal trim of the aircraft. Finally figure 4.17 shows the maximum negative oscillation of the wing and the final configuration of control surfaces deflection and structural displacements, which is maintained for 5 seconds after the instant of time for which the FCS detects a load factor *NZ1* greater than *0.3g* (this is made in order to avoid undesired vibrations of the control surfaces). All these comments can be referred also to figure 4.18, which reports elevator, aileron and CG load factor time histories versus time. It can be seen the start of the FCS intervention, the reaching of the aileron saturation limit and the 5 seconds of constant deflection of the aileron.

Table 4.6, 4.7 and figures 4.19, 4.20 report the results obtained for the DTG analysis in terms of nonlinear model (FCS ON) design and time correlated loads with respect to the linear (FCS OFF) ones. Important information can be caught from this comparison about the entity of the bending moment alleviation and the indirect effects that the FCS has over other loads. Obviously these are only qualitative indications about what it is expected from the CT analysis methods shown below because DTG *(1-cos)* excitation is short (also with the longest gradient *H=350 ft*) so the load response is dominated by the structural dynamics. On the contrary CT is typically longer and the effects of rigid body modes can be relevant. So the responses of the two models are dominated by different dynamics and bring to different quantitative results.
The WRS4 bending moment reduction is in the order of the 10% of the linear PSD value, while it can be clearly seen the great increment in torsion moment (WRS5) due to the deflection of the aileron. HTP loads are affected by the dynamics of the aircraft and by the positive deflection of the elevator, which causes the increment in shear force and bending moment and the decrement in torsion moment. We remark that all design and time correlated loads in this and next sections are incremental with respect to *1g* loads.

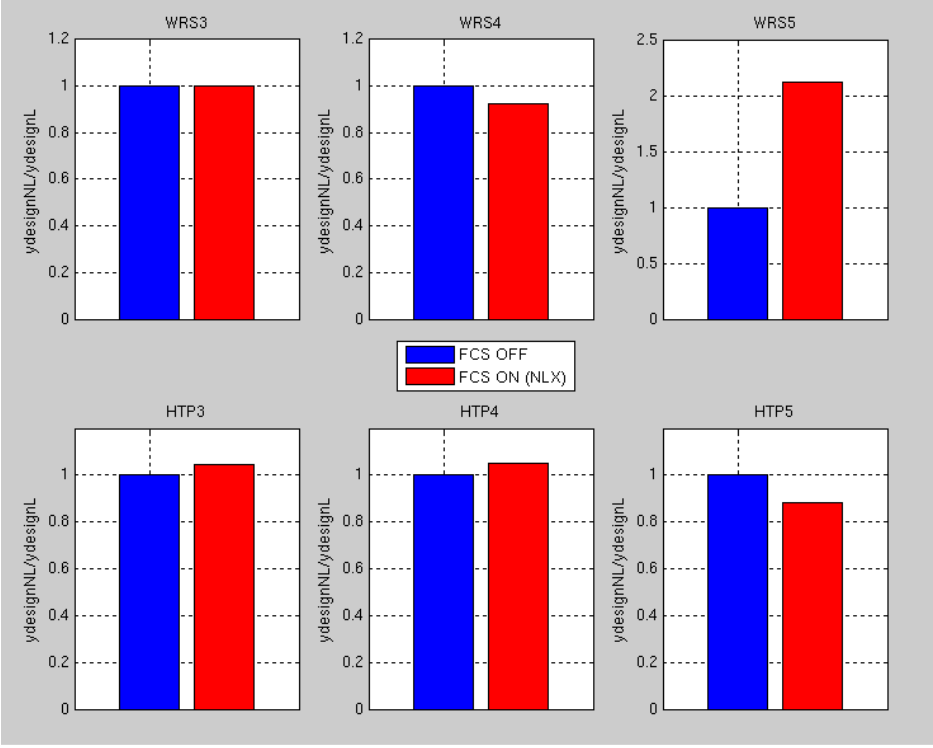

Figure 4.19. DTG design loads.

Load	Linear % diff	Nonlinear % diff
WRS3	-	0.05
WRS4	-	-7.66
WRS5	-	112.28
HTP3	-	4.46
HTP4	-	5.01
HTP5	-	-12.01

Table 4.6. DTG design loads.

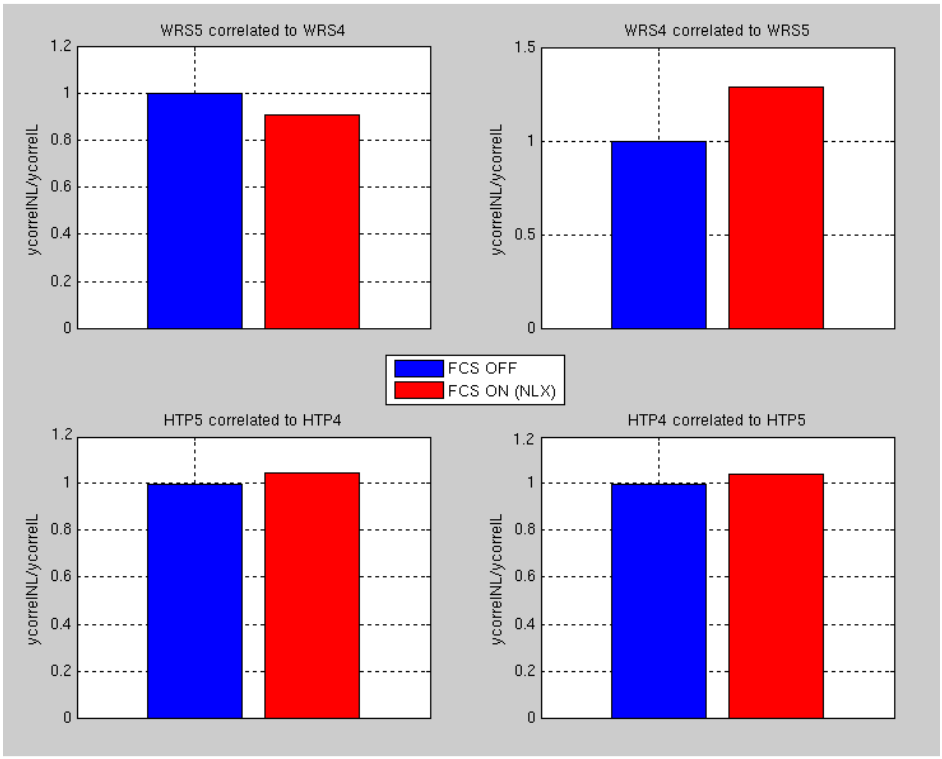

Figure 4.20. DTG correlated loads.

Design Load	Correlated Load	Linear % diff	Nonlinear % diff
WRS4	WRS5	-	-8.65
WRS5	WRS4	-	28.66
HTP4	HTP5	-	4.78
HTP5	HTP4	-	4.18

Table 4.7. DTG correlated loads.

4.3.2 Matched Filter

The operation flow of the MF method is recalled in figure 4.21, for a wider explanation see previous chapters. Referring to figure 4.21 and figures from 4.22 to 4.31, points *(a)* and *(b)* are referred to as *1st loop* and show the Hoblit gust filter impulse response and the impulse response of the considered load. Points *(c)*, *(d)* and *(e)* are called *2nd loop* and show respectively the matched excitation, the critical gust shape and the final response. Finally figure 4.32 shows a typical design load trend versus the initial impulse strength *k* sweep. For reasons of brevity next images refer only to WRS section bending moment (denominated N3 or WRS4), except where different specified.

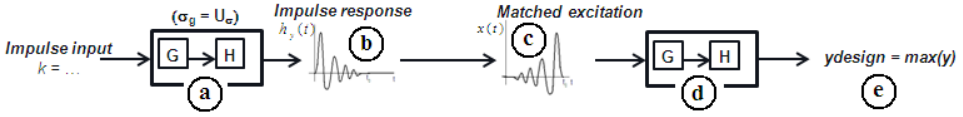

Figure 4.21. Matched Filter operation flowchart.

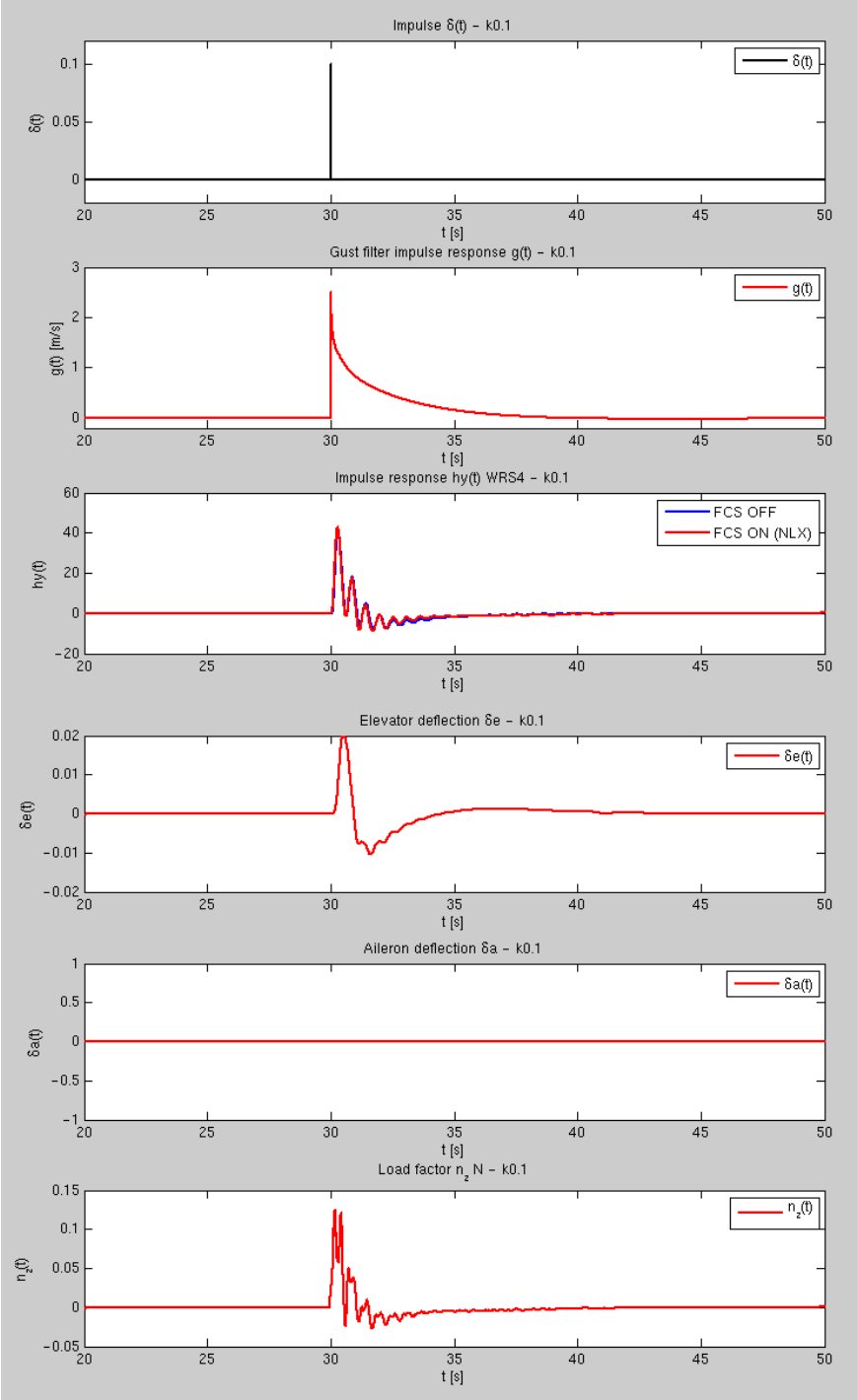

Figure 4.22. MF 1st loop, loadID=N3 (WRS bending moment), k = 0.1.

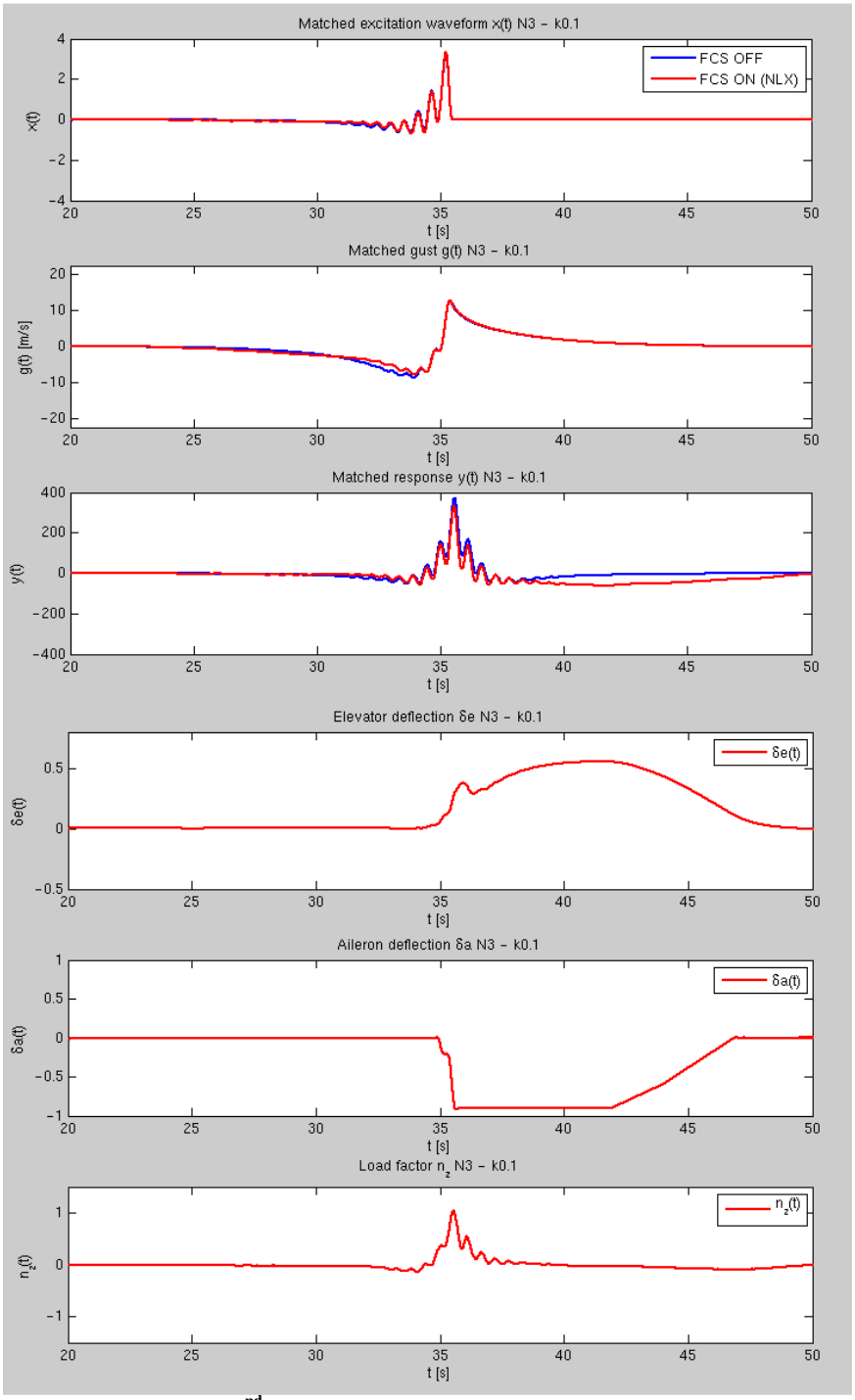

Figure 4.23. MF 2nd loop, loadID=N3 (WRS bending moment), k = 0.1.

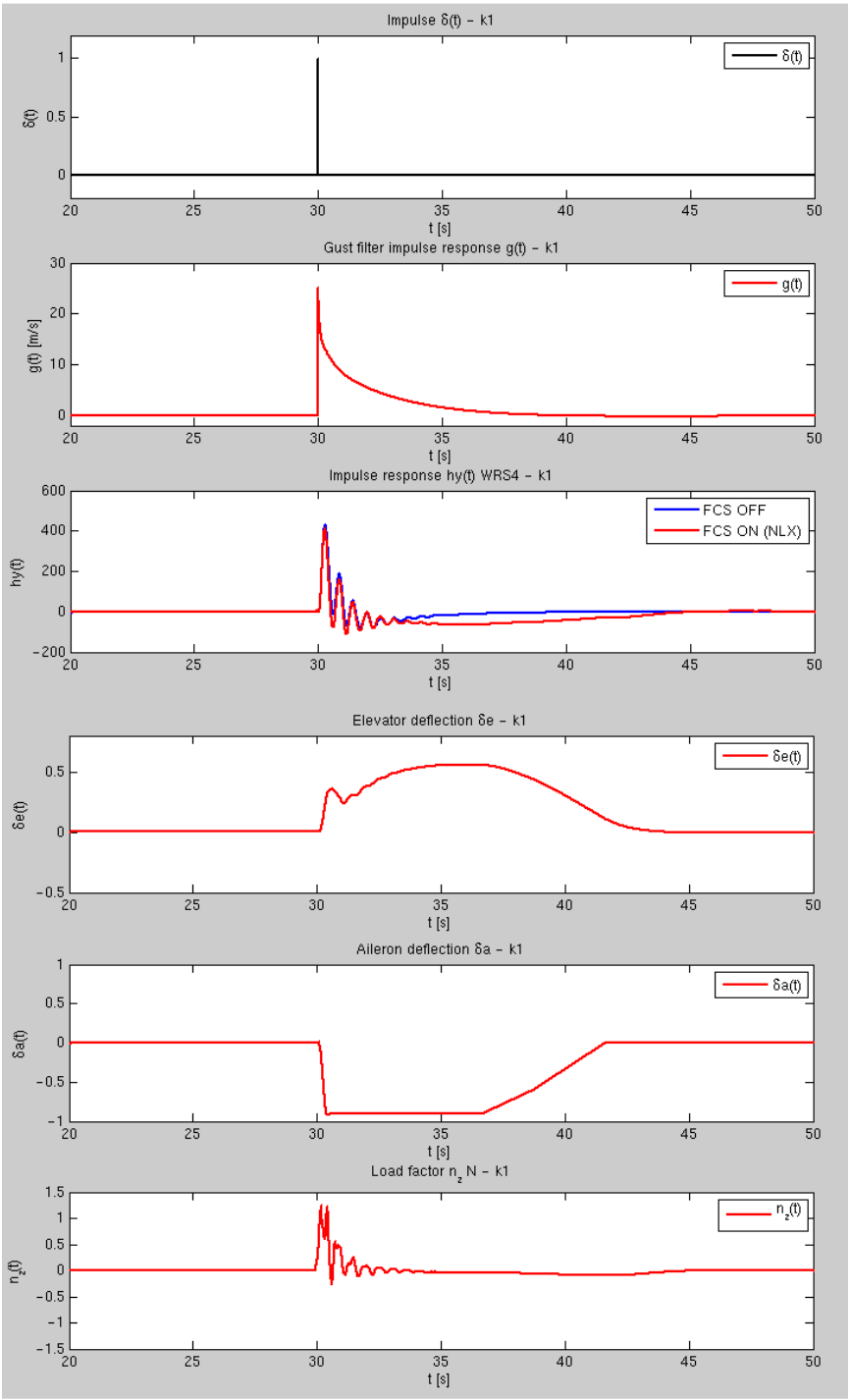

Figure 4.24. MF 1st loop, loadID=N3 (WRS bending moment), k = 1.

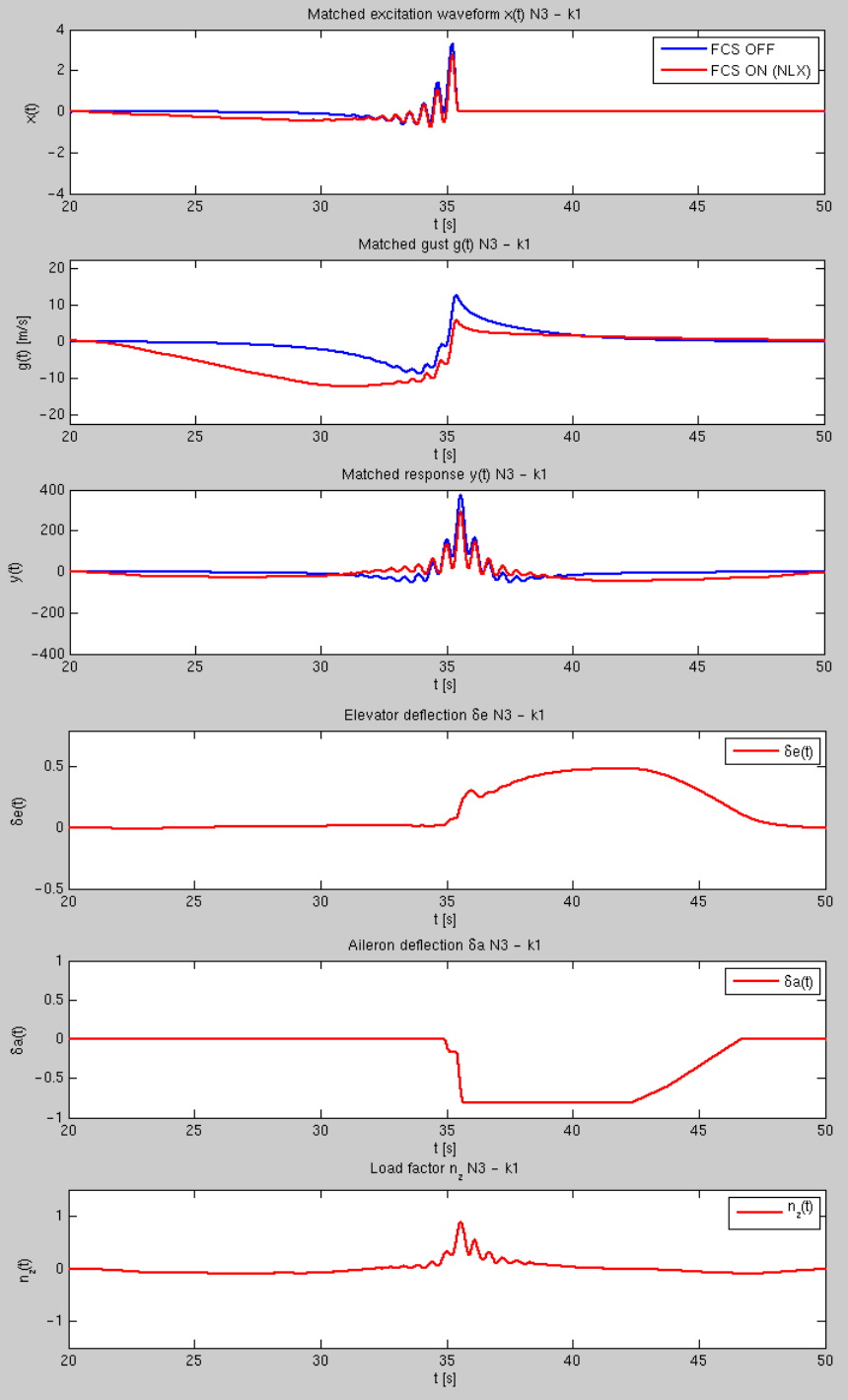

Figure 4.25. MF 2nd loop, loadID=N3 (WRS bending moment), k = 1.

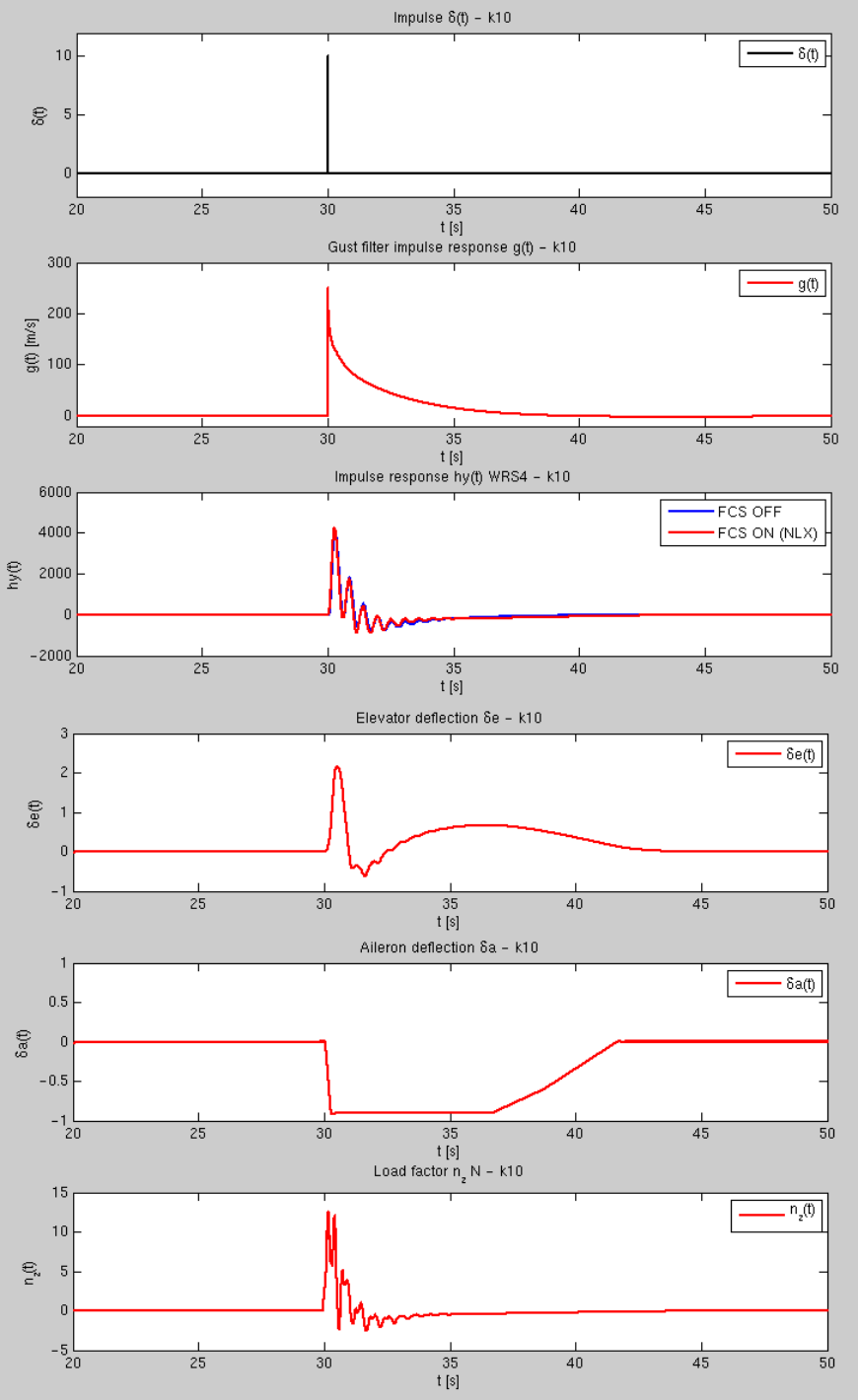

Figure 4.26. MF 1st loop, loadID=N3 (WRS bending moment), k = 10.

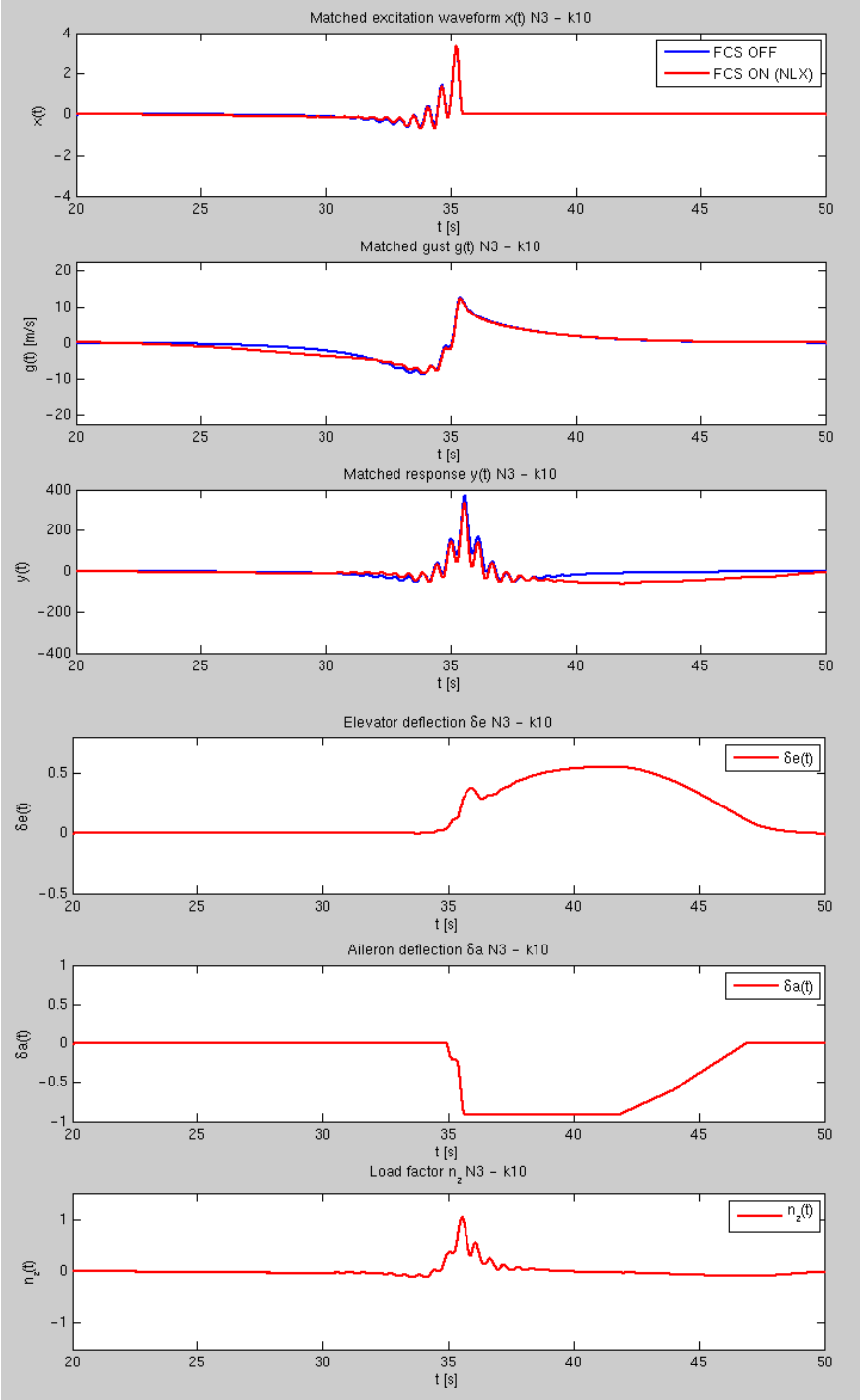

Figure 4.27. MF 2nd loop, loadID=N3 (WRS bending moment), k = 10.

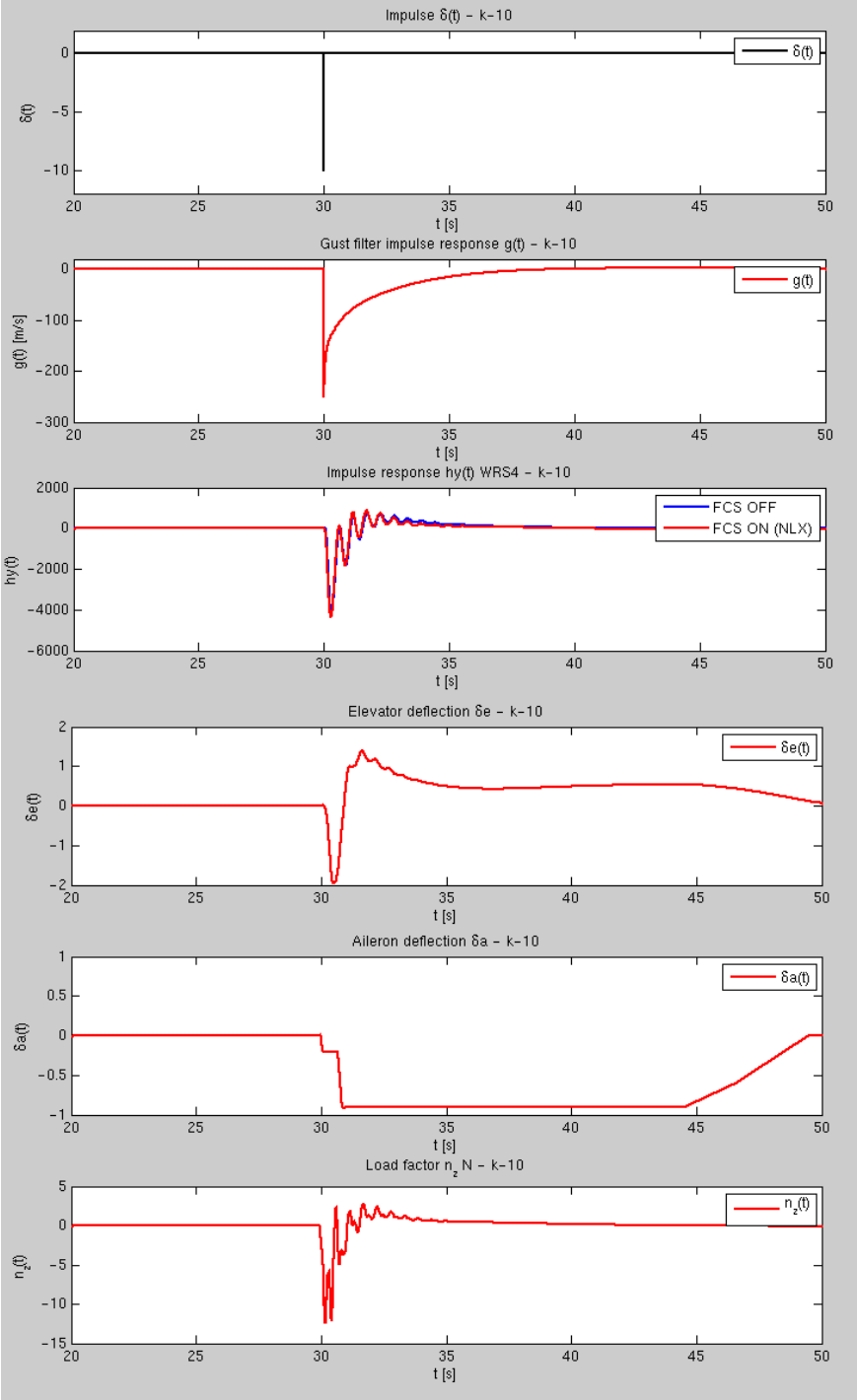

Figure 4.28. MF 1st loop, loadID=N3 (WRS bending moment), k = -10.

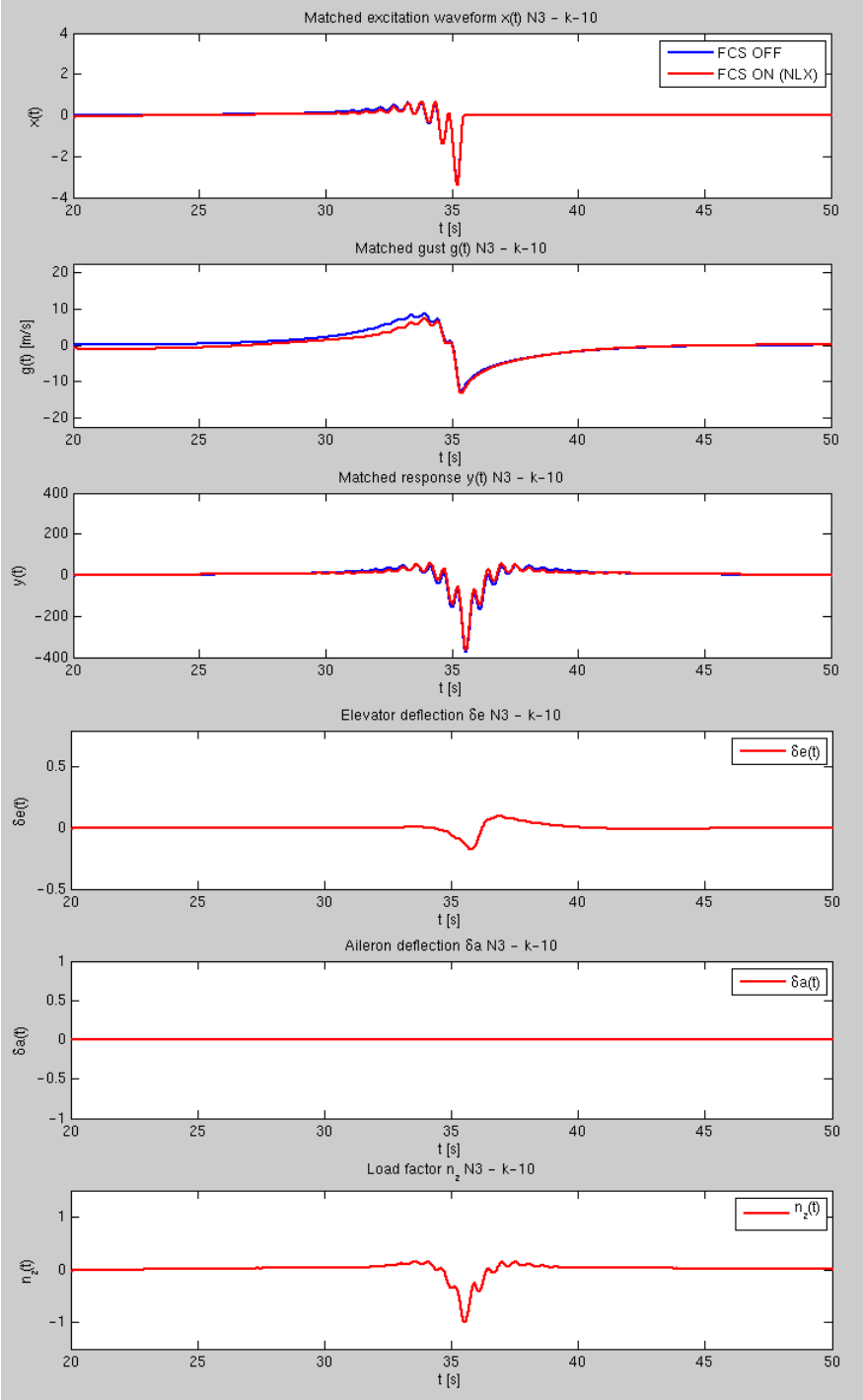

Figure 4.29. MF 2nd loop, loadID=N3 (WRS bending moment), k = -10.

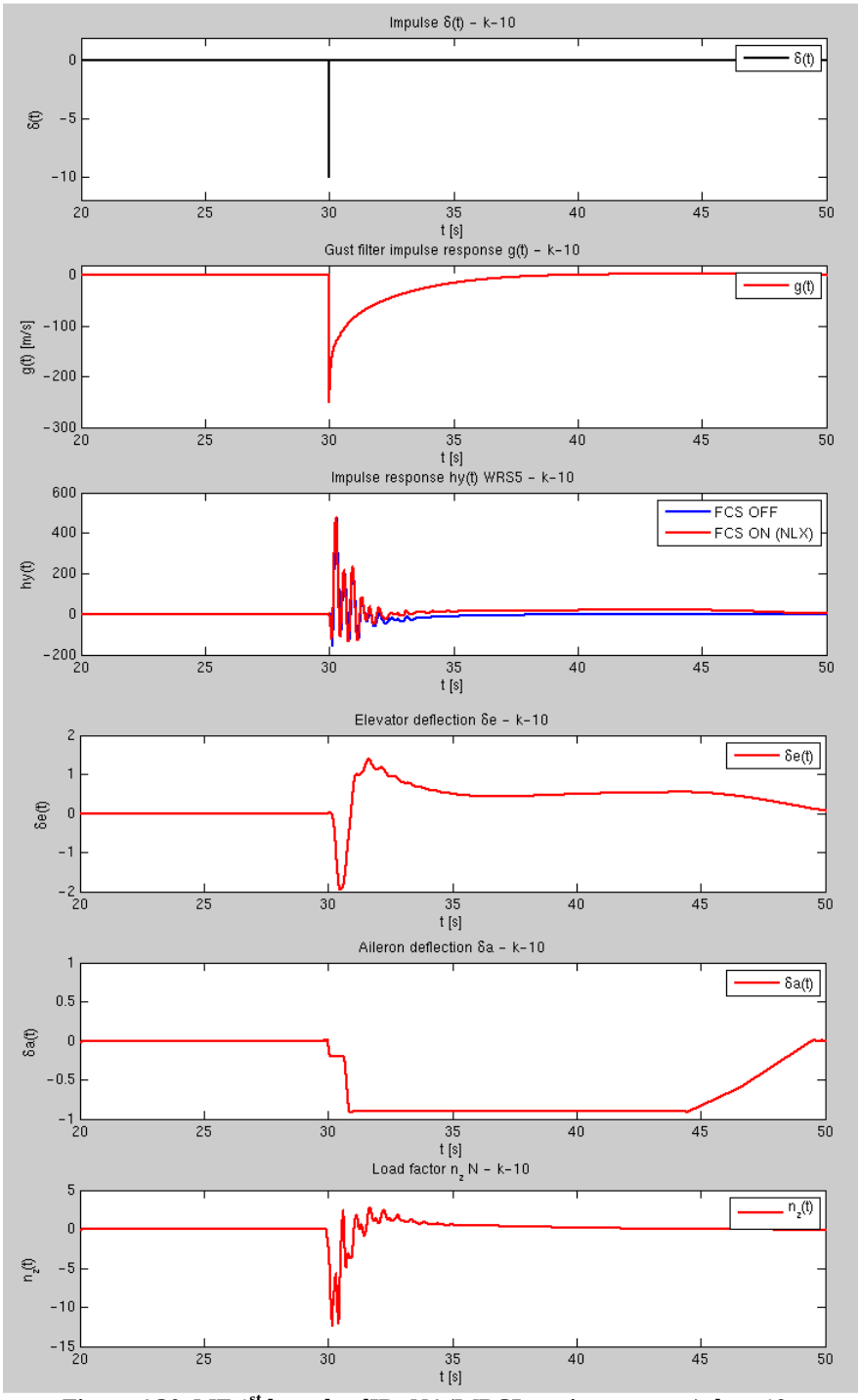

Figure 4.30. MF 1st loop, loadID=N4 (WRS5 torsion moment), k = -10.

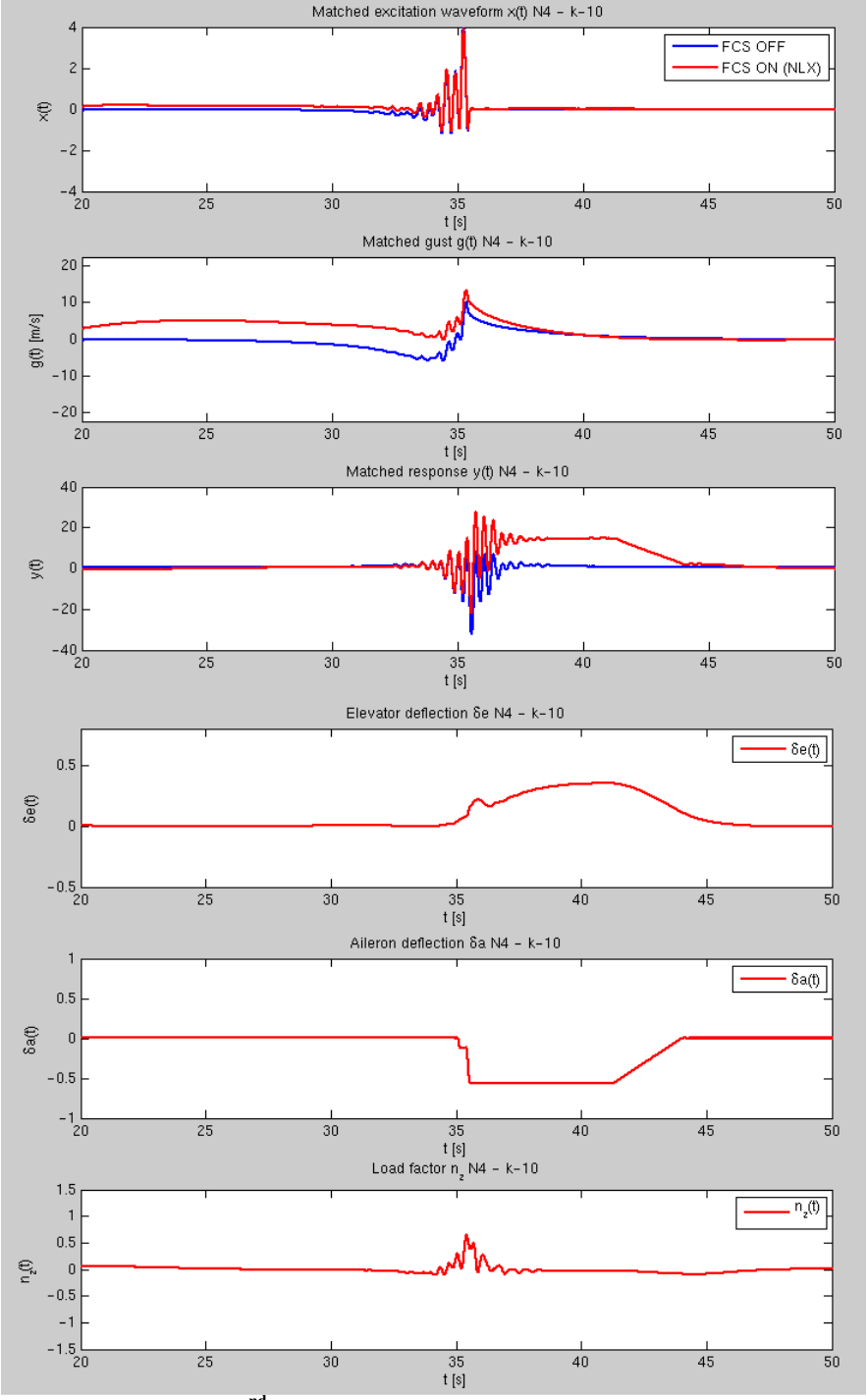

Figure 4.31. MF 2nd loop, loadID=N4 (WRS5 torsion moment), k = -10.

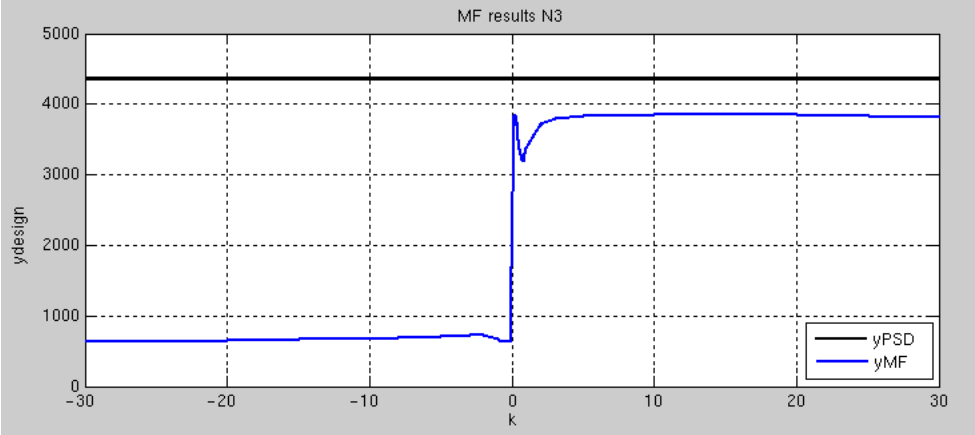

Figure 4.32. Nonlinear model (FCS ON), zoom on a typical variation of MF design loads with initial *k* sweep (WRS4).

Comments:
Interesting comments can be made about the previous images:

- With the smaller *k=0.1* the first impulse response (figure 4.22) is almost linear, because the reduced amplitude of the impulse excitation is not sufficient to activate the aileron displacement. The small differences between linear (FCS OFF) and nonlinear (FCS ON) responses are due to the elevator displacement. The second response (figure 4.23) is fully nonlinear because the matched excitation is normalized by its own RMS, hence has a "normal" amplitude which is sufficient to activate the nonlinear MLA block. The nonlinear FCS activation can be seen in figure 4.23, where the aileron deflection reaches the saturation limit.
- For *k=1* we can notice important differences between all the linear and nonlinear time histories. Both responses (figures 4.24, 4.25) are fully nonlinear and this brings to the bigger gap between the final time histories.
- For *k=10* (figures 4.26, 4.27) the behaviour of the system is similar to *k=0.1*, but for different reasons. In fact the amplitude of the first impulse excitation is considerably high: this fact brings to a fully nonlinear response (figure 4.26), but the capacity of load alleviation of the FCS is small respect to the magnitude of the excitation so the linear (FCS OFF) and nonlinear (FCS ON) impulse responses are almost identical, like their matched excitations. These have a "normal" amplitude because they have been normalized by their own RMS value. The second loop (figure 4.27) is nonlinear and the differences between the final responses are due to the FCS OFF/ON option.

- Finally also negatives initial impulse strengths have been tested (figures 4.28, 4.29, 4.30, 4.31, *k=-10*), because the opportunity of exciting an output of the system with its own matched excitation depends on the sign of its response function respect to the initial impulse excitation. We can notice that for the second loop of the WRS bending moment excitation (figure 4.29) the nonlinear block of the FCS doesn't activate, because the matched response for a negative *k* is negative hence the load factor never reach the positive threshold of *0.3g*. On the contrary for the WRS torsion moment (figure 4.31) the matched excitation for a negative *k* is positive, hence the nonlinear block activates. So still negative impulse excitations has to be taken in to account in the maximum search procedure.

4.3.3 Spectral Gust

SG method consists in: excite the system with the so called spectral excitation and calculate design and time-correlated loads as a time domain norm of the final response and by means of a time defined correlation coefficient. So just a simple deterministic response is needed (figure 4.33). Following figures reports the spectral excitation and the linear and nonlinear response time histories obtained for the WRS section bending moment (WRS4).

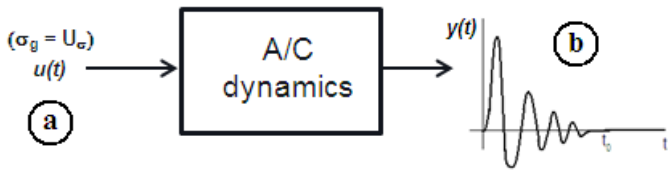

Figure 4.33. Spectral Gust operation flowchart.

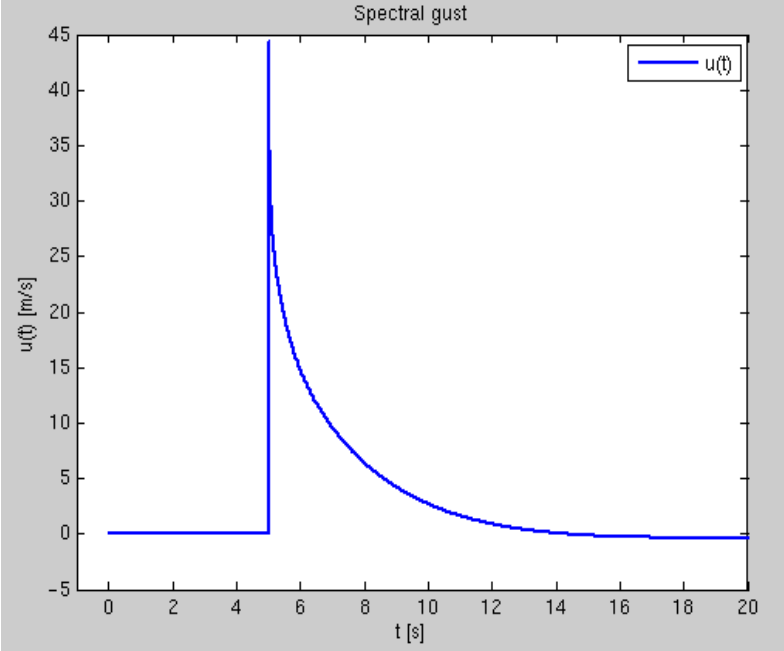

Figure 4.34. SG excitation (a).

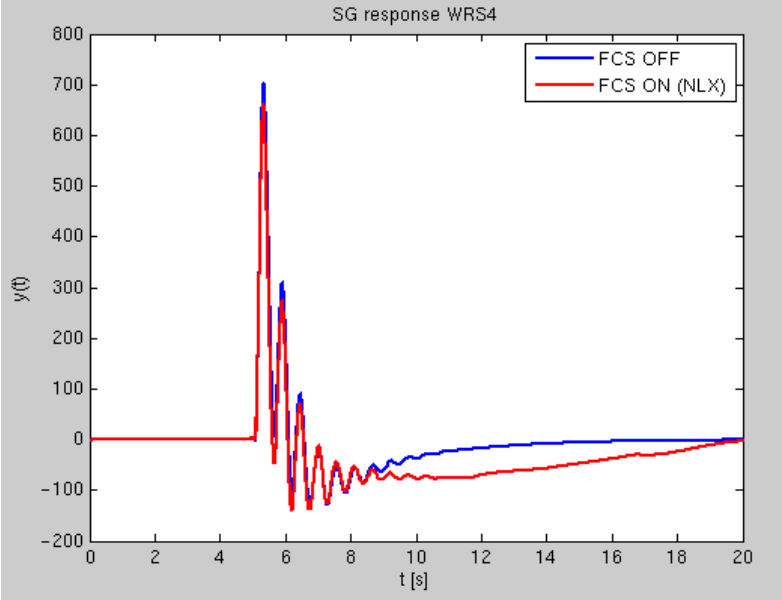

Figure 4.35. SG response, loadID=N3 (WRS bending moment) (b).

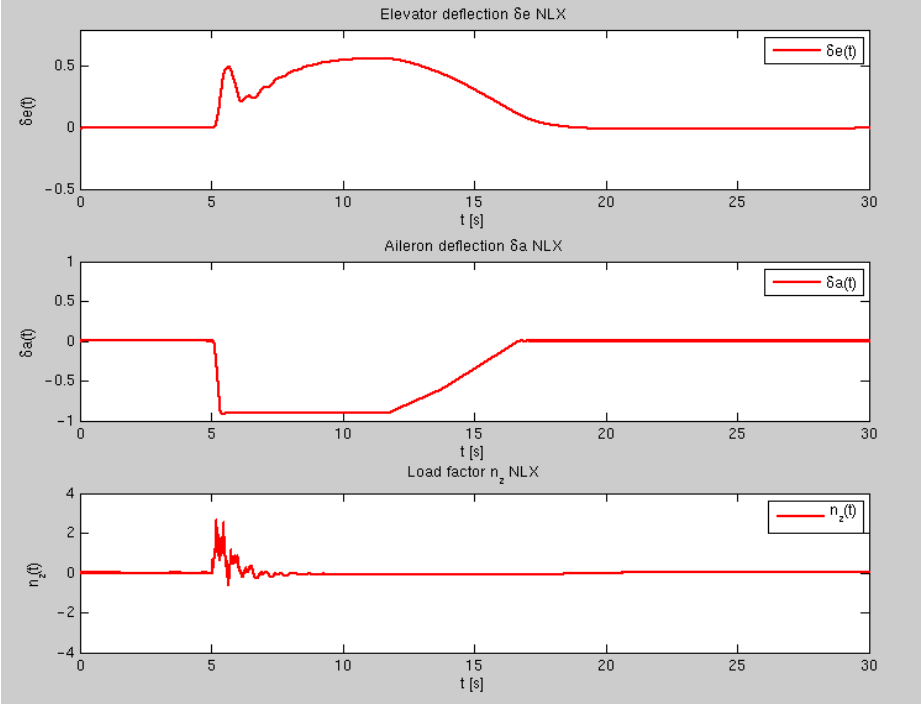

Figure 4.36. SG response, control surfaces and CG load factor.

Comments:

The three pictures reported above demonstrates that the SG is by far the most simple, straight forward and time saving method, although its reliability has to be proven. The excitation waveform (figure 4.34) is the impulse response of a Hoblit gust filter that suites well the von Karman turbulence spectrum (section 3.2). In figure 4.36 (control parameters) it is clearly visible the activation of the nonlinear FCS and the 5 seconds delay in the withdrawal of the ailerons (about *t=12s*), showed by the divergence and subsequent convergence of the linear (FCS OFF) and nonlinear (FCS ON) load responses of figure 4.35.

4.3.4 Statistical Method

The SM, as the SG, only consists in time responses calculation and post processing. Figures from 4.38 to 4.40 reports the waveforms obtained.

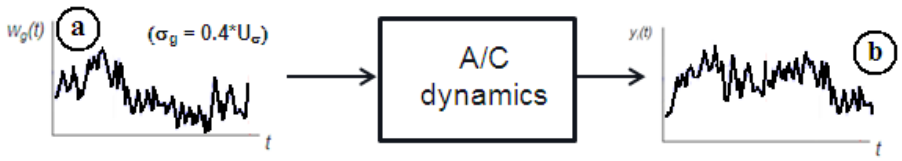

Figure 4.37. Statistical Method operation flowchart.

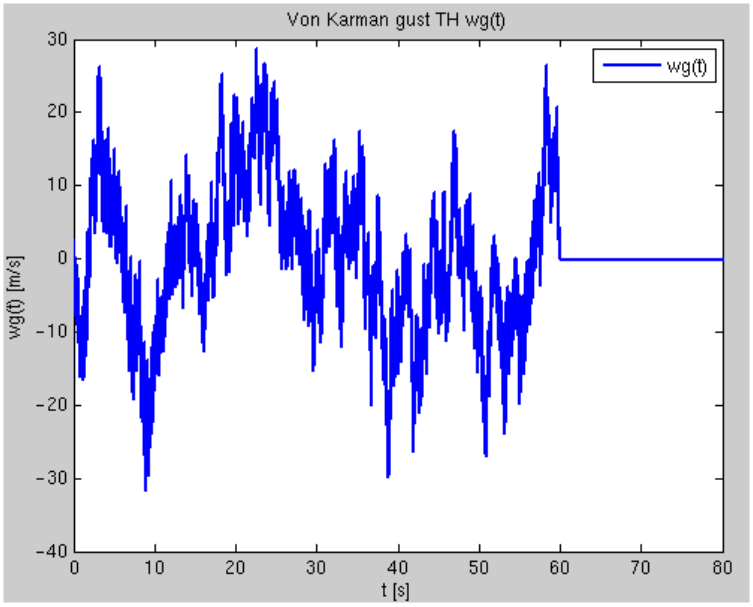

Figure 4.38. SM random excitation (a).

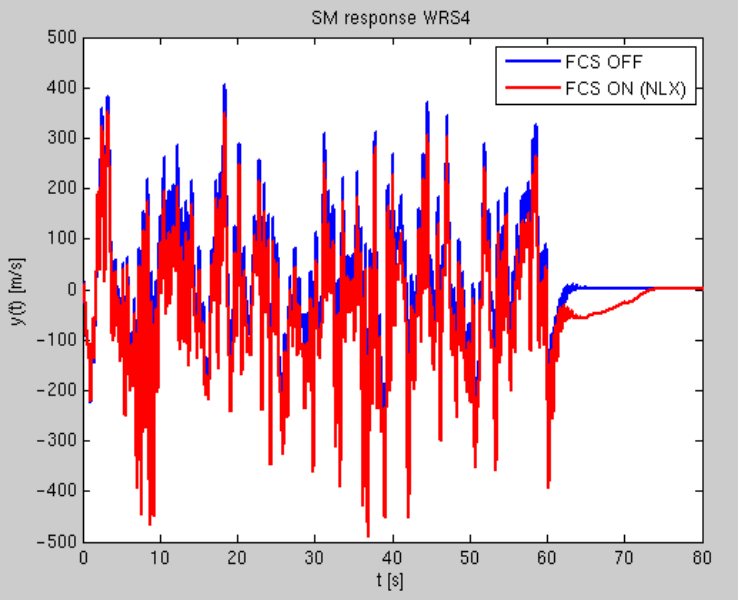

Figure 4.39. SM response, loadID=N3 (WRS bending moment) (b).

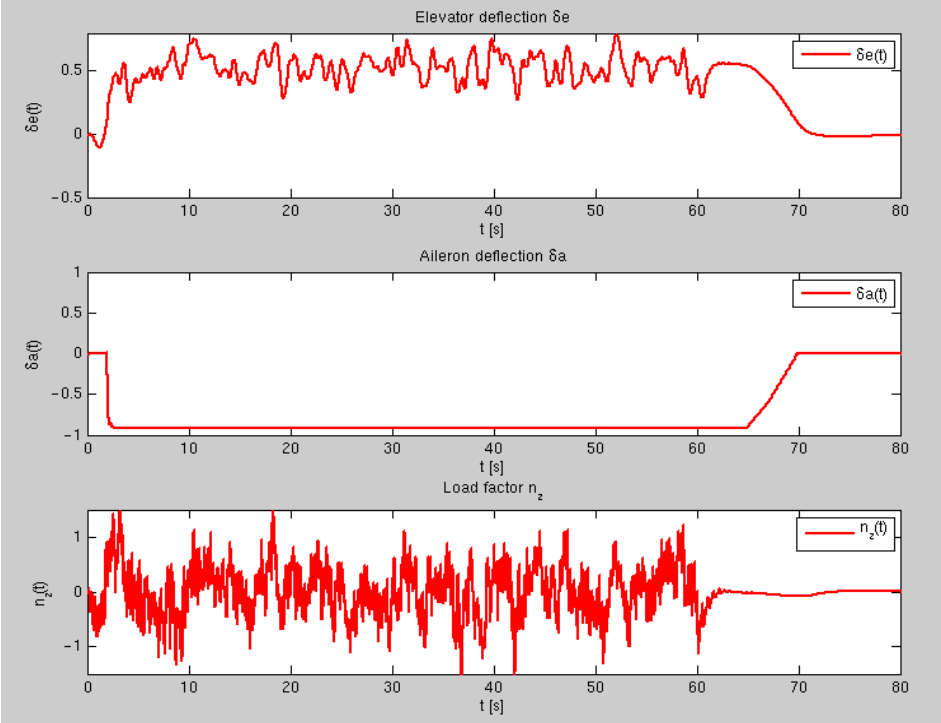

Figure 4.40. SM response, control surfaces and CG load factor.

Comments:
Figure 4.38 reports an example of input gust waveform generated as described in section 2.5.1. In figure 4.39 it is evident the load alleviation action of the nonlinear FCS and again it can be seen the 5 seconds delay in the cessation of FCS activity from *t=60* to *t=65s.*

4.4 Results comparison

Following sections present the results obtained with the three methods object of study (MF, SG, SM) for the *A400M* dynamic model. Design and time correlated loads have been calculated for the design stations indicated above (table 4.5 and figure 4.13). Design loads have been computed for all design section-load component combinations, while correlated loads have been calculated for the couples WRS4-WRS5 and HTP4-HTP5 (bending and torsion moment insisting on the same section). In the loads presentation actual values are omitted for reasons of industrial confidentiality, hence loads values are reported with respect to the linear PSD results. For the linear model the PSD loads represent the actual term of comparison as they are prescribed by regulations. For the nonlinear model (FCS ON) linear PSD loads (FCS OFF) are used just as a factor to get adimensional design and time correlated loads; nevertheless this is useful to understand the effectiveness of the FCS and how much loads decrease (or increase) for its activation.

4.4.1 Linear model (FCS OFF)

The first step to validate the quantitative behaviour of the methods is to apply them to the linear model (FCS OFF) for which the "exact" solution is known from PSD based criterions given by regulations (see section 1.1). The results are reported in tables 4.8, 4.9 and figures 4.41, 4.42 with respect to the PSD design and time correlated loads.

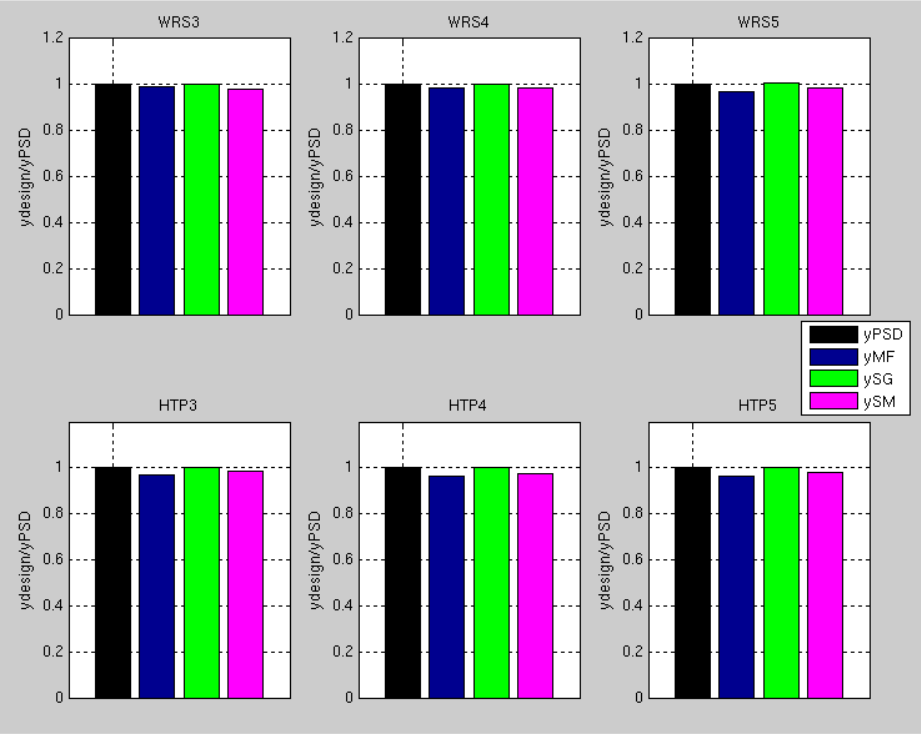

Figure 4.41. Linear model (FCS OFF) design loads.

Load	PSD % error	MF % error	SG % error	SM % error
WRS3	-	-1.17	-0.04	-2.14
WRS4	-	-1.27	-0.08	-1.68
WRS5	-	-3.10	0.65	-1.43
HTP3	-	-3.06	0.06	-1.71
HTP4	-	-3.61	0.06	-2.30
HTP5	-	-3.57	0.06	-1.92

Table 4.8. Linear model (FCS OFF) design loads % errors (with respect to linear PSD design loads).

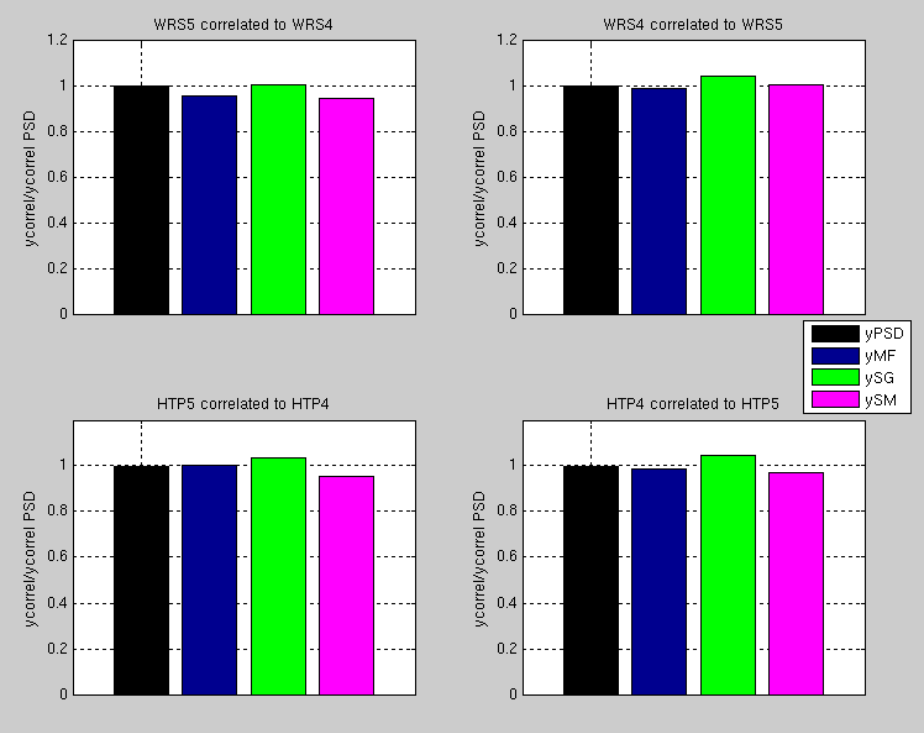

Figure 4.42. Linear model (FCS OFF) correlated loads.

Design Load	Correlated Load	PSD % error	MF % error	SG % error	SM % error
WRS4	WRS5	-	-4.07	0.73	-5.22
WRS5	WRS4	-	-1.07	4.51	0.70
HTP4	HTP5	-	0.05	3.53	-4.61
HTP5	HTP4	-	-1.57	4.33	-2.93

Table 4.9. Linear model (FCS OFF) correlated loads % errors (with respect to linear PSD correlated loads).

Comments:
The design loads calculated with the three methods fit very well the reference data, with maximum errors around -3.50%. The best approximation is represented by SG procedure which maximum error is below 1% .
It is interesting to take a look to how correlated loads time histories (confidentially called "potatoes") comply with the PSD based equiprobability ellipse, which represent the regulation reference for the calculation of correlated loads (see section 1.3). This "potatoes" are obtained plotting on each axis the desired loads time histories, for example WRS4 vs WRS5 (wing root bending versus torsion moment). Every point of the curve represents an instant of time and gives the loads combination in that instant. The design load condition is given by the point of tangency named *T* in figure 1.3.
Figures 4.43 and 4.44 report the correlated time histories obtained with the MF procedure. The matched responses (WRS4 and WRS5 or HTP4 and HTP5 time histories obtained with their own matched excitation) are painted in red, while the dotted blue lines represents the non matched responses (i.e. calculated with excitations matched to others outputs). We can notice that the method perfectly fit with the PSD equiprobability ellipse giving exactly the *T* point of tangency.
For the SM method the detection of the correlated design condition respect to the ellipse is a bit more complicated. Taking as an example the WRS4 vs WRS5 potato for one of the 64 responses needed for the SM procedure (figure 4.45) it can be noticed that the time history often goes out from the ellipse: this is normal since the design and time correlated loads definition is based on the frequency of exceedance concept. Green points represent the correlated load values (for example WRS5) taken at the instant of time when the design load (for example WRS4) time history crosses its own design value (see section 2.5, figure 2.10 for a better comprehension). Doing this for every one of the 64 time responses and averaging all the related correlation points we obtain the red crosses of figure 4.46, which represent the correlated design load condition for the SM.
SG correlated loads are calculated by means of the time definition of correlation coefficients, so it can't be plotted in form of "potato" nor compared with the equiprobability ellipse.
In conclusion correlated loads errors with respect to PSD reference are a bit greater than the ones obtained for the limit loads, especially for SG which gave exceptional results in the design load calculation. However approximation level reached complies with literature survey results.

In this section it has been demonstrated that the three methods approximate quite well the linear PSD results both for design and correlated loads. This is a good starting point for the following nonlinear application.

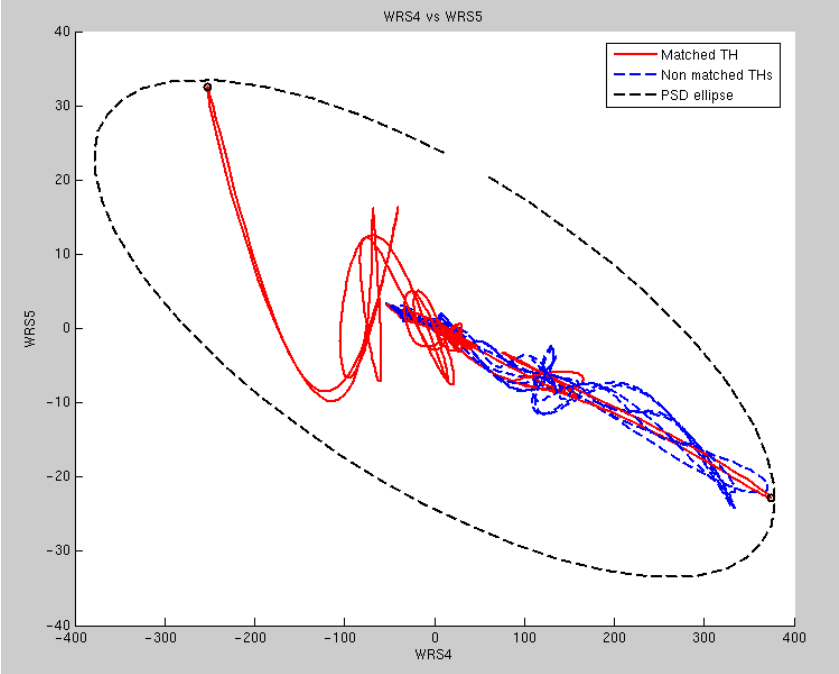

Figure 4.43. Linear model (FCS OFF), MF WRS correlated time histories.

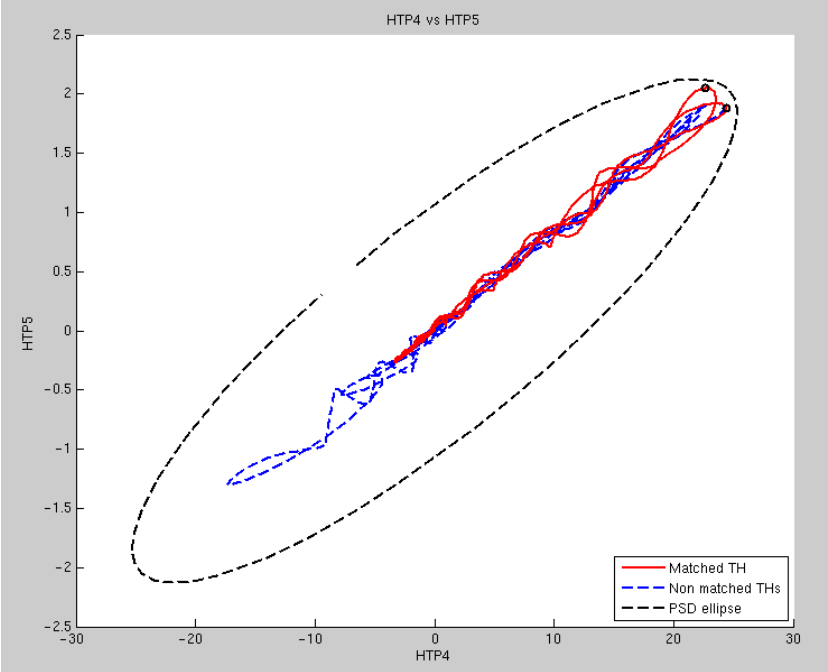

Figure 4.44. Linear model (FCS OFF), MF HTP correlated time histories.

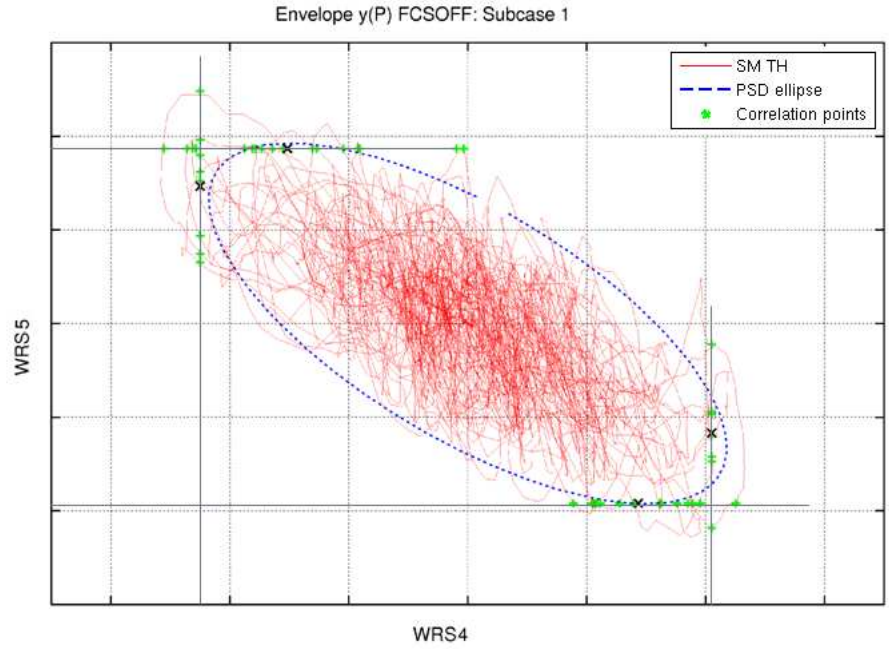

Figure 4.45. Linear model (FCS OFF), SM WRS example of correlated time history.

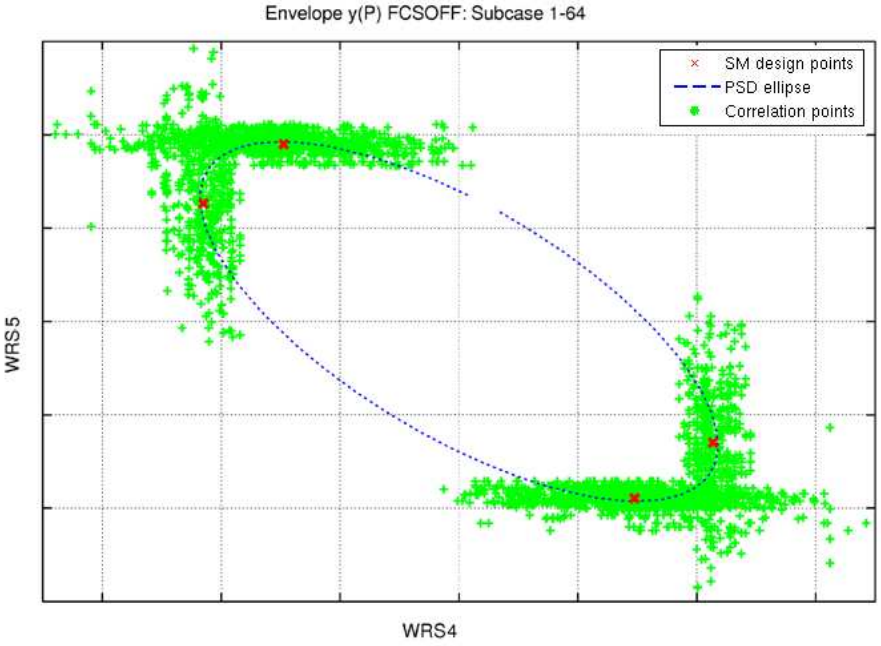

Figure 4.46. Linear model (FCS OFF), SM WRS envelope of 64 correlated time histories.

4.4.2 Nonlinear model (FCS ON)

This section reports the results of the application of MF, SG and SM to the nonlinear dynamic model of the *A400M*, where for nonlinear it is intended with the presence of the nonlinear FCS (FCS ON). PSD loads are still considered as reference even if they are calculated for a linear model; this is not useful for an error comparison but could be interesting to see the behaviour of the FCS in terms of decrement (or increment) of design and correlated loads. Figures 4.47, 4.48 and tables 4.10, 4.11 show the design and time correlated loads comparison while figure 4.49 reports a typical design load dependence on the *k* sweep for the MF method.

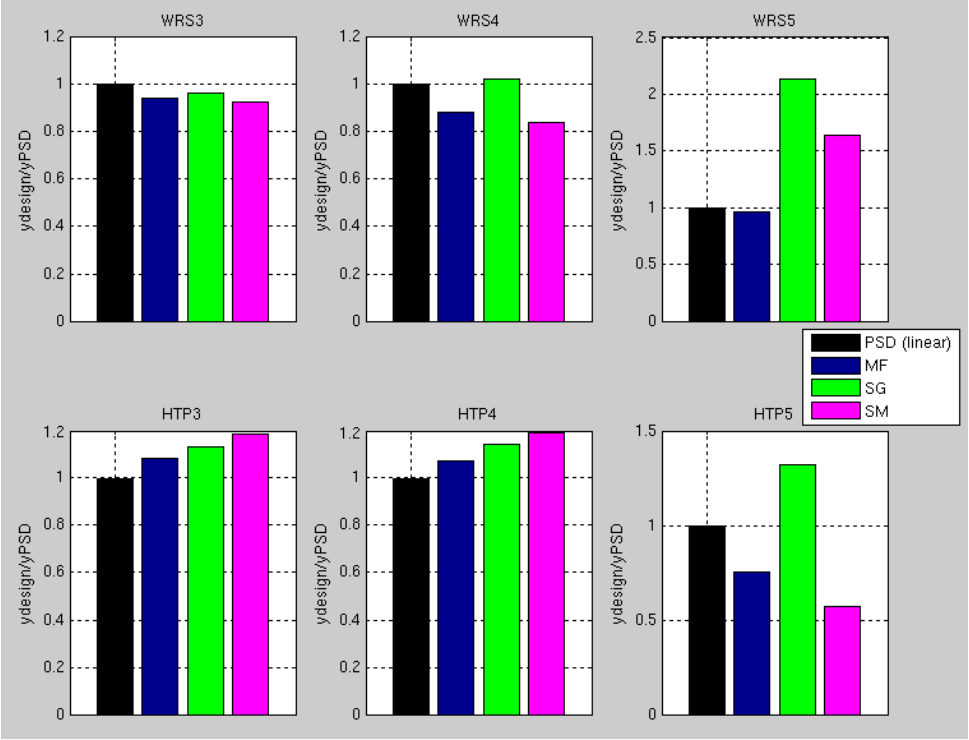

Figure 4.47. Nonlinear model (FCS ON) design loads.

Load	PSD % diff	MF % diff	SG % diff	SM % diff
WRS3	-	-5.41	-3.55	-7.05
WRS4	-	-11.67	2.41	-15.77
WRS5	-	-3.32	113.44	63.43
HTP3	-	8.19	13.41	18.61
HTP4	-	7.47	14.45	19.33
HTP5	-	-24.81	32.37	-42.87

Table 4.10. Nonlinear model (FCS ON) design loads % difference with respect to linear PSD design loads.

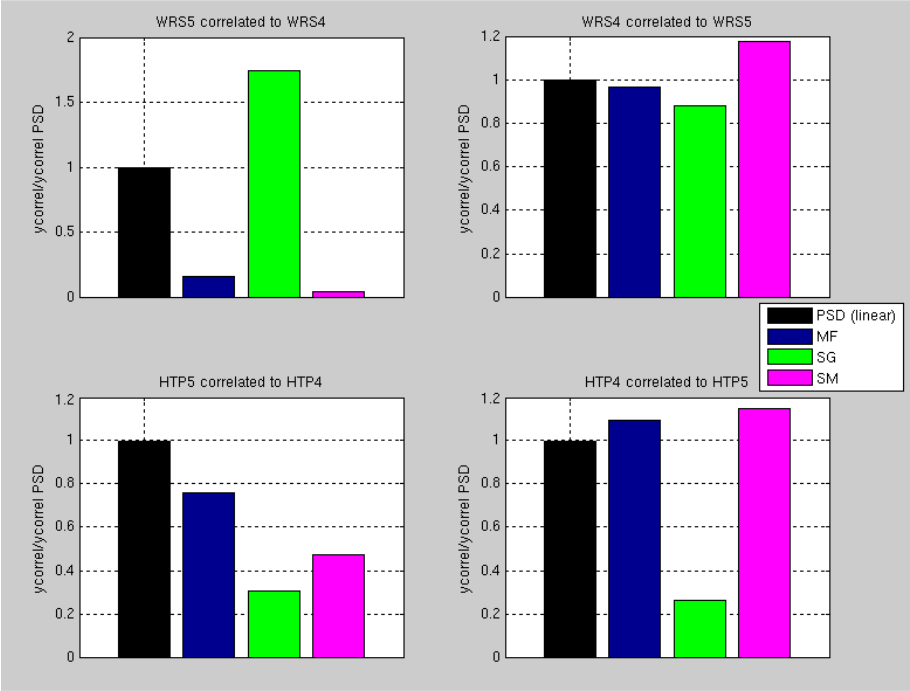

Figure 4.48. Nonlinear model (FCS ON) correlated loads.

Design Load	Correlated Load	PSD % diff	MF % diff	SG % diff	SM % diff
WRS4	WRS5	-	-83.99	74.16	-96.28
WRS5	WRS4	-	-2.95	-11.55	18.20
HTP4	HTP5	-	-24.19	-69.42	-52.66
HTP5	HTP4	-	9.73	-73.71	14.70

Table 4.11. Nonlinear model (FCS ON) correlated loads % errors with respect to linear PSD correlated loads.

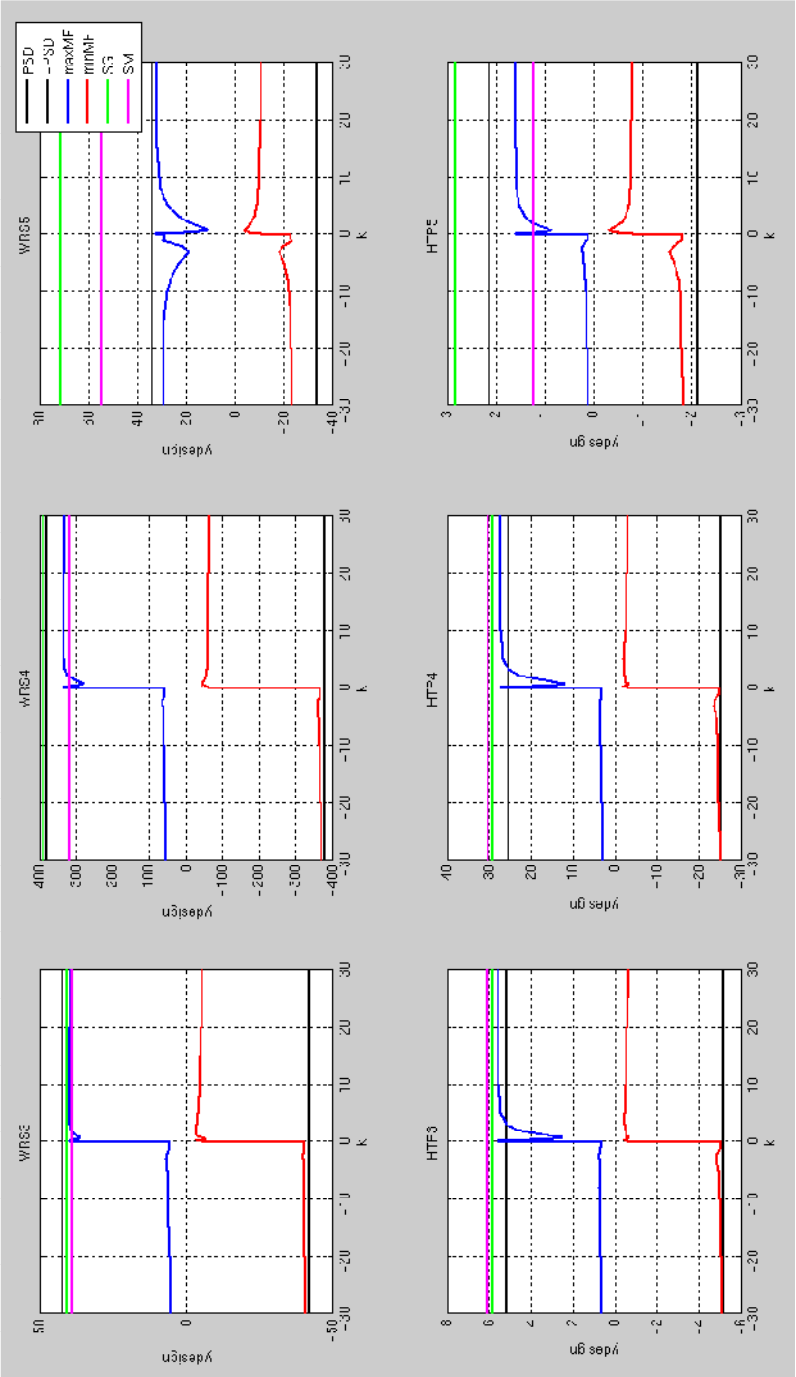

Figure 4.49. Nonlinear model (FCS ON), variation of MF design loads with initial *k* sweep.

Comments:
Unexpectedly the results spread around the reference values and it is not possible to recognize a dominant tendency. Starting from WRS design loads results, it can be noticed a reasonable behaviour of all three methods for the shear force WRS3, while for the bending moment WRS4 the results are contradictory: MF and SM detect the FCS effect decreasing the bending moment limit value, while the SG fails the bending moment evaluation which is greater than the linear (without FCS) design value. This fact shouldn't be possible since the FCS is designed for WRS4 alleviation (and effectively get it, see section 4.3.1 about DTG nonlinear analysis). HTP shear force and bending moment design loads show relatively small difference, about *10%* around of the linear PSD value. The mayor problems are detectable in WRS5 and HTP5 (torsion moments) design load calculation, where limit values spread in a huge range of values. Taking DTG nonlinear design values as a qualitative reference we can deduct that MF WRS5 design load is probably wrong, because it is almost identical to the linear PSD value while, due to the aileron deflection, it should be appreciably higher (as shown by SG method and SM). SG HTP5 design load is probably wrong too, because the positive deflection of the elevator should give lower design loads than the linear case, without elevator deflection.

Correlated loads show great differences between the three methods. For the SG procedure correlated loads are calculated by multiplication of the design limit loads by a time defined correlation coefficient, hence if the limit loads are bad calculated neither correlated loads can be taken in to account. With respect to DTG results SM approximates in a reasonably manner shear forces correlated to torsion moments (WRS4 correlated to WRS5 and HTP4 correlated to HTP5), while gives very low values for the torsion moments correlated to shear forces. Finally the MF procedure gives reasonable values only for HTP4 correlated to HTP5, while for the other cases the results don't comply with the nonlinear DTG logic.

A final comment can be made about the time length of the excitations: MF and SG calculate CT design loads through short excitations (gust filter and A/C dynamics impulse responses) while SM excitation represents a sort of true turbulence field in which the aircraft flight for about *60s*. So the responses of the different methods are dominated by different dynamics and this can be a further explanation for the different results obtained, even if further investigations are required to clear up this aspect of the phenomenon.

4.4.3 Nonlinear model (FCS ON) calculation times

Table 4.12 reports the total number of analysis and the length of each response needed for the calculation of design and time correlated loads for the nonlinear model. Actual CPU times are not reported for reasons of industrial confidentiality and should comprehend the DYNRESP dynamic response, load recovery with summation of forces method for the above mentioned design section and time histories post processing (including also iterative cycles if required).

Method	Number of responses	Length of each response [s]
MF*	$k(1+N_{design\ section}*N_{loadcomponents})$	65
SG	1	65
SM	64	100

Table 4.12. Nonlinear model (FCS ON) total calculation times.

From table 4.12 and from previous data showed for the 2 DOF test system (section 3.4.3) it should be clear that the faster method should be the SG procedure. It requires only one time response to get all desired design and correlated loads and this great advantage remains also if the number of design stations increase, with only a small increase in post processing times. Hence, even if the SG nonlinear design and time correlated loads didn't prove to be reliable, further investigations have to be carried out because of this really promising time performances of the method.
MF is depicted with a star symbol *(*)* because the total time depends on case by case duration of the one dimensional search procedure (a typical number can be *30-40* iterations) and it can be deducted the high calculation effort required. In fact for every combination design station-load component the search procedure has to be repeated, because any output of the system has its own matched excitation which varies with the initial impulse strength *k*. This is a big disadvantage respect to SG and SM, because increasing the number of design stations the total calculation time increase in an exponential manner.
Finally the SM: single responses are long because of the sensitivity of the gust time history spectrum to the frequency step *df*, hence big periods *T=1/df* are required to approximate quite well the von Karman spectrum. The number of time responses (*N=64*) seems to be big but it remains constant independently of the number of design station considered. Increasing the number of combinations design station-load component we will detect an increment only in post processing time, which represents the minor part of the total CPU time.

Chapter 5

Conclusions and further developments

Three methods for calculating continuous turbulence aircraft response in the presence of nonlinearities have been compared:

- Matched Filter (MF) based method and Spectral Gust (SG) procedure have been implemented from public literature.
- Statistical Method (SM) has been evaluated from AI-Military developments.

Loads comparisons for the *A400M* case provide the following conclusions:

- For the linear model (FCS OFF) all the three methods prove to be sufficiently reliable. The reference loads are those prescribed by regulations calculated with the Design Envelope criterion (ref. [2]). Correlated loads show bigger deviations from the reference results but the consistency of the procedures has been proven through the equiprobability ellipse comparison.
- For the nonlinear model (FCS ON) the SG procedure (which gives excellent results in the linear case) doesn't prove to be reliable, because it gives design and time correlated loads contradictory with respect to DTG tendency and others CT methods results. SM seems to be the most reliable method for design loads, while MF follows the SM results except for wing root section torsion moment. Nonlinear correlated loads presents a great results dispersion and don't follow the DTG tendency.
- The fastest method to compute nonlinear loads is the SG procedure, because it requires only one response analysis to obtain design and time correlated loads. MF is the most expensive method in terms of calculation time especially with a relevant number of design stations, because every output of the system has its specific matched excitation hence a number of analysis proportional to the number of outputs has to be performed. Furthermore the method is based on an iterative procedure which duration depends on system dynamics. SM procedure lays between SG and MF because it always requires a fixed number of responses (64 in this application) and increase or decrease the number of design stations will affect only the post processing time.

So the linear application of the method can be certainly defined as satisfactory, while the nonlinear application results are not as good as expected. Some hypothesis about this unexpected behaviour and actions that could be taken to improve the results are reported in table 5.1.

Method	Comments	Action
MF	- Solid formulation. - Bad behaviour for nonlinear design torsion moments. - Bad behaviour for nonlinear correlated loads.	- Improve von Kármán spectrum approximation. - Further investigation over correlated loads. - Improve the search procedure (*k* sweep).
SG	- Great time saving. - Good matching with linear design and correlated loads. - Unexpected nonlinear results.	- Further investigation? - Improve von Kármán spectrum approximation.
SM	- Solid formulation. - Good linear and nonlinear results. - Bad behaviour for nonlinear correlated torsion moments.	- Further investigation over correlated loads calculation procedure.

Table 5.1. Methods comparison and further developments.

Table 5.1 clearly depicts the main characteristics of each method and future developments in the implementation that are felt to be important. A general investigation over nonlinear correlated loads calculation and definition has to be carried out. An improvement on the gust filter definition is necessary for the methods which generate the initial exciting gust as the impulse response of the filter (MF and SG) itself, to a better matching with the von Kármán power spectrum.
An interesting comment can be made about the discrete representation of continuous turbulence in time domain: MF method and SG procedure calculate CT design loads using very short time excitations (series of gust filter and A/C dynamics impulse responses and the impulse response itself), for which the load response should be completely dominated by structural dynamics. On the contrary the SM procedure uses a very long excitation (about *60s*) that should represent the true turbulence field that the aircraft can encounter, for which rigid body modes contribution can be relevant. So the question is if methods like MF

and SG can excite all the relevant dynamics involved in the CT response giving the correct design and correlated loads.

The MF method demonstrates to be promisingly reliable but, independently of the problems which presents today, it requires the biggest calculation effort among the methods considered; so its utility is felt to be academic or only for a limited number of critical cases, in which the MF can reproduce the critical design loads and directly provide nodal loads. SG procedure nonlinear results should suggest stopping the development of the method but its surprisingly good linear results and its great capacity of time saving can be good reasons to further investigate it. Finally the SM proves to be reliable in the linear and nonlinear design load calculation and is very promising for the future, despite further investigation are needed about the nonlinear correlated loads definition and calculation.

Bibliography and References

[1] - Thomas A. Zeiler, Matched Filter Concept and Maximum Gust Loads, Journal of Aircraft Vol. 34 (1997).

[2] - European Aviation Safety Agency, Certification Specifications for Large Aeroplanes CS-25, (2003).

[3] - Robert C. Scott, Anthony S. Pototzky, Boyd Perry III, Maximized Gust Loads for a Nonlinear Airplane using Matched Filter Theory and Constrained Optimization, Langley Research Center, Hampton, Virginia, NASA Technical Memorandum 104138 (1991).

[4] - H. Lusebrink, J. Brink-Spalink, Treatment of Non-Linear Systems by Timeplane-Transformed C.T. Methods, The Spectral Gust Method, Hamburg, Germany: Deutsche Aerospace Airbus GmbH - Structural Dynamics (1994).

[5] - R. Noback, The Deterministic Power Spectral Density Method, Amsterdam, The Netherlands: National Aerospace Laboratory NLR, NLR TP 92114 U (1992).

[6] - Panel NATO RTO Applied Vehicle Technology, Design Loads for Future Aircraft, RTO-TR-045 (2002).

[7] - W.J. Vink, A stochastic simulation procedure compared to deterministic methods for PSD gust design loads, National Aerospace Laboratory NLR, NLR-TP-98240 (1998).

[8] - Anthony S. Pototzky, Thomas A. Zeiler, Boyd Perry III, Calculating Time-Correlated Gust Loads using Matched Filter and Random Process Theories, Journal of Aircraft Vol. 28, No. 5 (1991).

[9] - F.M. Hoblit, Gust Loads on Aircraft: Concepts and Applications, AIAA Education Series (1988).

[10] - NATO Advisory Group for Aerospace Research and Development, Manual on the Flight of Flexible Aircraft in Turbulence, AGARD-AG-317 (1991).

[11] - Enrique González Sánchez, Continuous Turbulence analysis on Time Domain, EADS-CASA, Airbus Military Structural Dynamic and Aeroelasticity Department, Getafe (Spain) (2010).

[12] - Joint Aviation Authorities, Gust and Continuous Turbulence Design Loads, Comment Response Document NPA 25C-309 (2002).

[13] - Moti Karpel, DYNRESP-7: Dynamic Response of Aircraft Structures to Gusts, Manuever Commands and Direct Forces – Theoretical Manual, KARPEL Dynamic Consulting Ltd (2011).

[14] - Paul F. Taylor, Laurence C. Hanson, Terence C. Barnes, A Brief History of Aircraft Loads Analysis Methods, AIAA 2003-1892 (2003).

[15] - Walter A. Silva, Maximized Gust Loads of a Closed-loop, Nonlinear Aeroelastic system using Nonlinear System Theory, AIAA 99-1474 (1999).

[16] - Robert C. Scott, Anthony S. Pototzky, Boyd Perry III, Further Studies using Matched Filter Theory and Stochastic Simulation for Gust Loads Prediction, AIAA 93-1365-CP (1993).

[17] - Robert C. Scott, Anthony S. Pototzky, Boyd Perry III, Matched-Filter and Stochastic-Simulation based methods of Gust Loads Prediction, Journal of Aircraft Vol. 32, No. 5 (1995).

[18] - Krzysztof J. Fidkowski, Frode Engelsen, Karen E. Willcox, Ilan M. Kroo, Stochastic Gust Analysis Techniques for Aircraft Conceptual Design, American Institute of Aeronautics and Astronautics (AIAA) paper.

[19] - J.C. Jones, Formulation of Design Envelope Criterion in terms of Deterministic Spectral Procedure, Royal Aerospace Establishment AD-A222 120 (1990).

[20] - W.J. Vink, J.B. de Jonge, A MATLAB program to study gust loading on a simple aircraft model, National Aerospace Laboratory NLR, NLR-TP-97379 (1997).

[21] - J.C. Jones, Nonlinear Aircraft Loads in Severe Atmospheric Turbulence, Journal of Aircraft Vol. 46, No. 5 (2009).

[22] - Harry Press, Bernard Mazelsky, A study of the application of Power-Spectral Methods of Generalized Harmonic Analysis to Gust Loads on Airplanes, NACA report 1172.

[23] - MSC.Nastran 2005, Aeroelastic Analysis User's Guide, Basic Dynamic Analysis User's Guide, Reference Manual, MSC.Software Corporation.

[24] - Walter A. Silva, Thomas W. Strganac, Muhammad R. Hajj, Higher-Order Spectral Analysis of a Nonlinear Pitch and Plunge Apparatus, American Institute of Aeronautics and Astronautics (AIAA) paper.

[25] - Raymond G. Kvaternik, Walter A. Silva, A Computational Procedure for Identifying Bilinear Representations of Nonlinear Systems Using Volterra Kernels, NASA Technical Memorandum 215320 (2008).

[26] - Walter A. Silva, Identification of Linear and Nonlinear Aerodynamic Impulse Responses using Digital Filter Techniques, NASA Technical Memorandum 112872 (1997).

[27] - Walter A. Silva, Muhammad R. Hajj, Shane Dunn, Thomas W. Strganac, Edward J. Powers, Ronald Stearman, Recent Applications of Higher-Order Spectral Analysis to Nonlinear Aeroelastic Phenomena, American Institute of Aeronautics and Astronautics (AIAA) paper.

[28] – Herbert S. Ribner, Propellers in Yaw, NACA report 820 (1945).

[29] – John C. Houbolt, Wilmer H. Reed III, Propeller-Nacelle Whirl Flutter, Journal of the Aerospace Sciences (March 1962).

[30] – K.E. Baker, R. Smith, K.W. Toulson, Notes on Propeller Whirl Flutter, Canadair Limited (1965).

[31] – Wilmer H. Reed III, Propeller-Rotor Whirl Flutter: a State of the Art review, NASA Technical Memorandum 56678 (1965).

[32] - Wilmer H. Reed III, Samuel R. Bland, An Analytical Treatment of Aircraft Propeller Precession Instability, NASA technical note D-659.